ABSTRACT

FULLY NONLINEAR INTERFACIAL WAVES IN A BOUNDED TWO-FLUID SYSTEM

by
Lyudmyla Leonidivna Barannyk

We study the nonlinear flow which results when two immiscible inviscid incompressible fluids of different densities and separated by an interface which is free to move and which supports surface tension, are caused to flow in a straight infinite channel. Gravity is taken into consideration and the velocities of each phase can be different, thus giving rise to the Kelvin-Helmholtz instability. Our objective is to study the competing effects of the Kelvin-Helmholtz instability coupled with a stably or unstably stratified fluid system (Rayleigh-Taylor instability) when surface tension is present to regularize the dynamics. Our approach involves the derivation of two- and three-dimensional model evolution equations using long-wave asymptotics and the ensuing analysis and computation of these models. In addition, we derive the appropriate Birkhoff-Rott integro-differential equation for two-phase inviscid flows in channels of arbitrary aspect ratios.

A long wave asymptotic analysis is undertaken to develop a theory for fully nonlinear interfacial waves allowing amplitudes as large as the channel thickness. The result is a set of evolution equations for the interfacial shape and the velocity jump across the interface. Linear stability analysis reveals that capillary forces stabilize short-wave disturbances in a dispersive manner and we study their effect on the fully nonlinear dynamics described by our models. In the case of two-dimensional interfacial deflections, traveling waves of permanent form are constructed and it is shown that solitary waves are possible for a range of physical parameters. All solitary waves are expressed implicitly in terms of incomplete elliptic integrals of the third kind. When the upper layer has zero density, two explicit solitary-wave solutions

have been found whose amplitudes are equal to $h/4$ or $h/9$ where $2h$ is the channel thickness. In the absence of gravity, solitary waves are not possible but periodic ones are. Numerically constructed traveling and solitary waves are given for representative physical parameters. The initial value problem for the partial differential equations is also addressed numerically in periodic domains, and the regularizing effect of surface tension is investigated. In particular, when surface tension is absent it is shown that the system of governing evolution equations terminates in a singularity after a finite time. This is achieved by studying a 2×2 system of nonlinear conservation laws in the complex plane and by numerical solution of the evolution equations. The analysis shows that a sinusoidal perturbation of the flat interface and a cosine perturbation to the unit velocity jump across the interface, develop a singularity at time $t_c = \ln \frac{1}{\varepsilon} + O\left(\ln(\ln \frac{1}{\varepsilon})\right)$ where ε is the initial amplitude of the disturbances. This result is asymptotic for small ε and is derived by studying the asymptotic form of the flow characteristics in the complex plane.

We also derive the analogous three-dimensional evolution equations by assuming that the wavelengths in the principal horizontal directions are large compared to the channel thickness. Surface tension is again incorporated to regularize short-wave Kelvin-Helmholtz instabilities and the equations are solved numerically subject to periodic boundary conditions. Evidence of singularity formation is found. In particular, we observe that singularities occur at isolated points starting from general initial conditions. This finding is consistent with numerical studies of unbounded three-dimensional vortex sheets (see Introduction for a discussion and references).

In the final part of this work we consider the vortex-sheet formulation of the exact nonlinear two-dimensional flow of a vortex sheet which is bounded in a channel. We derive a Birkhoff-Rott type integro-differential evolution equation for the velocity of the interface in terms of the vorticity as well as the evolution equation for the unnormalized vortex sheet strength. For the case of a spatially periodic vortex

sheet, this Birkhoff-Rott type equation is written in terms of Jacobi's functions. The equation is shown to recover the limits of unbounded and non-periodic flows which are known in the literature.

FULLY NONLINEAR INTERFACIAL WAVES IN A BOUNDED TWO-FLUID SYSTEM

by
Lyudmyla Leonidivna Barannyk

A Dissertation
Submitted to the Faculty of
New Jersey Institute of Technology and
Rutgers, The State University of New Jersey – Newark
in Partial Fulfillment of the Requirements for the Degree of
Doctor of Philosophy in Mathematical Sciences

Department of Mathematical Sciences
Department of Mathematics and Computer Science, Rutgers-Newark

May 2003

APPROVAL PAGE

FULLY NONLINEAR INTERFACIAL WAVES IN A BOUNDED TWO-FLUID SYSTEM

Lyudmyla Leonidivna Barannyk

Dr. Demetrius T. Papageorgiou, Dissertation Advisor — Date
Professor of Mathematical Sciences, NJIT

Dr. Nadine Aubry, Committee Member — Date
Distinguished Professor and Chair of Mechanical Engineering
Professor of Mathematical Sciences, NJIT

Dr. Lou Kondic, Committee Member — Date
Associate Professor of Mathematical Sciences, NJIT

Dr. Robert M. Miura, Committee Member — Date
Professor of Mathematical Sciences, NJIT

Dr. Michael Siegel, Committee Member — Date
Associate Professor of Mathematical Sciences, NJIT

BIOGRAPHICAL SKETCH

Author: Lyudmyla Leonidivna Barannyk

Degree: Doctor of Philosophy

Date: May 2003

Date of Birth: April 17, 1972

Place of Birth: Poltava, Ukraine

Undergraduate and Graduate Education:

- Doctor of Philosophy in Mathematical Sciences,
  New Jersey Institute of Technology, Newark, NJ, 2003
- Master of Science in Applied Mathematics,
  New Jersey Institute of Technology, Newark, NJ, 2000
- Candidate of Physical and Mathematical Sciences,
  Institute of Mathematics, National Academy of Sciences of Ukraine, Kyiv, Ukraine, 1997
- Specialist in Mathematics and the Teaching of Mathematics,
  Kharkiv State University, Kharkiv, Ukraine, 1994

Major: Mathematical Sciences

Presentations and Publications:

Barannyk, L.L., and Papageorgiou, D.T.
Fully nonlinear gravity-capillary solitary waves in a two-fluid system of finite depth, *J. Engng. Math., 42* (2002) 321–339.

Barannyk, L.L., and Papageorgiou, D.T.
Three-dimensional fully nonlinear interfacial long waves in a bounded two-fluid system, 55^{th} *Annual Meeting of the Division of Fluid Dynamics*, American Physical Society, Dallas, TX, November 24–26, 2002.

Barannyk, L.L., and Papageorgiou, D.T.
Effect of the surface tension on the fully nonlinear capillary-gravity waves of bounded two-fluid systems, *Invited Lecture*, The Mathematics-Physics-Technical Section of the Shevchenko Scientific Society, New York, NY, November 9, 2002.

Barannyk, L.L., and Papageorgiou, D.T.

Strongly nonlinear interfacial waves of two-fluid system with the surface tension: solitary and traveling waves, 54^{th} *Annual Meeting of the Division of Fluid Dynamics*, American Physical Society, San Diego, CA, November 18–20, 2001.

Barannyk, L.L.

Some new solitary waves in two-fluid flows and their connection to elliptic integrals, *Graduate Research Seminar*, Center for Applied Mathematics and Statistics, New Jersey Institute of Technology, July 10, 2001.

Barannyk, L.L., and Papageorgiou, D.T.

The effect of surface tension on strongly nonlinear interfacial waves in a channel, 53^{rd} *Annual Meeting of the Division of Fluid Dynamics*, American Physical Society, Washington, DC, November 18–21, 2000.

To my Beloved Mama and Papa, without whom this would not have been possible

ACKNOWLEDGMENT

I would like to express my sincere gratitude and appreciation to my advisor, Dr. Demetrius Papageorgiou, who introduced me to the interesting and beautiful subject of this work, for his expert guidance and patience, encouragement and support throughout my time as a graduate student.

Special thanks are given to Dr. Nadine Aubry, Dr. Lou Kondic, Dr. Robert Miura, Dr. Michael Siegel for actively participating in my committee, for taking time out of their busy schedules to read this dissertation, provide help and offer constructive comments.

I would like to thank Professor Daljit S. Ahluwalia, Chair of the Department of Mathematical Sciences at NJIT, for the help, patience, and support all these years. Padma Gulati, Susan Sutton, Mónica Figueroa, and Liliana Boland deserve my appreciation for the help given me. I am grateful to the department for providing financial support for this research.

I wish to express my deepest gratitude to Professor Roman Voronka who became my "in loco parentis" since I came to the United States of America, and made the world of difference to my stay here in this country.

Many of my fellow present and former graduate students in the Department of Mathematical Sciences are deserving of recognition for their support. I would like to express my gratitude to my friends Dr. Adrienne James and Hoa Tran for adapting the dissertation LaTeX style file. I am very grateful to Hoa Tran and my brother, Oleksandr Barannyk, for their help in creating and modifying figures. I wish to extend my thanks to Tetyana Segin, Valery Lukyanov, Jyoti Champanerkar, Arnaud Goullet, Urmi Ghosh-Dastidar, Yuriy Mileyko, Tsezar Seman as well as Dr. Said Kas-Danouche, Dr. Stephen Kunec and Dr. Knograt Savettaseranee for their help in mathematical discussions, their friendship and support.

I am grateful to Mr. Michael Forrow for saving my dissertation in the Montclair direct train and proofreading it.

I would like to express my gratitude to Paata Tsiklauri, my husband, and Oleksandr Barannyk, my brother, for their love, patience, understanding and support. My heartfelt thanks to my Mama and Papa, Mariya and Leonid Barannyk, who always believed in me and supported me in my decision to come to the United States to pursue further academic study. I am very grateful to my parents for inspiring me to study mathematics and learn foreign languages, for their continuing encouragement, love and support.

TABLE OF CONTENTS

TABLE OF CONTENTS
(Continued)

Chapter **Page**

TABLE OF CONTENTS
(Continued)

Chapter **Page**

LIST OF FIGURES

LIST OF FIGURES
(Continued)

Figure **Page**

LIST OF FIGURES
(Continued)

Figure **Page**

CHAPTER 1

INTRODUCTION

Interfacial waves are waves which propagate at the interface of two fluids and are encountered in many physical situations. Applications range from oceanography, meteorology, cooling systems, lubricated transport, as well as applications in aerodynamics, for example, wakes behind aerofoils or flows in turbomachinery. Waves propagating in two-layer fluid flows may be observed in the seasonal thermocline in the ocean and in the inversion in the atmosphere. An example of environmental interest are flows in estuaries where lighter fresh water flows into the heavier brine with the potential of interfacial instabilities developing which can affect mixing, for example. The fundamental understanding of interfacial waves and their nonlinear response is of great interest both from a mathematical point of view as well as in gaining a quantitative understanding of fundamental physical mechanisms.

It is well known that nonlinearity and dispersion are two fundamental mechanisms that are responsible for wave propagation in fluids. During the course of the wave evolution, nonlinearity tends to steepen a wave form, while dispersion tends to flatten steep free-surface gradients; thus it creates a competing mechanism to that of nonlinearity. Possibly one of the simplest examples that exhibits the interplay between nonlinearity and dispersion is the case of free-surface waves of a homogeneous layer of incompressible and inviscid fluid. Free surface waves are waves propagating at the interface of a fluid with a passive upper region, i.e. the density of the upper layer being zero. When the two competing effects of nonlinearity and dispersion balance each other, this can result in a single wave of elevation, called a solitary wave, which propagates at a constant amplitude-dependent speed, without change in shape. The relative importance of nonlinearity and dispersion can be measured if we introduce two independent non-dimensional parameters: the nonlinearity ratio $\mathfrak{a} = \frac{a}{h_1}$ where a

in the wave amplitude and h_1 is the thickness of the fluid layer, and the aspect ratio $\varepsilon = \frac{h_1}{l}$, ratio of the layer thickness to the typical wavelength l. The balance when a solitary wave arises is usually taken to be a scaling relation between $\mathfrak{a}$ and ε for values $\mathfrak{a} \ll 1$ and $\varepsilon \ll 1$. The regime $\mathfrak{a} \ll 1$ and $\varepsilon \ll 1$ is called a weakly nonlinear regime since in this case, the amplitude of the wave is much smaller than the thickness of the layer.

Nonlinear waves propagating on the surface of fluid of finite or infinite depth have been studied extensively. Gravity waves were studied by Stokes [85], Schwartz [80] and Longuet-Higgings [59] and exact solutions for capillary waves were found by Crapper [26] for the case of fluid of infinite depth and Kinnersley [50] for fluid of finite depth. Gravity-capillary waves in irrotational fluid were considered by Schwartz and Vanden-Broeck [81], Chen and Saffman [20, 21], Hogan [39] and Hunter and Vanden-Broeck [43]. When vorticity is also present, calculations for gravity-capillary waves can be found in Kang and Vanden-Broeck [48] and references therein.

Of course, most physical processes (particularly those with environmental applications) occur when the density of the fluid does not remain constant throughout the layer, but has some variation with the height of the layer. Although most of the density stratifications which take place in nature are continuous, it is reasonable to use the two-layer fluid model with a density discontinuity, due to its simplicity and the fact that it gives a good approximation when the interfacial wavelength is sufficiently longer than the length scale of the density variation [87]. The case of waves at the interface of two immiscible fluids of different density brings an additional level of complexity into the wave propagation problem. To see this, let h_2 be the thickness of the lower layer. Then in addition to $\mathfrak{a}$ and ε, one can introduce another independent parameter, the depth ratio $D = \frac{h_1}{h_2}$. The balance between nonlinearity and dispersion can vary according to D even in the weakly nonlinear case. Different regimes are possible depending on the depth ratio. They range between the two extremes, one

of which is when the lower fluid layer is also small compared to the wavelength, and when the lower fluid layer is infinitely deep compared with the upper one.

The shallow water wave regime is characterized by $D = O(1)$ and $\mathfrak{a} = O(\varepsilon^2)$, $\varepsilon \ll 1$. These assumptions lead to the Korteweg-de Vries equation that governs the evolution of the unidirectional weakly nonlinear waves - see Benjamin [10]). Miles [64, 65], Kakutani and Yamasaki [47], Helfrich, Melville and Miles [37] study the internal waves at the interface of two fluids with applications to oceanography. The central interest of the above investigators is the weakly nonlinear evolution of traveling waves over varying topography. Surface tension is usually excluded and the evolution equations are of Korteweg-de Vries type. Rosales and Papanicolaou [76] derived fairly general Korteweg-de Vries evolution equations for gravity waves in a channel with a rough bottom, the roughness being both rapidly varying periodic and (small amplitude) random.

Another case is when the depth of the lower layer is much larger than that of the upper layer ($D \gg 1$) and $\mathfrak{a} = O(\varepsilon)$. This limit leads to the Intermediate Long Wave equation studied by Joseph [46] and Kubota, Ko & Dobbs [54]. In the limit as $D \to \infty$, this equation reduces to the Benjamin-Ono equation (Benjamin [11], Davis & Acrivos [29], Ono [70]). Matsuno [62] and Choi & Camassa [22] derived more general equations valid for arbitrary D using the weakly nonlinear assumption.

Gravity waves in the case of two fluids have been modelled by Liska, Margolin and Wendroff [57], and Choi and Camassa [23] among others. In particular, the latter study contains the Kortweg-de Vries and Intermediate Long Wave equations as special cases. The effect of a Kelvin-Helmholtz instability when a second fluid is introduced, is likely to render these results unstable to short waves, and such effects were excluded from the above studies.

The common feature of the models briefly described above, is the presence of small parameters like $\mathfrak{a}$ and ε that allow us to eliminate the dependence on

the vertical coordinate, thereby substantially simplifying the problem and making analytical progress possible. For these approximations to the original Euler equations to be practically useful, however, they have to be accurate even when the parameters $\mathfrak{a}$ and ε, for example, take moderate values rather than the asymptotically small ones assumed in the derivations, since this can ensure some compensation for other neglected physical effects like viscosity, for instance. Experiments conducted by Koop & Butler [51], however, reveal that just when these weakly nonlinear models give a good approximation to the Euler equations, the effects of viscosity become important and compete with nonlinearity and dispersion, thus possibly making these models of limited validity. Experimental data collected by these authors provide evidence that the weak nonlinearity (small amplitude) assumption may be inadequate to describe their experiments, at least.

Despite their physical relevance, the effects of finite amplitude have been investigated significantly less than weakly nonlinear models. The challenge is to have fully nonlinear models comparable in simplicity to weakly nonlinear ones and at the same time have the potential to capture and describe accurately finite-amplitude dynamical effects. One of our motivations in this study, is to derive asymptotically fully nonlinear models that contain several competing physical effects (nonlinearity, shear instability, density stratification and surface tension). Ultimately, we study these models analytically and computationally in order to gain a quantitative understanding of such flows.

Another interesting problem that arises in the study of an interface between two fluids of different density is the problem of nonlinear stability. When the heavier fluid lies above the lighter one, the interface may be subject to Rayleigh-Taylor instability due to the destabilizing force of gravity (Taylor [88]). This results in the characteristic "spike-bubble"interfacial shape pattern as the interface amplitude grows with time. For this reason, this kind of instability is sometimes called the *fingering instability*.

Taylor recognized that all such types of problem are equivalent to those where the net acceleration is directed from the lighter fluid towards the heavier one. This instability can be observed by rapidly accelerating a glass of water downwards, for example. Let us denote the density in the upper layer by ρ_1 and density in the lower one by ρ_2 (we are assuming that a given continuous density distribution can be replaced by a piecewise smooth distribution - see discussion above). We also introduce the density ratio $\rho = \frac{\rho_1}{\rho_2}$ and the Atwood ratio $\alpha = \frac{1-\rho}{1+\rho}$. The Rayleigh-Taylor mode has $\alpha < 0$ since the heavier fluid lies above the lighter one, then. When the lighter fluid is above the heavier one, i.e., $\alpha > 0$, the configuration is statically stable, but once there is a difference in velocities across the interface, i.e., the tangential velocity has a jump discontinuity, an inertially induced Kelvin-Helmholtz instability can be generated (Kelvin [49]) giving another classical example of hydrodynamic instability. The Kelvin-Helmholtz instability is a fundamental instability of incompressible fluid flow at high Reynolds number. A vortex sheet separating the regions of potential flow has been often used as an idealization of a shear layered flow in studies of mixing properties, boundary layers and coherent structures in fluids. In the case when surface tension is absent and the two fluids are both incompressible and inviscid, the linear stability analysis for both of these instability modes, predicts that as the wavelength decreases, the growth rate of disturbances increases without any bound. In this case, the vortex sheet problem is ill-posed. Moreover, nonlinear interaction of high frequency modes can lead to the formation of a singularity in a finite time.

In real fluids, interfacial surface tension and viscosity regularize this behavior. Chandrasekhar [19] deduced that for the inviscid Kelvin-Helmholtz mode, the surface tension acts to inhibit the onset of linearized instability at all wavelengths for a value of the velocity difference not exceeding a certain critical value. Greater velocity differences are unstable but only for wavelengths above a certain minimum value that depends on the velocity difference as well as fluid properties.

There is a fair number of experiments which address the Kelvin-Helmholtz instability in a bounded two fluid system in a channel. Among them are experiments by Thorpe [89, 89], and a photograph from [89] is also contained in "An Album of Fluid Motion" by Van Dyke [91], photo 145, p. 85. This experiment on stratified shear flow is presented in Figure 1.1 reveals that an initial sinusoidal perturbation of the interface occurs after a few seconds and grows nonlinearly into regular spiral rolls. The phenomenon of roll-up is highly nonlinear and is related to several aspects of the vortex sheet problem as we discuss later.

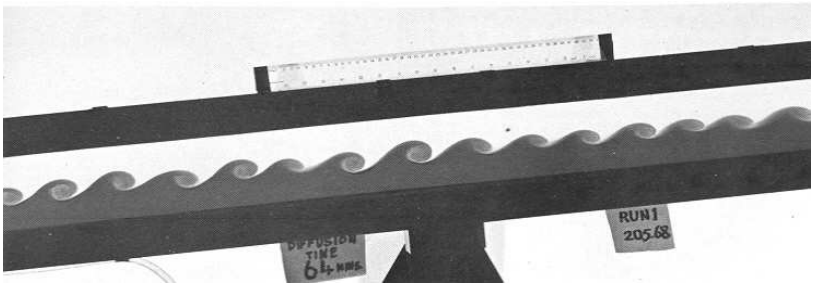

Figure 1.1 Kelvin-Helmholtz instability of stratified shear flow. Taken from Van Dyke's album [91], photo 145, p. 85.

Another photo from the experiment on the Kelvin-Helmholtz instability of superposed streams by Roberts, Dimotakis & Roshko (presented in Van Dyke's album [91], photo 146, p. 85) is shown in Figure 1.2. In both photos, the upper layer moves faster then the lower one. In the left photograph (Figure 1.2 (a)), the faster stream is perturbed sinusoidally at the most unstable frequency, and at half that frequency in the right (Figure 1.2 (b)). The motion the latter case produces an evolution which locks into the subharmonic mode.

The study of interfacial stability problems beyond the range of linear theory, as well as nonlinear free-surface wave behavior required the development of various numerical methods. The time-dependent Navier-Stokes equations were numerically integrated by Harlow & Welch [36], Daly [27, 28], Hirt, Cook & Butler [38] in their analysis of Rayleigh-Taylor instability. Daly [28] also investigated the effect of surface

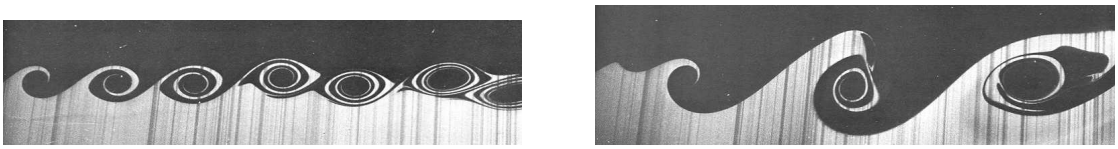

Figure 1.2 Kelvin-Helmholtz instability of superposed streams. Taken from Van Dyke's album [91], photo 146, p. 85. (a) Perturbation at most unstable mode; (b) at half that frequency.

tension on the late-time formation of a heavy-fluid spike for cylindrical geometry. In the case when the two fluids may be assumed to be irrotational, Kelvin's Circulation Theorem guarantees that the vorticity will be confined to the interface for all times. Hence, the interface may be regarded as a generalized vortex sheet. (The *classical vortex sheet* model is used for the two-fluid flow of different velocities but the same constant density. The *generalized vortex sheet* means that in addition to different velocities, fluids also have different densities in each layer, i.e. there is a finite density discontinuity across the interface.) Using the above result, Birkhoff [12] formulated the two-dimensional inviscid interfacial motion in terms of variables that describe the shape and circulation distribution of a vortex sheet representing the interface. This approach allowed him to reduce the effective space dimensionality of the problem by one. Birkhoff argued that the nonlinear initial value problem is ill-posed without the smoothing effect of surface tension and/or viscosity because of the unbounded growth rate at decreasing wavelength in the linear stability analysis. Since the presence of the surface tension removes its ill-posedness in the linear theory, Birkhoff suggested that it may likewise do so in the nonlinear case.

For constant-density fluid motions modeling shear-layers, surface tension cannot be included on physical grounds but it may be used as an artificial smoothing method, i.e., as a regularization method. Rosenhead [77] was the first who studied this problem numerically by modeling the vortex sheet by a row of point vortices whose mutually self-induced motion was supposed to approximate the true vortex-sheet motion. Unfortunately, Rosenhead found the vortices exhibited chaotic behavior in

regions where smooth roll-up should be expected. Moore [68] examined in detail the special case of a uniform circular vortex sheet. Combining a spectral analysis of the growing numerical error and an analytical study of the discrete-model behavior, Moore concluded that the mechanism of chaotic motion is indeed a discrete form of Kelvin-Helmholtz instability. Fink & Soh [31] proposed a method of redistributing the vortices at each time step that eliminated the error. Longuet-Higgins & Cokelet [60] used a linear-smoothing technique to suppress a saw-tooth-like instability in related free-surface flows. These methods were effective means of inhibiting the growth of the error.

Generalized vortex-sheet-like formulations of interfacial motion for the case of a finite-density discontinuity, have been developed by several authors. Among them is the paper by Zaroodny & Greenberg [93] where the authors studied the free-surface wave without inclusion of the surface tension term. Zalosh [92] includes surface tension in a vortex-type treatment of interfacial motion. He uses the simple point-vortex model to study Kelvin-Helmholtz instability and finds that for unstable conditions, irregularities develop on the interface profile where some coherent roll-up is expected.

The boundary integral technique is another powerful method for studying the evolution of an interface between incompressible fluids. In the case of inviscid fluids, methods based on the representation of the interface by a dipole or vortex sheet strength have been used to study Rayleigh-Taylor instability (Baker, Meiron & Orszag [4], Pullin [73], Tryggvason [90]), the motion of water waves and internal waves (Baker, Meiron & Orszag [6], Beale, Hou & Lowengrub [9, 8], [41], Pullin [73], Rangel & Sirignano [74], Roberts [75], Baker & Nachbin [5]). Although there are some differences in these methods, they all use markers to represent the interface, and simple approximations to the boundary integrals that are used to determine the

velocity of the markers. Bernoulli's equation, or some version of it, is used to update the velocity potential, dipole strength or the vortex sheet along the interface.

For flows when the upper fluid is absent (i.e., the case of an upper liquid with zero density), numerical simulations reveal evidence that the motion is well behaved (Baker, Caflisch & Siegel [3]). However, when the motion of an interface is studied numerically for fluids of nonzero densities, the rapid formation of curvature singularities is observed in the absence of surface tension. The underlying mechanism that causes such singularities to form is the Kelvin-Helmholtz instability (Krasny [53], Shelley [82], Baker, Caflisch & Siegel [3]). As the interface moves, there will be regions where speeds of liquid flow are different on either side of the interface. At a local level these regions are vortex sheets with almost uniform strength. In the absence of stabilizing effects like surface tension or viscosity, these regions develop the nonlinear Kelvin-Helmholtz instability which causes the formation of curvature singularities in finite time.

The singularity formation in two-dimensional vortex sheets has been the subject of intensive study in the last two decades. Early contributions are due to Moore [67] who studied the nonlinear evolution of a vortex sheet with a small initial sinusoidal disturbance of amplitude ε. Moore predicted that near the singularity, the curvature of the vortex sheet is proportianal to $|\Gamma - \Gamma_s|^{-1/2}$, where Γ is the circulation of the sheet measured from a fixed reference point to point s and Γ_s is the position of singularity. Moore's result was based on asymptotic analysis and was confirmed by Meiron, Baker & Orszag [63] who investigated a power series solution in time. Later this result was supported numerically by Krasny [53] and Shelley [82]. Validating rigorously Moore's analysis, Caflisch & Orellana [15] proved the existence for a slightly perturbed vortex sheet up to $t = O(|\ln \varepsilon|)$ for Moore's initial condition. More recently, Cowley, Baker & Tanveer [25] studied in detail the singularity formation on a two-dimensional vortex sheet problem. They showed how the $\frac{3}{2}$ singularity in the vortex sheet is selected at

an early time in the extended complex plane. Authors also obtained an asymptotic description of the sheet shape as the physical singularity forms.

Most studies of two-dimensional vortex sheet problems are performed using a complex variable formulation. However, such formulations cannot naturally be generalized to the three-dimensional case. Ishihara & Kaneda [44, 45] provided some evidence that singularities form on three-dimensional vortex sheets by directly generalizing Moore's analysis to the three-dimensional problem. However, their result does not give a clear description of the singularity structure. Brady & Pullin [13] investigated three-dimensional vortex sheets of cylindrical shape and normal mode initial conditions. They showed that for this special type of initial data, the problem can be reduced exactly to a two-dimensional vortex sheet problem. Recently, Hou and Hu [40] have resolved a long-outstanding open problem on the singularity formation induced by the three-dimensional Kelvin-Helmholtz instability. They found that when viewed in appropriate physical variables and coordinates, the three-dimensional problem is essentially the same as the corresponding two-dimensional problem. These authors investigated an interesting open question about whether the singularity in a three-dimensional vortex sheet first appears as isolated points or along a one-dimensional line segment. They studied the motion of a singularity in the extended complex plane and used analytic continuation to argue that at the time when physical singularities form, they appear either at some isolated points or along entire one-dimensional curves in the plane of real parameters. They showed that the interface cannot develop finite time singularities along a segment of a one-dimensional curve.

The purpose of the present work is to derive two-fluid models when surface tension and gravity are present, and at the same time allowing tangential slip at the interface making it a vortex sheet. The surface tension is a physical regularization of the system and we are concerned, among other aspects, with the construction of

solitary waves for a range of parameters. These solutions along with finite-length waves add gravity and an upper fluid to the study of Kinnersley [50]. No exact solutions are possible in general when gravity is present, but our fully nonlinear long wave model supports a class of solitary waves expressible in terms of elliptic integrals. Some explicit solutions are also found. We are also interested in evaluating our models for singularity formation in the absence of surface tension and presence of a Kelvin-Helmholtz instability, along with the analogous surface tension regularizations of such motions by increasingly larger amounts of regularization. We pursue such studies using numerical methods for both two- and three-dimensional disturbances. In addition, we derive Birkhoff-Rott type equations for vortex sheets in channels. Such models can be used to make theoretical comparisons with available experiments but this is left for future work.

The rest of the thesis is organized as follows. In Chapter 2, we use a long wave approximation to develop a theory for fully nonlinear interfacial waves allowing amplitudes as large as the channel thickness. The result is a set of evolution equations for the interfacial shape and the velocity jump across the interface. Linear stability analysis reveals that capillary forces stabilize short-wave disturbances in a dispersive manner. Traveling waves of permanent form are studied, and it is shown that solitary waves are possible for a range of physical parameters. All solitary waves can be expressed implicitly in terms of incomplete elliptic integrals of the third kind. When the upper layer has zero density, two explicit solitary-wave solutions have been found whose amplitudes are equal to $h/4$ or $h/9$ where $2h$ is the channel thickness. In the absence of gravity, solitary waves are not possible but periodic ones are. Numerically constructed traveling and solitary waves are given for representative physical parameters. The initial value problem for the partial differential equations is also addressed numerically, and the regularizing effect of surface tension is investigated. An explicit pseudo-spectral scheme is used in

numerical analysis. The system of evolution equations has three conserved quantities, corresponding to mass, total circulation and energy. These constants of motion have been used as a check on the accuracy of computational solutions. It is also shown that the system of governing equations terminates in infinite slope singularities. This is achieved by studying a 2×2 system of nonlinear conservation laws in the complex plane and by numerical solution of the evolution equations. This analysis shows that a sinusoidal perturbation of the flat interface and a cosinusoidal perturbation to the unit velocity jump across the interface develop a singularity at time $t_c = \ln \frac{1}{\varepsilon} + O(\ln(\ln \frac{1}{\varepsilon}))$ where ε is the initial amplitude of the disturbances. This result is asymptotic for small ε and is derived by studying the asymptotic form of the flow characteristics in the complex plane.

In Chapter 3, the problem under consideration is generalized to the three-dimensional case, where two fluids with different density and velocities bounded between two infinite horizontal plates are studied. Three-dimensional long-wave model equations are derived by assuming that the wavelengths in the principal horizontal directions are large compared to the channel thickness. Surface tension is again incorporated to regularize short-wave Kelvin-Helmholtz instabilities and the equations are solved numerically subject to periodic boundary conditions. Evidence of singularity formation is found. In particular, we observe that singularities occur at isolated points starting from general initial conditions. This finding is consistent with numerical studies of unbounded three-dimensional vortex sheets, in particular, with the results by Hou & Hu [40]. Integral invariants of motion that correspond to mass, total circulation in the principal horizontal directions, and energy provided a useful accuracy check for the numerics.

Chapter 4 presents the vortex-sheet formulation of the exact nonlinear two-dimensional motion of the interface for the case when the vortex sheet is bounded by the channel walls. The model includes a Birkhoff-Rott type integro-differential

evolution equation for the velocity of the interface in terms of the vorticity as well as the evolution equation for the unnormalized vortex sheet strength. For the case of a spacially periodic vortex sheet, this Birkhoff-Rott type equation is written in terms of Jacobi's functions. The equation is shown to recover the limits of unbounded and non-periodic flows which are known in the literature. Appendix A gives the details of the problem formulation in the three-dimensional case that are used as well for the two-dimensional problem as a partial case. In Appendix B, we derive equation (2.58) that governs the evolution of nonlinear traveling waves. Appendix C contains necessary definitions, relations and properties of Legendre's Elliptic Integrals, Jacobi's Elliptic Functions and Jacobi's Z, Π, Θ and H Functions. Finally, in Appendix D, we present Sohotskij-Plemelj Formulae used in the derivation of a Birkhoff-Rott type integro-differential equation in Section 4.1.

CHAPTER 2

TWO-DIMENSIONAL NONLINEAR WAVES

2.1 Problem Formulation

We consider a system of two immiscible fluid streams each with a different constant density and different velocity, one stream above the other. The fluids are assumed to be inviscid, incompressible, and the motion irrotational. The fluids are of infinite horizontal extent and they are bounded in a channel with straight, horizontal parallel walls. We are interested in the evolution of interfacial waves when both gravity and surface tension act. The unperturbed depth of each layer is initially h. Denote upper and lower fluid quantities by subscripts 1 and 2, respectively, with corresponding densities ρ_1 and ρ_2. Using Cartesian coordinates, the undisturbed interface is at $y = 0$ and at subsequent times it is given by $y = S(x,t)$, where x is the horizontal coordinate and t is time. Throughout the thesis, both top and the bottom boundaries are assumed to be rigid, so that problems such as the interaction between surface waves and interfacial waves do not arise. The configuration is schematically shown in Figure 2.1.

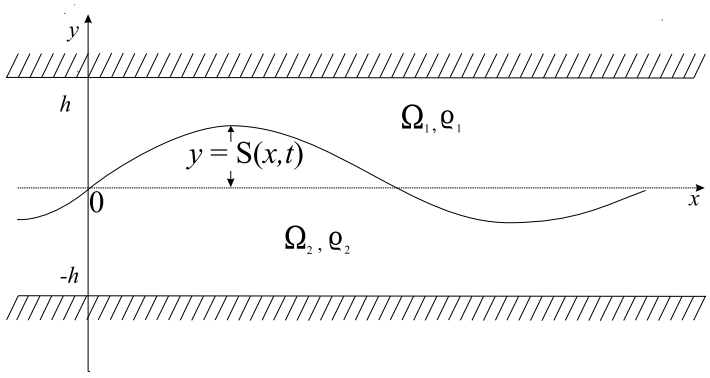

Figure 2.1 The configuration of the problem.

The flow is taken to be irrotational away from the interface (in what follows we allow the interface to be a vortex sheet). Under these assumptions, the motion of

the upper fluid can be expressed in terms of the velocity potential $\phi_1(x, y, t)$, and the lower in terms of $\phi_2(x, y, t)$. These potentials are governed by the Laplace equations

$$\phi_{ixx} + \phi_{iyy} = 0 \quad \text{in} \quad \Omega_i, \tag{2.1}$$

subject to the following boundary conditions

$$\phi_{iy} = 0 \quad \text{at} \quad y = \pm h, \tag{2.2}$$

$$S_t + \phi_{ix} S_x = \phi_{iy} \quad \text{on} \quad y = S, \tag{2.3}$$

$$\begin{aligned} \rho_2 \phi_{2t} \quad &+ \quad \frac{1}{2}\rho_2 \left[(\phi_{2x})^2 + (\phi_{2y})^2\right] + (\rho_2 - \rho_1) g S \\ &- \quad \rho_1 \phi_{1t} - \frac{1}{2}\rho_1 \left[(\phi_{1x})^2 + (\phi_{1y})^2\right] = p_1 - p_2 \quad \text{on} \quad y = S, \end{aligned} \tag{2.4}$$

where $i = 1, 2$; the subscripts x, y, and t mean partial differentiations with respect to x, y, and t, respectively. The boundary conditions (2.2)-(2.4) represent zero normal flow (impermeability) at solid walls, the kinematic constraint, and the Bernoulli equation at the interface derivable by starting from the Euler equations and using the velocity potentials ϕ_i, $i = 1, 2$. These conditions are derived from the Navier-Stokes model in Appendix A. The pressure difference across the interface is due to surface tension and is directly proportional to the curvature of S. Note that if the flow is undisturbed far away, and there is an underlying horizontal velocity $V^{\pm}(t)$ in each layer, then an appropriate function of t must be added to (2.4). This is removed when (2.4) is differentiated with respect to x; the underlying flow is important, however, because it provides linear instability through the Kelvin-Helmholtz mechanism, and ill-posedness of the nonlinear problem, at least in the absence of surface tension.

The pressure difference across the interface balances surface tension forces by the normal stress condition, giving the pressure jump

$$p_1 - p_2 = \sigma_0 \frac{S_{xx}}{(1 + \varepsilon^2 S_x^2)^{\frac{3}{2}}}, \tag{2.5}$$

where σ_0 is the surface tension coefficient.

Assuming l to be a typical horizontal length scale (e.g., a wavelength), and c_0 to be a typical velocity (e.g., a wavespeed given by linear theory if the waves are dispersive, or a typical underlying velocity in the case of Kelvin-Helmholtz flow), the problem is made dimensionless by introducing the following variables (superscripts * denote dimensionless quantities and are subsequently dropped from the resulting equations):

$$x^* = \frac{x}{l}, \quad y^* = \frac{y}{h}, \quad t^* = \frac{c_0}{2l}t, \quad S^* = \frac{S}{h}, \quad \phi_i^* = \frac{\phi_i}{c_0 l}, \quad p_i^* = \frac{2}{\rho_2 c_0^2}p_i. \tag{2.6}$$

The coefficient $\frac{1}{2}$ in the scaling for time t^* is introduced to remove coefficient $\frac{1}{2}$ in the Bernoulli equation (2.4). The dimensionless system to be addressed becomes

$$\varepsilon^2\phi_{ixx} + \phi_{iyy} = 0 \quad \text{in} \quad \Omega_i, \tag{2.7}$$

$$\phi_{iy} = 0 \quad \text{on} \quad y = \pm 1, \tag{2.8}$$

$$\varepsilon^2\left(\frac{1}{2}S_t + \phi_{ix}S_x\right) = \phi_{iy} \quad \text{on} \quad y = S, \tag{2.9}$$

$$\begin{aligned}\phi_{2t} \quad &+ \quad \left[(\phi_{2x})^2 + \frac{1}{\varepsilon^2}\left(\phi_{2y}\right)^2\right] + \frac{1}{F}(1-\rho)S \\ &- \quad \rho\phi_{1t} - \rho\left[(\phi_{1x})^2 + \frac{1}{\varepsilon^2}\left(\phi_{1y}\right)^2\right] = \tilde{\sigma}\varepsilon\frac{S_{xx}}{(1+\varepsilon^2 S_x^2)^{\frac{3}{2}}} \quad \text{on} \quad y = S\end{aligned} \tag{2.10}$$

where the dimensionless parameters

$$\varepsilon = \frac{h}{l}, \quad \rho = \frac{\rho_1}{\rho_2}, \quad F = \frac{c_0^2}{2gh}, \quad \tilde{\sigma} = \frac{2\sigma_0}{l\rho_2 c_0^2}, \tag{2.11}$$

are a shallowness parameter, density ratio, Froude number and a surface tension parameter. The right-hand side of (2.10) is the contribution to the pressure jump across the interface due to surface tension. The Froude number F measures the importance of inertial forces to gravitational forces, whereas the surface tension parameter $\tilde{\sigma}$ is proportional to the ratio of surface tension to inertial forces. Note that

$\tilde{\sigma}$ is inversely proportional to the Weber number We, and is large when surface tension is large. The Weber number measures the importance of inertial forces relative to the dispersive forces of surface tension forces.

In what follows, canonical equations are derived in the limit $\varepsilon \to 0$ with both gravity and surface tension retained. In the long-wave analysis, the curvature of the interface is small relative to its amplitude, and in order to allow for surface tension effects to enter and compete with gravity, the distinguished limit,

$$\tilde{\sigma} = \frac{\sigma}{\varepsilon} \tag{2.12}$$

is considered, with σ an order one parameter. Using this, equation (2.10) becomes

$$\varepsilon^2 \left[\phi_{2t} - \rho\phi_{1t} + (\phi_{2x})^2 - \rho(\phi_{1x})^2\right] + (\phi_{2y})^2 - \rho(\phi_{1y})^2 + \frac{\varepsilon^2}{F}(1-\rho)S$$
$$= \frac{\sigma\varepsilon^2 S_{xx}}{(1+\varepsilon^2 S_x^2)^{3/2}} \quad \text{on} \quad y = S. \tag{2.13}$$

The problem stated above is exact and results from the chosen non-dimensionalization; for example, setting $\varepsilon = 1$, (2.7)-(2.9), (2.13) are the equations for a non-slender two-fluid system in a channel. In what follows we study strongly nonlinear solutions valid in the limit $\varepsilon \to 0$.

2.2 Derivation of the Nonlinear Evolution Equations

In the limit $\varepsilon \to 0$, the only small parameter appearing in the governing equations (2.7)-(2.9), (2.13) is ε^2 and we assume the following asymptotic expansions,

$$S = S^{(0)} + \varepsilon^2 S^{(1)} + \varepsilon^4 S^{(2)} + \ldots, \tag{2.14}$$

$$\phi_i = \phi_i^{(0)} + \varepsilon^2 \phi_i^{(1)} + \varepsilon^4 \phi_i^{(2)} + \ldots, \quad i = 1, 2. \tag{2.15}$$

When (2.14) and (2.15) are substituted into (2.7)-(2.9) and (2.13) and successive orders of ε^2 are equated, the following problems emerge:

$$\phi_{iyy}^{(j)} = a_i^{(j)}(x, y, t) \quad \text{in} \quad \Omega_i, \tag{2.16}$$

$$\phi_{i_y}^{(j)} = 0 \quad \text{at} \quad y = \pm 1, \tag{2.17}$$

$$\phi_{i_y}^{(j)} = c_i^{(j)}(x, y, t) \quad \text{at} \quad y = S^{(0)}(x, t), \tag{2.18}$$

where $j = 0, 1, 2, \ldots$. The functions $a_i^{(j)}$ and $c_i^{(j)}$ force the linear operators on the left-hand side and contain information from the previous stage $j-1$, $j = 1, 2, \ldots$. The first few of these functions are

$$a_i^{(0)} = 0, \quad a_i^{(j)}(x, y, t) = -\phi_{i_{xx}}^{(j-1)}, \quad j = 1, 2, \ldots, \tag{2.19}$$

$$c_i^{(0)} = 0, \quad c_i^{(1)} = \frac{1}{2} S_t^{(0)} + S_x^{(0)} \phi_{i_x}^{(0)}, \tag{2.20}$$

$$c_i^{(2)} = \frac{1}{2} S_t^{(1)} + S_x^{(1)} \phi_{i_x}^{(0)} + S_x^{(0)} \phi_{i_x}^{(1)} + S^{(1)} \phi_{i_{xx}}^{(0)}, \tag{2.21}$$

where the potential functions and their derivatives in equations (2.20) and (2.21) are evaluated at $(x, y) = (x, S^{(0)}(x, t))$. For each j the problem is a linear boundary value one, which has a solution (unique up to a constant) if and only if the following compatibility condition is satisfied (see [76] for a situation involving elliptic operators on the left):

$$\langle a_1^{(j)} \rangle = \int_0^1 dx \int_{S^{(0)}}^1 a_1^{(j)}(x, y, t) dy = -\int_0^1 c_1^{(j)}(x, t) dx, \tag{2.22}$$

$$\langle a_2^{(j)} \rangle = \int_0^1 dx \int_{-1}^{S^{(0)}} a_2^{(j)}(x, y, t) dy = \int_0^1 c_2^{(j)}(x, t) dx. \tag{2.23}$$

The above conditions assume (without loss of generality) periodic solutions with period one in the x-direction. The leading order problem can be easily solved to give solutions that are independent of y

$$\phi_1^{(0)} = \Phi_1(x, t) \quad \text{in} \quad \Omega_1 \quad \text{and} \quad \phi_2^{(0)} = \Phi_2(x, t) \quad \text{in} \quad \Omega_2. \tag{2.24}$$

At the next order $j = 1$, the kinematic condition (2.18) together with solutions (2.24) gives

$$\frac{1}{2} S_t^{(0)} + \Phi_{i_x} S_x^{(0)} = \phi_{i_y}^{(1)}. \tag{2.25}$$

Since $\phi_{i_{yy}}^{(1)} = -\phi_{i_{xx}}^{(0)} = -\Phi_{ixx}$ from (2.16) and (2.24), and $\phi_{i_y}^{(1)} = 0$ at $y = \pm 1$ from (2.17), it follows that

$$\phi_{1_y}^{(1)} = (1-y)\Phi_{1xx} \quad \text{and} \quad \phi_{2_y}^{(1)} = -(1+y)\Phi_{2xx}. \tag{2.26}$$

Using expressions for $\phi_{1_y}^{(1)}$ and $\phi_{2_y}^{(1)}$ from (2.26) in the kinematic condition (2.25) yields

$$\frac{1}{2}S_t^{(0)} + \Big((S^{(0)} - 1)\Phi_{1x}\Big)_x = 0, \tag{2.27}$$

$$\frac{1}{2}S_t^{(0)} + \Big((S^{(0)} + 1)\Phi_{2x}\Big)_x = 0. \tag{2.28}$$

The Bernoulli equation (2.13) is satisfied identically at order ε^0, and at order ε^2 yields,

$$\Phi_{2t} - \rho\Phi_{1t} + (\Phi_{2x})^2 - \rho(\Phi_{1x})^2 + \frac{1-\rho}{F}S^{(0)} = \sigma S_{xx}^{(0)}. \tag{2.29}$$

Equations (2.27)-(2.29) are three equations for the three unknown functions Φ_1, Φ_2 and $S^{(0)}$. They can be reduced to a set of two coupled nonlinear partial differential equations by defining new variables Φ and V by

$$\Phi = \frac{1}{2}(\Phi_1 + \Phi_2), \quad V = \frac{1}{2}(\Phi_1 - \Phi_2). \tag{2.30}$$

Addition and subtraction of (2.28) and (2.27) and integration with respect to x in the latter instance gives

$$S_t^{(0)} + 2(\Phi_x S^{(0)} - V_x)_x = 0, \tag{2.31}$$

$$\Phi_x = S^{(0)}V_x + \chi(t), \tag{2.32}$$

where the function $\chi(t)$ is a result of the x integration. The value of $\chi(t)$ can be found by considering the unperturbed flow at large $|x|$. Assuming that far away the interface is flat, gives $S^{(0)}(\pm\infty, t) = 0$; Φ_x is the average of the undisturbed fluid velocities in the two layers and if the fluids are at rest far away, it follows that $\chi(t) = 0$. The

general case has $\Phi_x \neq 0$ and thus $\chi \equiv \chi(t)$. The case $\chi = const.$ corresponds to uniform inviscid streams while any time oscillatory far fields, for example, give rise to a time dependence. Substitution of (2.32) into (2.31) eliminates Φ and yields the equation

$$S_t^{(0)} + 2\chi S_x^{(0)} + 2\left({S^{(0)}}^2 V_x\right)_x = 2V_{xx}.$$

A second equation is obtained by differentiation of (2.29) with respect to x and elimination of Φ_i, $i = 1, 2$, in terms of the new variables (2.30), and with subsequent elimination of Φ using (2.32). The evolution equations become

$$S_t + 2\chi S_x + 2(S^2 W)_x = 2W_x, \tag{2.33}$$

$$(W - \alpha SW)_t + 2\chi(W - \alpha SW)_x - (\alpha S^2 W^2 - 2SW^2 + \alpha W^2)_x$$

$$= \frac{\alpha}{F} S_x - \frac{\sigma}{1+\rho} S_{xxx}, \tag{2.34}$$

where $W = V_x$, and the superscript zero has been dropped from $S^{(0)}$. Changing to the inertial frame

$$(x, t) \rightarrow \left(x - 2\int^t \chi(t')dt', t\right),$$

is seen to remove χ from the problem. The parameter α is the *Atwood ratio* defined by

$$\alpha = \frac{1-\rho}{1+\rho},$$

and $-1 \leq \alpha \leq 1$. Denote the coefficient of S_{xxx} as

$$\gamma = \frac{\sigma}{1+\rho}. \tag{2.35}$$

Therefore, the resulting evolution equations are

$$S_t + 2(S^2 W)_x = 2W_x, \tag{2.36}$$

$$(W - \alpha SW)_t - (\alpha S^2 W^2 - 2SW^2 + \alpha W^2)_x = \frac{\alpha}{F} S_x - \gamma S_{xxx}. \tag{2.37}$$

In what follows, then, we study equations (2.36) and (2.37). When α is positive/negative the heavier fluid is on the bottom/top; the latter case introduces a Rayleigh-Taylor instability into the problem. The case $\alpha = 0$ is that of density matched fluids. The system (2.36), (2.37) contains various physical mechanisms of interest including a Kelvin-Helmholtz instability and its modification due to surface tension and/or gravity.

The case $\alpha = 1$ that corresponds to the upper fluid having zero density ($\rho_1 = 0 \Rightarrow \rho = 0 \Rightarrow \alpha = 1$) is particularly interesting because it yields closed form solitary waves (see Section 2.5). Setting $\alpha = 1$ in (2.37) and defining a new dependent variable by $U = (1 - S)W$, casts the system (2.36), (2.37) into the simpler form

$$S_t - 2\left(U(1 + S)\right)_x = 0, \qquad U_t - (U^2)_x = \frac{1}{F} S_x - \sigma S_{xxx}. \tag{2.38}$$

In view of the fact that explicit solitary waves exist, it would be interesting to study the system (2.38) for complete integrability.

2.3 Integral Invariants of the Motion

There exists several integral properties of the flow which remain invariant with time whatever is the motion of the interface S. These quantities can be monitored in a computational solution of equations (2.36) and (2.37) as a check on its accuracy.

The following integrals, corresponding to mass, total circulation and energy, are conserved quantities of the system

$$\mathcal{I}_1 = \int S dx, \quad \mathcal{I}_2 = \int (W - \alpha SW) dx, \tag{2.39}$$

$$\mathcal{I}_3 = \int \left[\frac{1}{2} W^2 (1 - \alpha S)(1 - S^2) - \frac{\alpha}{4F}(1 - S^2) + \frac{\gamma}{4} S_x^2 \right] dx. \tag{2.40}$$

The energy integral is derived by starting from the exact energy of the system and applying the perturbation scheme of Section 2.2. It is easy to check *a posteriori* that equation (2.34) follows from $\mathcal{I}_3$. The details of the derivation follow next.

2.3.1 Conservation of Mass

Considerations of overall mass conservation show that the mass per wavelength remains invariant. We use the dimensional notation of Section 2.1. At time t, consider two strips Ω_1 and Ω_2 of the upper and lower fluids, respectively, each of x-dimension equal to one wavelength l and of average y-dimension h as shown in Figure 2.2.

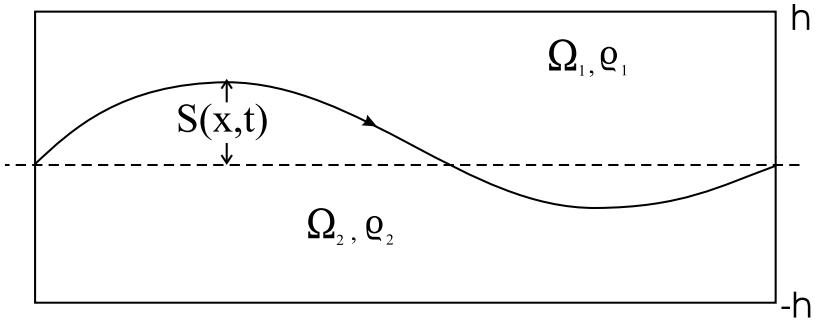

Figure 2.2 Regions Ω_1 and Ω_2 for determining mass and energy.

The total mass of the fluid instantaneously in Ω_1 and Ω_2 is

$$M = \rho_1 \int_S^h \int_0^l dxdy + \rho_2 \int_{-h}^S \int_0^l dxdy.$$

Changing to dimensionless variables by using (2.6) and then subsequently dropping the superscript $*$, we obtain

$$M = \rho_2 lh \left\{ \frac{\rho_1}{\rho_2} \int_S^1 \int_0^1 dxdy + \int_{-1}^S \int_0^1 dxdy \right\}.$$

Integrating with respect to y and using the density ratio $\rho = \frac{\rho_1}{\rho_2}$, we can write

$$M = \rho_2 lh \int_0^1 \{\rho(1-S) + (S+1)\}\, dx = \rho_2 lh \int_0^1 \{(\rho+1)$$

$$+(1-\rho)S\}\, dx = \rho_2 lh(1+\rho) \int_0^1 (1+\alpha S)dx,$$

where we used the definition of Atwood ratio $\alpha = \frac{1-\rho}{1-\rho}$. Then the dimensionless mass is

$$\tilde{M} = \frac{M}{\rho_2 lh} = (1+\rho) \int_0^1 (1+\alpha S)dx$$

and this quantity is conserved. Then

$$M_0 \equiv \frac{\tilde{M}}{1+\rho} = \int_0^1 (1+\alpha S)dx = 1 + \alpha \int_0^1 S(x,t)dx = const.$$

Therefore, the integral

$$\int_0^1 S(x,t)dx = \mathcal{I}_1$$

is the first constant of motion.

The same result may be obtained if we note that equation (2.36) may be written in the conservation law form

$$S_t + \left[2(S^2-1)W\right]_x = 0,$$

and hence S is the *conserved density*, and $-2(S^2-1)W$, the *flux* of S. Since we assume periodicity of S and W, it follows that

$$\mathcal{I}_1 = \int_0^1 S(x,t)dx$$

is the constant of motion [66].

2.3.2 Total Circulation Conservation

Let us write equation (2.37) in the conservative form, i.e.

$$[(1-\alpha S)W]_t + \left[\frac{\sigma}{1+\rho}S_{xx} - \frac{\alpha}{F}S - (\alpha S^2 - 2S + \alpha)W^2\right]_x = 0.$$

By the above reasonings, we conclude that

$$\mathcal{I}_2 = \int_0^1 (1-\alpha S)W dx \tag{2.41}$$

is the second constant of motion.

Let us analyze the above conserved quantity. For this purpose consider the expression under the integral sign in (2.41) using definitions of α, ρ and W.

$$(1-\alpha S)W = W - \frac{1-\rho}{1+\rho}SW = \frac{1}{1+\rho}\left\{(1+\rho)W - (1-\rho)SW\right\}$$

$$= \frac{1}{1+\rho}\left\{W + \rho W - SW + \rho SW\right\} = \frac{1}{1+\rho}\left\{W(1-S) + \rho W(1+S)\right\}$$

$$= \frac{1}{1+\rho}\left\{\int_S^1 W dy + \rho \int_{-1}^S W dy\right\} = \frac{1}{1+\rho}\frac{1}{\rho_2}\left\{\rho_2 \int_S^1 W dy + \rho_1 \int_{-1}^S W dy\right\}$$

$$= \frac{1}{(1+\rho)\rho_2}\left\{\rho_2 \int_S^1 V_x dy + \rho_1 \int_{-1}^S V_x dy\right\}.$$

Therefore, equation (2.41) may be written as

$$\mathcal{I}_2 = \frac{1}{(1+\rho)\rho_2}\left[\int_0^1 \int_S^1 \rho_2 V_x dx dy + \int_0^1 \int_{-1}^S \rho_1 V_x dx dy\right] \tag{2.42}$$

where $V = \frac{1}{2}(\Phi_1 - \Phi_2)$ and V_x is the leading order component of the velocity jump across the interface or the vortex sheet strength. Therefore, the conserved quantity in (2.41) is the total amount of circulation of vorticity or the circulation of the vortex sheet in one periodic cell. The total circulation may be obtained by changing from the double integral in (2.42) to the line integral along the interface using Green's theorem. Due to the long wave approximation used to derive our modeling equations, $\frac{\partial}{\partial s} \sim \frac{\partial}{\partial x}$ in the dimensional variables, where s is the arc length, that justifies the physical meaning of the constant of motion $\mathcal{I}_2$. The total circulation is conserved since we assumed flows to be irrotational.

2.3.3 Conservation of Energy

Strictly speaking, the total energy for two-dimensional stratified flow is infinite. However, the perturbation energy of the disturbed flow away for a steady-state value, evaluated over one spatial period of the flow, is finite and conserved [6]. The dimensional notation of Section 2.1 is used to obtain the total energy of the system at a given time. The energy of the motion has three components, namely (i) the kinetic energy, (ii) the potential energy, and (iii) the interfacial surface energy associated with work done against surface tension in deforming the interface S. The datum line for potential and interfacial surface energy is taken at $y = 0$. Without loss of

generality we assume the flow to be periodic with period l. Then the total energy per unit width of the channel and in a single periodic cell is

$$\begin{aligned} E &= \frac{1}{2}\rho_1 \int_0^l \int_S^h ((\phi_{1x})^2 + (\phi_{1y})^2) dxdy + \frac{1}{2}\rho_2 \int_0^l \int_{-h}^S ((\phi_{2x})^2 + (\phi_{2y})^2) dxdy \\ &+ \rho_1 g \int_0^l \int_S^h y dy dx + \rho_2 g \int_0^l \int_{-h}^S y dy dx + \sigma_0 \int_0^l (1 + S_x^2)^{1/2} dx. \end{aligned} \tag{2.43}$$

The non-dimensionalization (2.6) in (2.43) (where we subsequently drop the superscript $*$) yields

$$\begin{aligned} E &= \frac{1}{2}\rho \int_0^1 \int_S^1 ((\phi_{1x})^2 + \frac{1}{\varepsilon^2}(\phi_{1y})^2) dxdy + \frac{1}{2} \int_0^1 \int_{-1}^S ((\phi_{2x})^2 + \frac{1}{\varepsilon^2}(\phi_{2y})^2) dxdy \\ &+ \frac{1}{4F}(\rho - 1) \int_0^1 (1 - S^2) dx + \frac{\tilde{\sigma}}{2\varepsilon} \int_0^1 (1 + \varepsilon^2 S_x^2)^{1/2} dx. \end{aligned} \tag{2.44}$$

Equation (2.44) is exact since it is the result of a change of variables alone. The long wave approximation of interest is achieved through the ansatz (2.14), (2.15) and the corresponding leading order solutions (2.24). This yields the functional

$$\begin{aligned} E &= \frac{1}{2}\rho \int_0^1 \int_S^1 (\Phi_{1x})^2 dxdy + \frac{1}{2} \int_0^1 \int_{-1}^S (\Phi_{2x})^2 dxdy \\ &+ \frac{1}{4F}(\rho - 1) \int_0^1 (1 - S^2) dx + \frac{\tilde{\sigma}}{2\varepsilon} \left(1 + \frac{1}{2}\varepsilon^2 \int_0^1 S_x^2 dx\right). \end{aligned} \tag{2.45}$$

It follows from (2.45) that strong surface tension of order ε^{-1} is required to compete with inertial and gravity terms, an observation already established in Section 2.1. Use of (2.12) along with the solutions (2.30), (2.32) with $\chi(t) = 0$ recasts (2.45) into

$$E_0 = \int_0^1 \left(\frac{1}{2}W^2(1 - \alpha S)(1 - S^2) - \frac{\alpha}{4F}(1 - S^2) + \frac{\gamma}{4}S_x^2\right) dx, \tag{2.46}$$

where E_0 is a constant since energy is conserved at each level of the expansion.

The expression (2.46) is a conserved quantity for the system. Finally we show that this is consistent with the governing equations (2.36) and (2.37). Differentiation of (2.46) with respect to t and elimination of S_t and W_t from (2.36), (2.37) yields

$$\begin{aligned} &\int_0^1 \frac{\partial}{\partial x} \Big(W(1 - S^2)W^2(\alpha - 2S + \alpha S^2) + \frac{\alpha}{F} WS(1 - S^2) \\ &- \gamma \left\{W(1 - S^2)S_{xx} - S_x[(1 - S^2)W]_x\right\}\Big) dx = 0. \end{aligned} \tag{2.47}$$

Clearly the integral is zero since the integrand is a derivative and consistency with the evolution equations is verified.

2.4 Linear Stability Properties of the Evolution Equations

Consider next the evolution of infinitesimal wavy disturbances at the interface according to the model (2.36), (2.37). Writing $S = \delta\tilde{S}(x,t)$ and $W = W_0 + \delta\tilde{W}(x,t)$ for infinitesimally small δ, yields the linear equation

$$\tilde{W}_{tt} - 4\alpha W_0 \tilde{W}_{xt} + \left(4W_0^2 - \frac{2\alpha}{F}\right)\tilde{W}_{xx} + 2\gamma\tilde{W}_{xxxx} = 0, \tag{2.48}$$

where W_0 measures the strength of the underlying vortex sheet flow. Using the method of normal modes, we assume that an arbitrary disturbance is proportional to $\exp(ikx + \omega t)$, i.e.,

$$\tilde{S} = \hat{S}\,\mathrm{e}^{ikx+\omega t}, \quad \tilde{W} = \hat{W}\,\mathrm{e}^{ikx+\omega t},$$

where k is wavenumber, ω is growth rate and $\hat{S}$, $\hat{W}$ are of order 1. This gives the dispersion relation

$$\omega = 2ik\alpha W_0 \pm k\sqrt{2}\left(2W_0^2(1-\alpha^2) - \frac{\alpha}{F} - \gamma k^2\right)^{1/2}. \tag{2.49}$$

Instability occurs when the real part of ω is positive. Surface tension stabilizes short-wave disturbances in a dispersive manner while in its absence, and for $\alpha \neq 1$ (i.e., when an upper layer is present), the nonlinear problem is ill-posed and is expected to encounter a finite-time singularity. For unbounded vortex sheets this has been analyzed by Moore [67, 69] (see also Caflisch and Orellana [15, 16]), and singularity formation was studied numerically by Krasny [53]. We will address the singularity formation problem in Section 2.7 but now we consider the construction of "exact" traveling wave solutions. Guided by the evolution of vortex sheets, we expect that the class of solutions found may emerge from the initial value problem as long as

the dispersion relation (2.49) gives neutrally stable waves or waves with only a small number of active modes. This can be quantified by a stability analysis of the nonlinear traveling waves, and is the subject of current work.

The dispersion relation (2.49) admits stable short waves even in the absence of surface tension, as long as $F \leq \frac{\alpha}{2W_0^2(1-\alpha^2)}$. This balance between Kelvin-Helmholtz instability and stable density stratification is a result of the long wave shallow-water type approximation used to derive the nonlinear system; in fact, the Kelvin-Helmholtz instability dominates at short waves giving growth rates of order k as opposed to the order $k^{1/2}$ that emerge from Rayleigh-Taylor stability or instability (see for example Drazin and Reid [30], p.14).

This apparent discrepancy can be explained by noting that the result (2.49) is the leading order in ε growth rate of the exact linear dispersion relation. This can be found in a routine way starting from (2.7)-(2.9), (2.13), looking for normal modes as above and solving in a channel of dimensionless thickness of 2. The result is

$$\begin{aligned} \omega &= -2ikV_c + 2ik\alpha W_0 \\ &\pm \left(4W_0^2(1-\alpha^2)k^2 - \frac{2k\alpha\tanh(\varepsilon k)}{\varepsilon F} - \frac{2\sigma k^3\tanh(\varepsilon k)}{\varepsilon(1+\rho)}\right)^{1/2}, \end{aligned} \tag{2.50}$$

where $V_c = \frac{1}{2}\left(\Phi_{1_0} + \Phi_{2_0}\right)_x$ is the average of unperturbed velocities in each layer, $W_0 = \frac{1}{2}\left(\Phi_{1_0} - \Phi_{2_0}\right)_x$ is as above, and Φ_{i_0}, $i = 1, 2$, are unperturbed velocity potentials. The relation (2.50) is exact for channels and the limit $\varepsilon \to 0$ recovers the relation (2.49) above once the term containing V_c is removed by a Galilean transformation. We can conclude, therefore, that the short-wave spectrum of the long-wave nonlinear equations gives a more stable behavior than that of the full spectrum. This could be important for solutions that violate the long wave approximation (e.g., infinite slope singularities), but our concern is with waves having sufficiently high surface tension that the flow is either linearly neutrally stable or only has a few unstable modes.

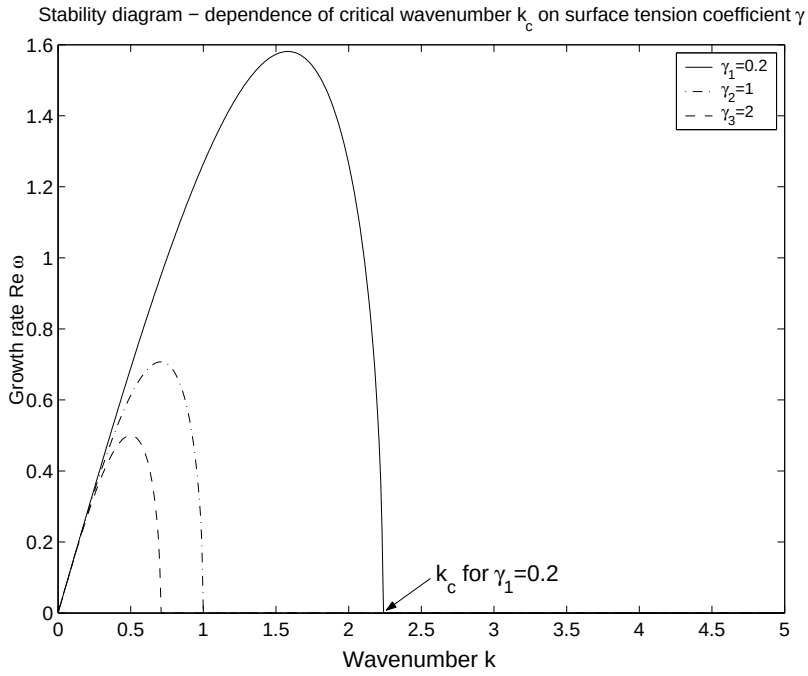

Figure 2.3 Stability diagram — dependence of critical wavenumber k_c on surface tension coefficient γ: $W_0 = 1$, $\alpha = 0.5$, $F = 1$ and $\gamma_1 = 0.2$, $\gamma_2 = 1$, $\gamma_3 = 2$.

According to (2.49) all waves with wavenumbers larger than

$$k_c = \left[\frac{2W_0^2(1-\alpha^2) - \alpha/F}{\gamma}\right]^{1/2},$$

are linearly neutrally stable. The value k_c is called a *critical wavenumber*. Dependence of the growth rate $\mathrm{Re}\,\omega$ on wavenumber k is presented in Figure 2.3 for representative values $W_0 = 1$, $\alpha = 0.5$, $\gamma_1 = 0.2$, $\gamma_2 = 1$, $\gamma_3 = 2$ and $F = 1$. As can be seen from this graph, as the surface coefficient γ becomes bigger, the critical wave number k_c gets smaller, therefore the number of linearly unstable modes decreases when γ increases.

It is also of interest to consider spatially periodic disturbances of finite length $2L$, say. It is easy to show that the system is linearly neutrally stable for any

$$\gamma > \left[\frac{L^2}{\pi^2}\left(2W_0^2(1-\alpha^2) - \frac{\alpha}{F}\right)\right].$$

The number of linearly unstable modes, k_c say, is given by

$$k_c = \mathrm{mod}\left[\frac{L^2}{\gamma\pi^2}\left(2W_0^2(1-\alpha^2) - \frac{\alpha}{F}\right)\right]^{1/2} \tag{2.51}$$

where mod means the integral part of a number. This result is used later in our discussion of nonlinear waves.

In the absence of surface tension, we have linear neutral stability as long as

$$F \leq \frac{\alpha}{2W_0(1-\alpha^2)}.$$

The nonlinear evolution of an unbounded vortex sheet in the absence of surface tension, encounters a singularity after a finite time due to the transfer of energy to high wavenumbers (Moore [67] and Caflisch & Orellana [16]). Setting $\gamma = \alpha = 0$ we recover the classical result $\omega = \pm 2kW_0$. For non-zero Atwood ratios but in the absence of surface tension still, the condition for instability is given by

$$-\left(1+\frac{1}{16W_0^4F^2}\right)^{1/2} - \frac{1}{4W_0^2F} < \alpha < \left(1+\frac{1}{16W_0^4F^2}\right)^{1/2} - \frac{1}{4W_0^2F}.$$

Clearly the lower limit is less than -1 and so is outside the range of α; the appropriate range of α which yields instability is, then

$$-1 < \alpha < \left(1+\frac{1}{16W_0^4F^2}\right)^{1/2} - \frac{1}{4W_0^2F}. \tag{2.52}$$

Condition (2.52) implies instability for any α smaller than zero as expected since such a case describes the motion with the heavier fluid on top. The reason the growth rate is $O(k)$ instead of the classical $O(k^{1/2})$ of Rayleigh-Taylor instability, lies in the long wavelength assumption used to derive our model equations. When the heavier fluid is below the lighter one there is a competing effect between the Kelvin-Helmholtz instability and the density stratification, and the system becomes linearly neutrally stable when (2.52) is violated, i.e., when α is in the range

$$\left(1+\frac{1}{16W_0^4F^2}\right)^{1/2} - \frac{1}{4W_0^2F} < \alpha < 1. \tag{2.53}$$

Growth rate curves corresponding to unstable (α, F) values exhibit a short wave instability which is reduced to a finite band of unstable waves when surface tension is included; any wavenumber larger than $k_c = \left[\frac{2W_0^2(1-\alpha^2)-\alpha/F}{\gamma}\right]^{1/2}$ is stabilized.

Note that in the absence of surface tension and Kelvin-Helmholtz instability, i.e. $\gamma \to 0$ and $W_0 \to 0$, inequality (2.53) reduces to $0 < \alpha < 1$, which is the classical stability criterion for the Rayleigh-Taylor instability mode. Indeed, denoting $\varepsilon = 16W_0^4F^2 \ll 1$ for small W_0, we can rewrite (2.53) as

$$\left(1+\frac{1}{\varepsilon^2}\right)^{1/2} - \frac{1}{\varepsilon} = \frac{1}{\varepsilon}(1+\varepsilon^2)^{1/2} - \frac{1}{\varepsilon} = \frac{1}{\varepsilon}\left(1+\frac{1}{2}\varepsilon^2 + O(\varepsilon^4)\right) - \frac{1}{\varepsilon} = O(\varepsilon).$$

In the absence of surface tension, the range of the Atwood ratio $0 < \alpha < 1$, i.e., when the lighter fluid is above the heavier one, $\rho_1 < \rho_2$, is called the gravitationally stable regime or regime with a gravitationally stable stratification.

2.5 Nonlinear Traveling Waves

This section is devoted to the construction of traveling-wave solutions to the system (2.36) and (2.37). Numerical results are presented in Section 2.6. Gravity and interfacial tension effects are taken to be of equal importance and solutions are sought in a Galilean steady moving frame of reference which has speed c. The transformation

$$S = S(\xi), \quad W = W(\xi), \quad \xi = x - ct$$

reduces the system (2.36), (2.37) to the ordinary differential equations that govern the shape and vortex sheet strength of the traveling wave:

$$-cS' + 2(S^2W)' = 2W', \tag{2.54}$$

$$-c(W - \alpha SW)' - (\alpha S^2W^2 - 2SW^2 + \alpha W^2)' = \frac{\alpha}{F}S' - \gamma S''', \tag{2.55}$$

with $'$ denoting differentiation with respect to ξ. Integration of (2.54), (2.55) yields

$$W = -\frac{1}{2}\frac{A + cS}{1 - S^2}, \tag{2.56}$$

$$-c(W - \alpha SW) - \alpha S^2W^2 + 2SW^2 - \alpha W^2 = \frac{\alpha}{F}S - \gamma S'' + B, \tag{2.57}$$

where A and B are constants of integration. Next, multiplication of (2.57) by S', elimination of W from (2.56) and integration gives the following equation for S (see Appendix B for details):

$$\frac{1}{2}\gamma(S')^2 = \frac{\alpha}{2F}S^2+BS-\frac{1}{4}\alpha c^2 S+D-\frac{1}{8}\frac{(A+c)^2(1-\alpha)}{1-S}-\frac{1}{8}\frac{(A-c)^2(1+\alpha)}{1+S} \quad (2.58)$$

where D is another constant of integration. We are interested in the range $-1 < S(\xi) < 1$. It is found that for a wide range of parameters, two roots of $(S')^2 = 0$ in $-1 < S < 1$ can exist. These values define the wave maximum and minimum and solutions easily follow by quadrature. Obviously, no traveling waves exist if $(S')^2 < 0$ for all $-1 < S < 1$.

2.5.1 Solitary Waves

We look for solitary waves by setting S and its derivatives equal to zero at infinity. This implies that $-\frac{A}{2}$ is equal to the undisturbed vortex sheet strength at infinity. In addition, a double root of $(S')^2 = 0$ is at $S = 0$ (this local double root behavior requires S to tend to zero as $|\xi|$ tends to infinity), and the construction is complete if another root exists in $(-1, 1)$. For solitary waves the constants B and D can be expressed in terms of A and c by,

$$B = \frac{A}{4}(2c - \alpha A), \quad D = \frac{1}{4}(A^2 + c^2 - 2\alpha A c), \quad (2.59)$$

and (2.58) becomes

$$\gamma(S')^2 = S^2\left[\frac{\alpha}{F} + \frac{\alpha S - 1}{2(1-S^2)}\left\{A^2 + c^2 - 2cA\beta(S)\right\}\right]. \quad (2.60)$$

The function $\beta(S)$ is given by

$$\beta(S) = \frac{S-\alpha}{\alpha S - 1} \quad \Rightarrow \quad -1 < \beta < 1, \quad (2.61)$$

and the double root at $S = 0$ is clearly seen in (2.60). Using (2.61) and the fact $A^2 + c^2 - 2cA\beta(S) = (A - c\beta)^2 + c^2(1 - \beta^2) \geq 0$, shows that $(S')^2 < 0$ whenever

$\alpha \leq 0$. Physically, this says that the model does not admit solitary waves if the densities are equal or if a heavier fluid lies above a lighter one. This is expected due to the Rayleigh-Taylor instability.

In what follows, then, we consider $\alpha > 0$ and re-write (2.60) as

$$\gamma(S')^2 = \frac{S^2}{1-S^2} p_2(S), \tag{2.62}$$

$$p_2(S) = -\frac{\alpha}{F}S^2 + \frac{\alpha}{2}\left(A^2 + c^2 - \frac{2cA}{\alpha}\right)S + \left(\frac{\alpha}{F} - \frac{A^2+c^2}{2} + \alpha A c\right). \tag{2.63}$$

The quadratic $p_2(S)$ plays a crucial role in the existence of solitary waves for unequal densities leading to a two-parameter family of solutions depending on A and c. The multiplying function $S^2/(1-S^2)$ in (2.62) is concave up, symmetric about $S = 0$ and tends to plus infinity as $S = \pm 1$ from below and above, respectively. In addition, p_2 is convex since $\frac{d^2 p_2}{dS^2} = -\frac{2\alpha}{F} < 0$. Four relevant possibilities emerge: (i) $p_2(S)$ has two real roots in $-1 < S < 1$ of opposite signs, (ii) $p_2(S)$ has two real roots in $-1 < S < 1$ with the same sign, (iii) $p_2(S)$ has only one real root in $-1 < S < 1$, (iv) $p_2(S)$ has no real roots in $-1 < S < 1$. Cases (ii) and (iv) preclude solitary waves while case (i) allows two distinct solitary waves with the same propagation speed and case (iii) only one. A schematic representation of these four possibilities is given in Figure 2.4. Only non-negative values of S_ξ^2 can be considered and the sketches are phase diagrams. For example, traversing the part of the phase plane in Figure 2.4 (i) from the negative root $S = S_2$ to $S = 0$, constructs half the "left" solitary wave (a wave of depression) from its global minimum value $S_2 < 0$ at $\xi = 0$ (the origin can be fixed by the translation invariance of the equations) to its zero asymptotic value at $\xi = +\infty$; the other half follows from symmetry. A similar construction gives the positive or "right" solitary wave (a wave of elevation) by starting at $S = S_1 > 0$ at $\xi = 0$ and monotonically decreasing to the zero asymptotic value at $\xi = +\infty$. Each solitary wave can be constructed independently and this becomes useful in our analysis that casts these solutions in terms of elliptic integrals. For case (ii), it is clear from the

canonical diagram in Figure 2.4 (ii), that it is impossible to connect either of the roots S_1, S_2 with the homoclinic point $S = 0$, without traversing a region where $S_\xi^2 < 0$ - this means that no real solitary waves exist in such instances.

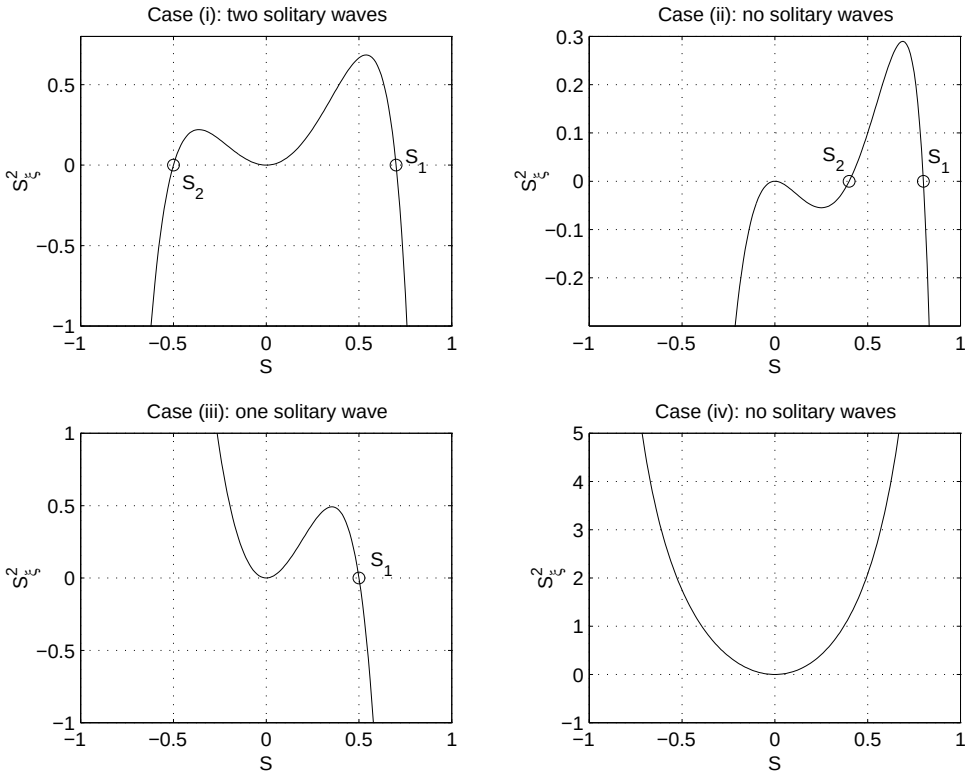

Figure 2.4 Schematic of the four canonical cases for solitary waves.

The Case $A = 0$ — Zero Vortex Sheet Strength

When $A = 0$, Kelvin-Helmholtz instabilities are absent; in addition, these solutions can be used to obtain others with $A \neq 0$ by continuation. For $A = 0$, equation (2.62) contains c^2 on its own and so constructed waves can have equal and opposite speeds. Note also that $\alpha > 0$ as explained previously, therefore, we have a gravitationally stable system.

Setting $A = 0$ in (2.63) and solving, we obtain the two roots

$$S_{1,2} = q \pm \left[q^2 - \frac{2}{\alpha}q + 1\right]^{1/2}, \quad q = \frac{1}{4}Fc^2, \tag{2.64}$$

and for real distinct roots we must have $q^2 - \frac{2}{\alpha}q + 1 > 0$, that is

$$q > q_1 = \frac{1+\sqrt{1-\alpha^2}}{\alpha} \quad \text{or} \quad q < q_2 = \frac{1-\sqrt{1-\alpha^2}}{\alpha}. \tag{2.65}$$

It is easy to establish the existence of two solitary waves for small values of q; the two roots of (2.64) for $0 < q \ll 1$ are

$$\begin{aligned} S_1 &= 1 - \frac{1-\alpha}{\alpha}q + O(q^2) \quad \Rightarrow \quad 0 < S_1 < 1, \\ S_2 &= -1 + \frac{1+\alpha}{\alpha}q + O(q^2) \quad \Rightarrow \quad -1 < S_2 < 0. \end{aligned} \tag{2.66}$$

Continuation to larger values of q provides solitary waves with larger speeds and smaller amplitudes. The inequalities (2.65) define two regions in the $q - \alpha$ plane where solitary waves may exist. These are depicted as regions 1 and 2 in Figure 2.5 and correspond to the right and left bounds of (2.65) respectively. Given $\alpha > 0$ and a Froude number F, we need to find values of c for which $S_1 < 1$ and/or $-1 < S_2 < 0$.

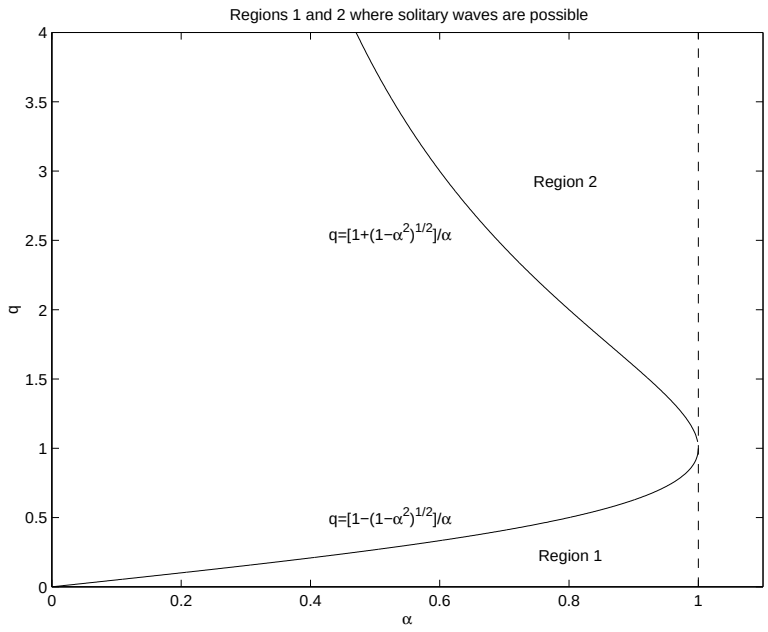

Figure 2.5 The regions 1 and 2 in the $q - \alpha$ plane where solitary waves may be possible.

A necessary condition for solitary waves to exist is for q and α to lie in either of regions 1 and 2 of Figure 2.5. The roots (2.64) in region 1 are

$$\begin{aligned} S_1(q) &= q + (q_1 - q)^{1/2}(q_2 - q)^{1/2}, \\ S_2(q) &= q - (q_1 - q)^{1/2}(q_2 - q)^{1/2}, \quad 0 < q < q_2 < 1. \end{aligned} \tag{2.67}$$

It is easy to establish that $S_1(0) = (q_1 q_2)^{1/2} = 1$, $S_1(q_2) = q_2 < 1$, $\frac{dS_1}{dq}(0) = 1 - (1/\alpha) < 0$, $\frac{dS_1}{dq}(q_2-) = -\infty$; the root $S_1(q)$ is monotonic decreasing from 1 to q_2 and all these values admit solitary waves of positive amplitude $q_2 \leq S_1(q) < 1$. Similarly, $S_2(0) = -1$, $S_2(q_2) = q_2$, $\frac{dS_2}{dq}(0) = 1 + (1/\alpha) > 0$ and $\frac{S_2}{dq}(q_2-) = +\infty$; the root $S_2(q)$ increases monotonically from -1 to q_2 and becomes zero at $q = \alpha/2$. Since $\frac{\alpha}{2} < q_2$, the interval $\frac{\alpha}{2} < q < q_2$ supports two positive roots both less than 1. This is case (ii) described earlier and depicted in Figure 2.4 (ii) and so is excluded. The conclusion, then, is that two solitary waves exist (waves of elevation and depression, respectively) for the range

$$0 < \frac{1}{4} F c^2 \leq \frac{\alpha}{2}. \tag{2.68}$$

The results presented above are summarized in Figure 2.6 for a typical case having $\alpha = 1/2$.

Next, we consider the possibility of solitary waves in Region 2 of Figure 2.5. The roots of (2.64) are

$$\begin{aligned} S_1(q) &= q + (q - q_1)^{1/2}(q - q_2)^{1/2}, \\ S_2(q) &= q - (q - q_1)^{1/2}(q - q_2)^{1/2}, \quad q > q_1 > 1. \end{aligned} \tag{2.69}$$

We find $S_1(q_1) = S_2(q_1) = q_1 > 1$, and $S_1(q)$ increases monotonically as q increases with an asymptote $S_1 \sim 2q$ at large q; $S_2(q)$ is monotonic decreasing with the asymptotic behavior $S_2 \to (1/\alpha)$ as $q \to \infty$. Since $(1/\alpha) > 1$, there can be no admissible solitary waves emerging from Region 2.

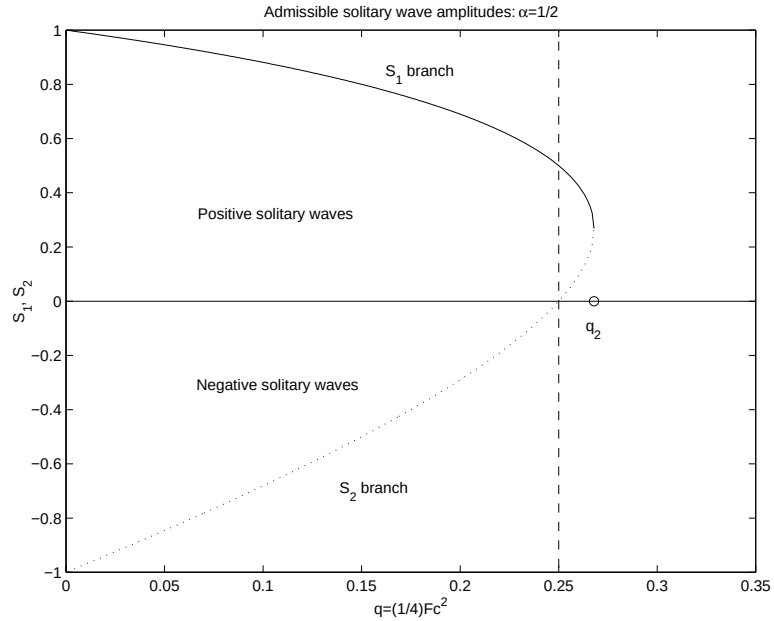

Figure 2.6 Admissible solitary waves in Region 1 ($0 < q < q_2$) for a typical value $\alpha = .5$. No solitary waves are possible to the right of the dashed line and two distinct waves exist to the left.

To summarize, we have found that for a given Froude number F and Atwood ratio $0 < \alpha < 1$, two solitary waves exist having the same speed. One wave is everywhere positive (the S_1 branch of Figure 2.6) and the other is everywhere negative (the S_2 branch of Figure 2.6). The wave speeds satisfy

$$|c| \leq \sqrt{\frac{2\alpha}{F}}, \tag{2.70}$$

with equality achieved when the negative solitary wave disappears and the positive one (see Figure 2.10 for this situation) has its smallest possible amplitude S_{1min}, say, given by $S_{1min} = \alpha$. At slower speeds, two solitary waves exist with amplitudes given by (2.67).

Having established the existence of solitary waves for $A = 0$, we can construct solutions for $A \neq 0$ by continuation methods. For asymptotically small values of A the solitary wave amplitudes and speeds change by order $|A|$ in a regular perturbation manner. We do not give details of such a calculation but instead use such results to guide the construction of waves numerically.

Some Exact Solutions for $\alpha = 1$ - Upper Layer of Zero Density

In certain cases exact solutions can be constructed depending on the wave amplitude S_0. With $\alpha = 1$, (2.63) is a perfect square and it is easily shown that (2.62) becomes

$$\gamma(S')^2 = \frac{S^2(S+S_0)}{F(1+S)}, \quad S_0 = 1 - \frac{F}{2}(A-c)^2. \tag{2.71}$$

From the form of the right-hand side of (2.71), the only admissible solitary waves have the amplitude $0 < S_0 < 1$. The resulting wave is negative everywhere and has a minimum amplitude of $-S_0$. In addition, the wave speed satisfies

$$A - \sqrt{\frac{2}{F}} < c < A + \sqrt{\frac{2}{F}}, \tag{2.72}$$

where A is related to the vortex sheet strength at infinity ($\lim_{|x|\to\infty} W(x) = -\frac{A}{2}$).

The solution to equation (2.71) is given implicitly by (half the wave in the region $\xi > 0$ where $S' > 0$ is constructed this way, the other half by reflection)

$$\int_{-S_0}^{S} \left(\frac{t+1}{t+S_0}\right)^{1/2} \frac{dt}{t} = \frac{\xi}{\sqrt{\gamma F}}. \tag{2.73}$$

The integral can be done exactly by making a substitution, for example $\tilde{Y}^2 = \frac{t+S_0}{t+1}$, giving

$$\frac{1+Y}{1-Y}\left(\frac{Y-\sqrt{S_0}}{Y+\sqrt{S_0}}\right)^{1/\sqrt{S_0}} = \exp(\frac{\xi}{\sqrt{\gamma F}}), \tag{2.74}$$

where $Y^2 = \frac{S+S_0}{S+1}$. It can be seen that for general values of the wave amplitude S_0, the solution must remain in implicit form. Explicit solutions are possible when $S_0 = \frac{1}{4}$ and $S_0 = \frac{1}{9}$ only, because (2.74) becomes a cubic or a quartic algebraic equation in Y, then. We construct the explicit solutions for these cases next.

Explicit Solution for $S_0 = \frac{1}{4}$

Manipulation of (2.74) leads to the following cubic equation for Y:

$$Y^3 - \frac{3}{4}Y - \frac{1}{4}\tau = 0, \quad \tau = \tanh(2\xi/\sqrt{\gamma F}). \tag{2.75}$$

Equation (2.75) has three real solutions that can be found explicitly by using Cardan's method [52]. We choose one of these roots which satisfies conditions $\lim_{\tau\to 0} Y = 0$, $\lim_{\tau\to 1} Y = -\frac{1}{2}$. The solution is

$$Y = -\cos\left(\frac{\arccos\tau + \pi}{3}\right), \quad S(\xi) = -\frac{(1/4) - Y^2}{1 - Y^2}. \tag{2.76}$$

It is easy to check, using the fact that $\tau(\xi = 0) = 0$ and $\tau \to 1$ as $\xi \to \infty$, that $S(0) = -1/4$ and $Y^2 \to (1/4)$ as $\xi \to \infty$, thus giving the required solitary wave behavior at infinity. The decay to zero at infinity is exponential. The graph of this solitary wave is presented in Figure 2.7.

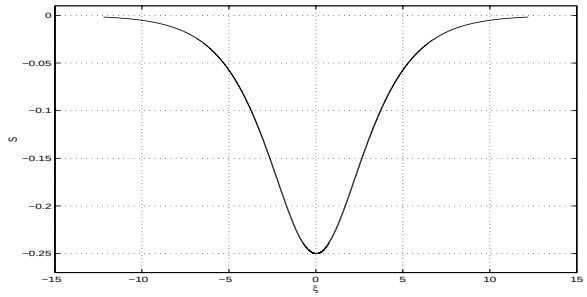

Figure 2.7 Solitary wave for $\alpha = 1$, $S_0 = 1/4$.

Explicit Solution for $S_0 = \frac{1}{9}$

Equation (2.74) in this case can be written in the form

$$Y^4 - \frac{2}{3}Y^2 - \frac{8}{27\tau}Y - \frac{1}{27} = 0, \quad \tau = \tanh(2\xi/\sqrt{\gamma F}). \tag{2.77}$$

Equation (2.77) can be solved, for instance, by Ferrari's method (see Abramowitz & Stegun[1]). We found that this equation has two real roots and two complex conjugate ones and the solitary wave solution is found explicitly by choosing one of the real roots that satisfies appropriate conditions for the solitary wave:

$$\begin{aligned} Y &= \frac{1}{3}\left\{\left(\eta + \frac{3}{2}\right)^{1/2} - \left(-\eta + \frac{3}{2} + 2\left[\eta^2 + \frac{3}{4}\right]^{1/2}\right)^{1/2}\right\}, \\ \eta &= \left(\frac{1}{\tau^2} - 1\right)^{1/3} - \frac{1}{2}, \\ S(\xi) &= -\frac{(1/9) - Y^2}{1 - Y^2}. \end{aligned} \tag{2.78}$$

As before, we can check that $S(0) = -\frac{1}{9}$ and $S(\xi) \to 0$ as $\xi \to \infty$, which are the properties that the solitary wave must satisfy.

Connection with Elliptic Integrals

The differential equation that gives solitary waves is equation (2.62) with (2.63). As discussed previously we have

$$p_2(S) \geq 0, \quad S \in [S_2, S_1], \quad -1 < S_2 \leq 0 \leq S_1 < 1. \tag{2.79}$$

Defining constants $a_2 = -\frac{\alpha}{F} < 0$, $a_1 = \frac{\alpha}{2}(A^2 + c^2 - \frac{2cA}{\alpha})$, $a_0 = \frac{\alpha}{F} - \frac{A^2+c^2}{2} + \alpha Ac$ and $\hat{\gamma} = \sqrt{\frac{-a_2}{\gamma}}$, and the ratios $a = \frac{a_1}{a_2}$, $b = \frac{a_0}{a_2}$, equation (2.62) is

$$\frac{dS}{d\xi} = \pm\hat{\gamma} S \sqrt{\frac{S^2 + aS + b}{S^2 - 1}} \equiv \pm F(S), \tag{2.80}$$

and in separated form

$$\frac{dS}{\pm F(S)} = d\xi \quad \text{or} \quad \frac{dS}{\pm\hat{\gamma} S \sqrt{\frac{S^2+aS+b}{S^2-1}}} = d\xi. \tag{2.81}$$

In view of (2.79), the polynomial $\tilde{p}_2(S) = S^2 + aS + b$ has two real distinct roots S_1, S_2, so that $\tilde{p}_2(S) = (S - S_1)(S - S_2) \leq 0$ for $S \in [S_2, S_1]$. Hence $(S')^2$ is positive there. Note the notation introduced earlier which fixes $0 < S_1 < 1$ and $-1 < S_2 < 0$. This is the general case of interest.

Since $(dS/d\xi)^2$ has a double root at zero and two simple roots S_1 and S_2, we have two distinct solitary waves and each wave is treated separately. First, we integrate (2.81) from S_2 to S, $S_2 \leq S \leq 0$, taking the plus sign of the square root. This choice constructs the right half of the solitary wave of depression; the other half of the wave follows by symmetry. Invoking Galilean invariance, we can shift the origin to be at the wave trough and the following implicit solution is found,

$$\xi = \int_{S_2}^{S} \frac{dt}{F(t)}, \quad S_2 \leq S \leq 0. \tag{2.82}$$

Integration of (2.81) from S to S_1, $0 \le S \le S_1$ and use of the minus sign of the square root, constructs the right half of the solitary wave of elevation (translation invariance is used also to fix the origin at the wave crest); the solution is

$$\xi = -\int_S^{S_1} \frac{dt}{F(t)}, \quad 0 \le S \le S_1. \tag{2.83}$$

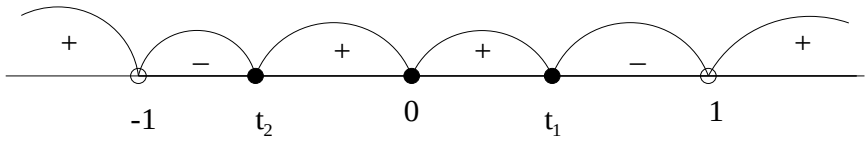

Figure 2.8 Polynomial $P_4(t)$ is positive in $(-\infty,-1)\bigcup(S_2,S_1)\bigcup(1,\infty)$ and negative in $(-1,S_2)\bigcup(S_1,1)$.

Consider equation (2.82) first. Introducing the polynomial

$$P_4(t) = (1-t)(S_1-t)(t-S_2)(t+1), \tag{2.84}$$

(note that $P_4(t)$ is positive for $t \in (-\infty,-1)\bigcup(S_2,S_1)\bigcup(1,\infty)$, see Figure 2.8), the solution becomes

$$\xi = \frac{1}{\hat{\gamma}}\left\{\int_{S_2}^{S} \frac{dt}{t\sqrt{P_4(t)}} - \int_{S_2}^{S} \frac{tdt}{\sqrt{P_4(t)}}\right\} \equiv \frac{1}{\hat{\gamma}}\left\{I_1(S) - I_2(S)\right\}. \tag{2.85}$$

The integrals $I_1(S)$ and $I_2(S)$ can be written as a linear combination of incomplete elliptic integrals of the third kind (see Appendix C for definition); they are special cases of the indefinite integrals covered in items 254.11 and 254.10 on page 113 of Byrd & Friedman [14]. It is useful to introduce the following constants:

$$\begin{aligned} k^2 &= \frac{2(S_1-S_2)}{(1-S_2)(S_1+1)}, \quad \lambda = \frac{2}{\sqrt{(1-S_2)(S_1+1)}}, \\ \beta^2 &= \frac{S_1-S_2}{1+S_1}, \quad \tilde{\beta}^2 = \frac{S_1-S_2}{1-S_2}, \end{aligned} \tag{2.86}$$

and functions

$$\varphi(S) = \sin^{-1}\sqrt{\frac{(S_1+1)(S-S_2)}{(S_1-S_2)(S+1)}}, \quad \tilde{\varphi}(S) = \sin^{-1}\sqrt{\frac{(1-S_2)(S_1-S)}{(S_1-S_2)(1-S)}}. \tag{2.87}$$

The incomplete elliptic integral of the third kind is central in our solutions. This is given by (see [14]):

$$\begin{aligned}\Pi(\varphi,\beta^2,k) &\equiv \int_0^S \frac{dt}{(1-\beta^2t^2)\sqrt{(1-t^2)(1-k^2t^2)}} \\ &= \int_0^\varphi \frac{d\theta}{(1-\beta^2\sin^2\theta)\sqrt{1-k^2\sin^2\theta}}.\end{aligned} \tag{2.88}$$

The solitary waves are given implicitly in terms of Π. The wave of depression has

$$\frac{\hat{\gamma}}{\lambda}\xi = \frac{1+S_2}{S_2}\Pi(\varphi,\beta^2/|S_2|,k) - (1+S_2)\Pi(\varphi,\beta^2,k), \tag{2.89}$$

and the wave of elevation is given by

$$\frac{\hat{\gamma}}{\lambda}\xi = \frac{S_1-1}{S_1}\Pi(\tilde{\varphi},\tilde{\beta}^2/S_1,k) + (S_1-1)\Pi(\tilde{\varphi},\tilde{\beta}^2,k). \tag{2.90}$$

2.5.2 Waves of Finite Periods

For finite periods equation (2.58) must be solved for all values of the constants A, B,D and c, providing a four-parameter family of solutions. The equation is conveniently written as

$$\gamma(S')^2 = \frac{1}{1-S^2}p_4(S), \tag{2.91}$$

where

$$\begin{aligned}p_4(S) = -\frac{\alpha}{F}S^4 + \left(\frac{\alpha c^2}{2} - 2B\right)S^3 + \left(\frac{\alpha}{F} - 2D\right)S^2 + \\ \left(2B - Ac + \frac{\alpha A^2}{2}\right)S + \left(2D - \frac{A^2+c^2}{2} + \alpha Ac\right).\end{aligned}$$

Since α and F are positive, $p_4(S)$ has at most two local maxima and one local minimum. Depending on the coefficients of $p_4(S)$, two, one or no admissible waves can be found. Any two successive roots in $-1 < S < 1$ describe the wave minimum and wave maximum respectively as long as the p_4 is positive between them. If the

function is concave between the roots no traveling wave exists since $(S')^2$ is negative then.

It is interesting to consider whether the periodic waves can be expressed in terms of elliptic integrals. Inspection of (2.91) and in particular its square root, indicates that the integrals that need to be calculated have integrands of the type

$$\frac{1-S^2}{\sqrt{(1-S)(1+S)p_4(S)}}, \tag{2.92}$$

that is they are rational functions of a polynomial and the square root of a sixth degree polynomial. This is not an elliptic integral. The integrand (2.92) degenerates to give a quartic under the radical and so elliptic integrals emerge. Comparing with solutions of the Kortweg-deVries (KdV) equation, for instance, we see that there is an additional level of complexity for the system studied here, in that the periodic waves of the KdV which are found in terms of elliptic integrals produce the well-known analytic sech^2 profiles as the period becomes infinite. In the present case, the periodic waves are not elliptic integrals but provide elliptic integral representations (albeit implicit) as the period becomes infinite to yield solitary waves.

In what follows we construct numerical solutions for both periodic and solitary waves.

2.6 Numerical Construction of Periodic and Solitary Waves

The results presented here were computed by integration of equation (2.58) for waves of finite periods and (2.60) for solitary waves. The wave profile is symmetric about some horizontal position which can be taken to be the origin, and it is enough to calculate the wave shape between trough and crest; a full wave follows by reflection. For definiteness, the plus sign is taken for S', and it is convenient to use S as the variable of integration and to compute the corresponding ξ. Consequently, without loss of generality, all traveling waves begin or end at $\xi = 0$. In the case of finite periods, for a given set of real constants A, B, c and D the possible values of S which

satisfy $(S')^2 = 0$ are found by Newton-Raphson iteration and the interval defined by the roots is subdivided into a regular mesh (typically 500 or 1000 points were used without any change in the solution to within graphical accuracy). The integration starts from the left-most root, the wave minimum, and is continued to the right-most, the wave maximum, calculating x at each S. Slight modifications are made in the solitary wave case since one of the wave extrema is at $S = 0$.

2.6.1 Periodic Waves

In order to fix things, we choose to study the behavior of the traveling waves as the Froude number and Atwood ratio vary with other constants held fixed. An extensive parameter study is not attempted here since the results are expected to be qualitatively similar. The numerical solutions presented in this sub-section have the following constants fixed:

$$A = 3.0, \quad B = 4.0, \quad c = 2.0, \quad D = 2.0, \quad \gamma = 1.0. \tag{2.93}$$

The first set of results examines the effect of the Atwood ratio α on interfacial profiles. The Froude number is fixed at unit value. Figure 2.9 (a) presents a family of curves in the phase plane for the cases $\alpha = 0.9, 0.8, 0.7, 0.5, 0.3, 0.1$ and the corresponding traveling waves over one complete period, are shown in Figure 2.9 (b). These results indicate that as the Atwood ratio decreases to smaller positive values, the wave height (crest to trough) decreases and at the same time the period increases. As the value of α increases, the effect of the upper fluid becomes less important and the wave can achieve larger amplitudes and smaller wavelengths for a given speed. Viscosity is absent from the present model and the reduction of amplitude is due to a transfer of momentum between the upper and lower fluids.

In the second set of results, the Atwood ratio is fixed at $\alpha = 0.5$ and the Froude number F is varied. Figure 2.10 (a) presents phase plane curves for $F = 3.0$, 0.5, 0.25, 0.05, 0.035 and Figure 2.10 (b) shows profiles of traveling waves obtained for

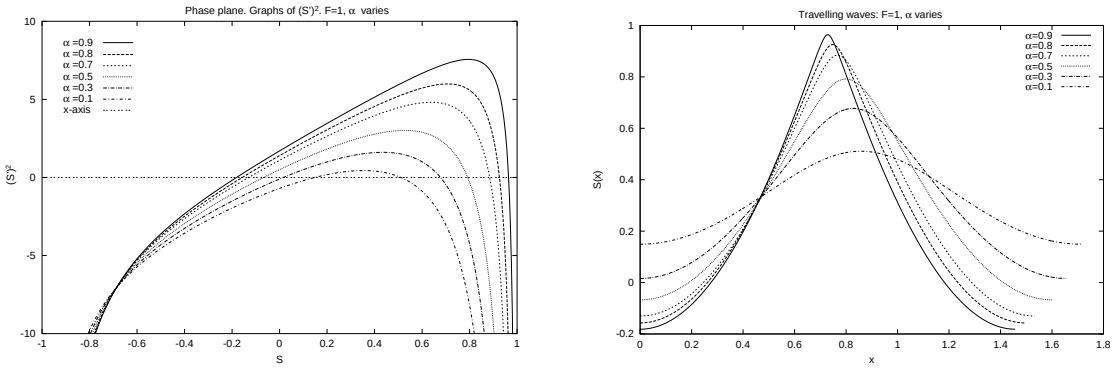

Figure 2.9 Traveling wave case: $F = 1$, α varies. Two simple roots. (a) Phase plane curves; (b) traveling waves.

the corresponding values of F. The wave profile is virtually unchanged at Froude

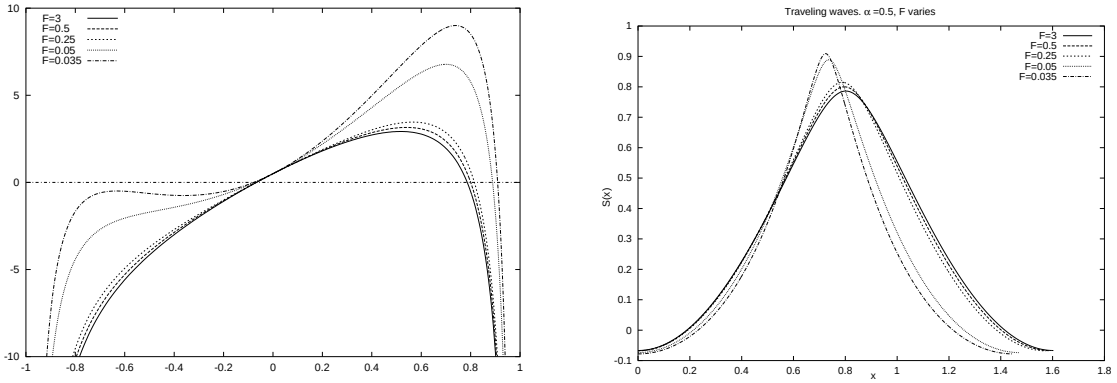

Figure 2.10 $\alpha = 0.5$ and F varies, $0.035 \leq F \leq 3.0$. Two simple roots. (a) Phase plane curves; (b) traveling wave profiles.

numbers larger than 3.0; this was checked numerically by dropping the $1/F$ term in (2.58). As indicated by Figure 2.10 (a), the wave amplitude and wavelength increase as the Froude number decreases; there is very little difference between the waves corresponding to $F = 3.0$ and $F = 0.5$. As the Froude number decreases further some interesting nonlinear behavior is found. The profile at $F = .05$, for example, has four inflexion points as opposed to that at $F = .25$ which has two. This feature carries through to lower values of F also. The amplitude of the wave also increases with decreasing Froude number and at the smallest value of $F = 0.01$ reported here, the wave almost touches the upper and lower channel walls (See Figure 2.11 for this

situation). Another interesting feature is that the wavelength of the periodic waves increases as F decreases; for $F = 0.05$ the wavelength is approximately 1.47. A further decrease in F below 0.05 yields traveling waves with increasing wavelengths, see Figures 2.14 (a) and (b).

We also observe that for values $0.035 \leq F \leq 3.0$, the phase plane curves have only two simple roots — points of intersection with x-axis. This corresponds to having only one traveling wave with positive amplitude for each value of F. As was mentioned above, phase curves for values $F \geq 0.25$ have only two points of inflexion. When F decreases, the left part of the phase curve, that it below x-axis, changes so that it has concave regions also (See Figure 2.10 (a)) which corresponds to the appearance of four points of inflexion instead of two. On the other hand, as F decreases, this left part of the phase curve approaches the x-axis and at the critical value $F = 0.0323627$ touches it as seen in Figure 2.12 (a). This double root will not produce any additional traveling wave. We still have one positive traveling wave shown in Figure 2.12 (b) and one "degenerate" wave corresponding to this double root. As F decreases further, the left part of the phase plane curve grows as well, i.e., the local max in Figure 2.13 moves above the horizontal axis giving two more points of intersection with the x-axis. Phase plane curves for representative waves for $F = 0.02$, 0.018 and 0.0169 are shown in Figure 2.13 (a). The amplified area where new roots appear is presented in Figure 2.13 (b). This left pair of roots gives rise to another traveling wave with negative amplitude. Therefore, for values of the Froude number below the critical one, i.e., $F < 0.0323627$, two traveling waves exist — one of elevation and one of depression. Traveling waves corresponding to the above values of F are depicted in Figure 2.14 (a) waves with positive amplitude and (b) with negative amplitude. Notice that at still lower values of F, the distance between the two middle roots decreases (see Figure 2.13 (b)) and at some value of F between 0.0169 and 0.01 these roots coincide. This corresponds to merging of negative and positive traveling waves

into one and we obtain what we term "combined" traveling waves as depicted in the representative case when $F = 0.01$ of Figure 2.11 (b)). Figure 2.13 gives details of the merging.

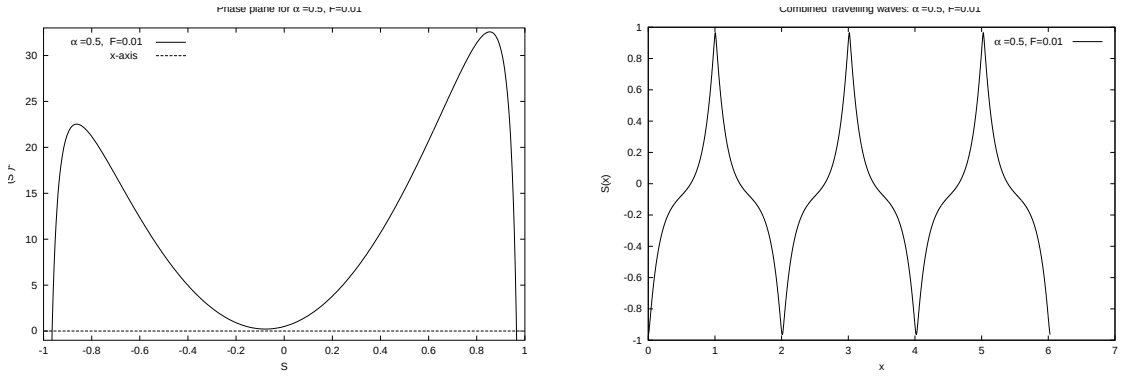

Figure 2.11 $\alpha = 0.5$, $F = 0.01$. (a) Phase plane curve; (b) two "combined" traveling waves.

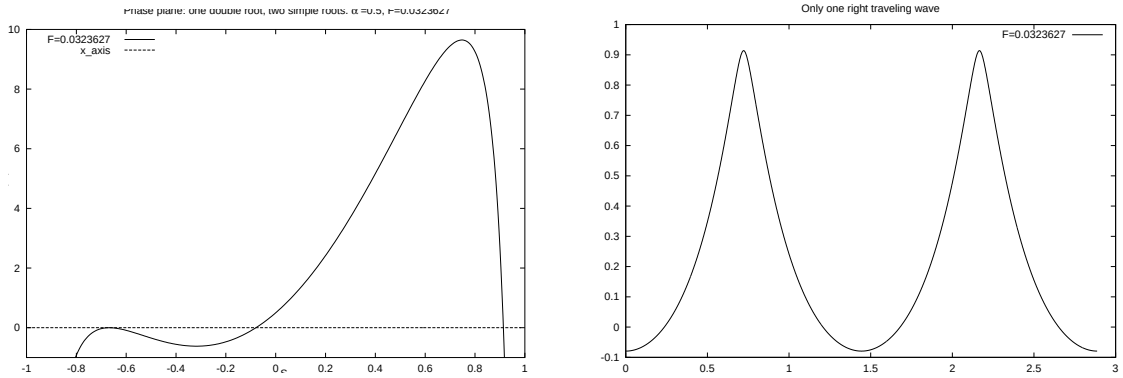

Figure 2.12 $\alpha = 0.5$, $F = 0.0323627$. Two simple roots, one - double. Only one right wave. Left wave is degenerate (trivial). (a) Phase plane curve; (b) traveling wave.

2.6.2 Representative Solitary Waves

Equation (2.60) can be readily integrated. Profiles are taken to be symmetric about the origin and it is enough to calculate the shape between trough and crest. For definiteness the plus sign is taken for S', and it is convenient to use S as the variable of integration and to compute the corresponding ξ. Consequently, all waves begin or end at $\xi = 0$. Solutions are obtained by quadrature by finding the ξ corresponding to

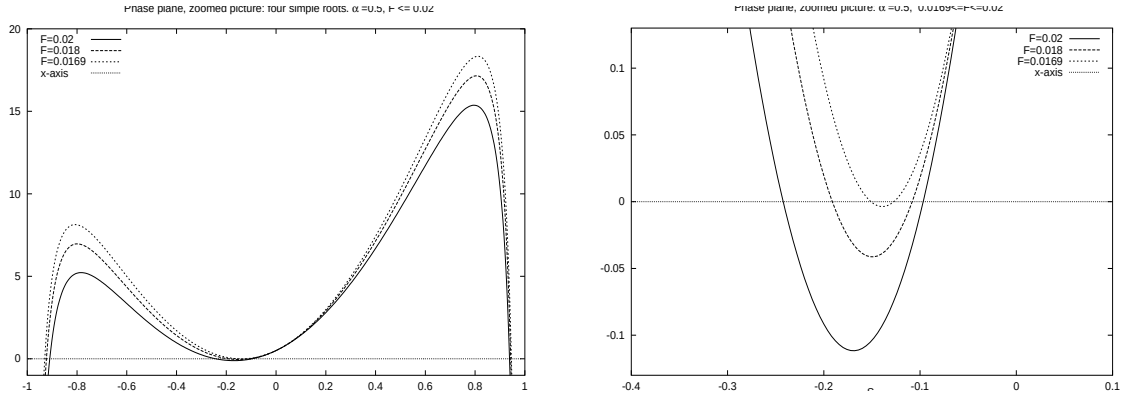

Figure 2.13 $\alpha = 0.5$, $F = 0.02, 0.018, 0.0169$. (a) Phase plane with four simple roots; (b) amplified picture of two interior roots.

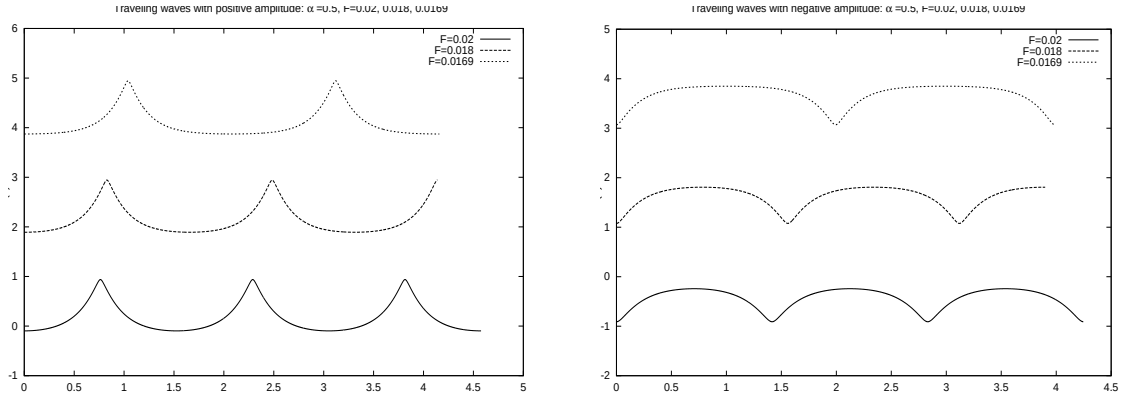

Figure 2.14 $\alpha = 0.5$, $F = 0.02, 0.018, 0.0169$. Two traveling waves with: (a) Positive amplitude; (b) negative amplitude.

the appropriate value of S. The asymptotic result (2.66) provides evidence regarding the existence of two solitary waves of equal speeds but different amplitudes. One wave has positive amplitude (this is a wave of elevation) while the other has negative amplitude (a wave of depression). It is easy to obtain values of A and c which produce a set of elevation and depression waves and in what follows we present solutions for the representative case

$$A = -0.1, \quad c = 0.9. \tag{2.94}$$

The main question we address is the dependence of the solitary wave shape on the physical parameters F and α.

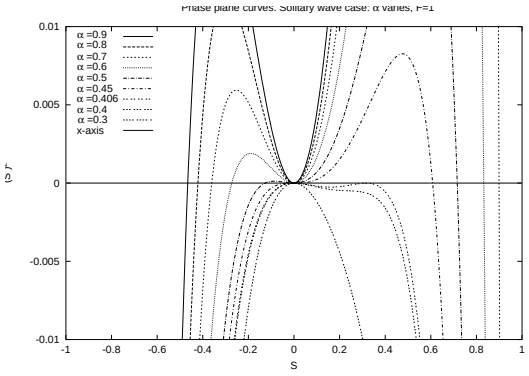

Figure 2.15 Phase plane curves for solitary wave case: $F = 1$, α varies.

Figure 2.15 is a graph of the right-hand side of equation (2.62), (2.63) for a fixed Froude number $F = 1.0$ and different Atwood ratios ranging from 0.9 to 0.3. A set of elevation and depression solitary waves exist for $\alpha = 0.9, 0.8, 0.7, 0.6, 0.5$. Note that the wave amplitudes decrease with α as does the maximum wave slope. A transition occurs between $\alpha = 0.5$ and $\alpha = 0.45$ when the left root coincides with the origin and the left solitary wave disappears. For $\alpha = 0.45$ only an elevation wave is present. The last curve in Figure 2.15 has $\alpha = 0.3$ and does not support any traveling waves since $S_x^2 < 0$ for all S. Representative solitary waves are shown in Figures 2.16 (a) and (b) for a range of α. For the choice of parameters (2.94) the amplitudes increase as the Atwood ratio increases towards unity.

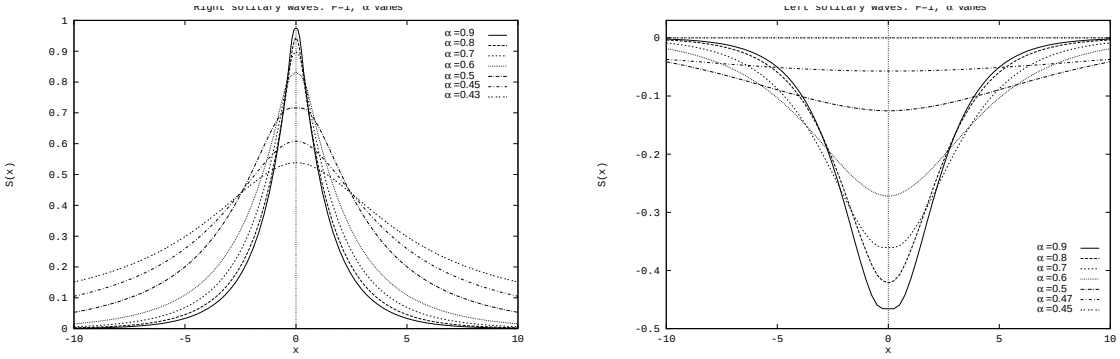

Figure 2.16 $F = 1$, α varies. (a) Waves of elevation; (b) waves of depression.

The effects of Froude number are considered next. Figure 2.17 shows the phase plane of (2.62) for a set of Froude numbers and fixed $\alpha = .5$. The figure covers the

range of $0.05 \leq F \leq 0.9$ with the following picture emerging. At the smallest value of $F = 0.05$ depicted, elevation and depression solitary waves coexist which almost touch the lower and upper walls, respectively. As the Froude number increases, the amplitudes of the left and right waves move away from the walls (See Figure 2.18 (a), (b) for left and right waves, respectively). This trend persists to higher values of $F > 1$, until a smooth transition at a value of F between 1.09 and 1.1 when the left wave disappears. In Figure 2.19 we follow the development of the interfacial traveling waves at still higher values of the Froude number. For $F = 1.125$ and 1.15, right waves are still present. At higher values of F only trivial solutions are possible - this is seen in Figure 2.19 with the phase-plane curve moving below the $S_\xi^2 = 0$ axis and so precluding a right wave. The last curve has $F = 1.25$ and is completely below the axis, so now waves are possible.

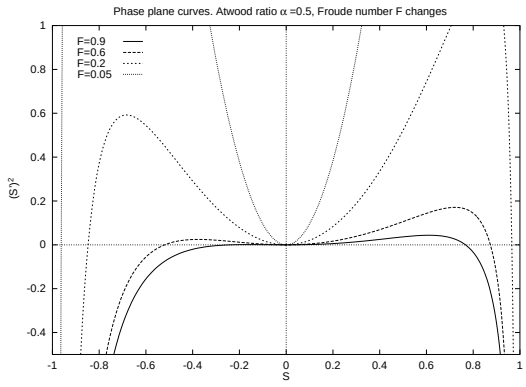

Figure 2.17 Phase plane curves for $\alpha = 0.5$, $0 < F < 1$.

2.7 Formation of an Infinite-Slope Singularities after a Finite Time in the Absence of Surface Tension and the Atwood Ratio $\alpha = 0$

The case when the Atwood ratio $\alpha = 0$ corresponds to the homogeneous layer of fluid, i.e., when both fluids have the same density. In the absence of surface tension, the system of governing equations (2.36) and (2.37) is

$$S_t + 2(S^2 W - W)_x = 0, \tag{2.95}$$

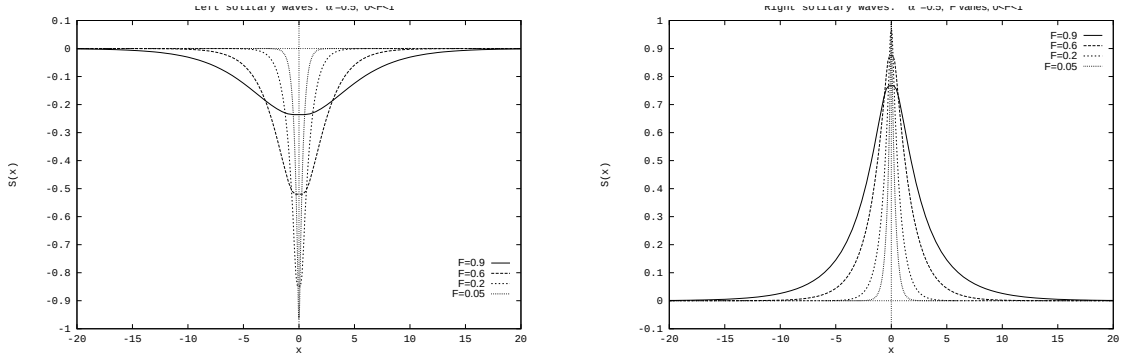

Figure 2.18 Solitary waves, $\alpha = 0.5$, $0 < F < 0$. (a) Waves of depression; (b) waves of elevation.

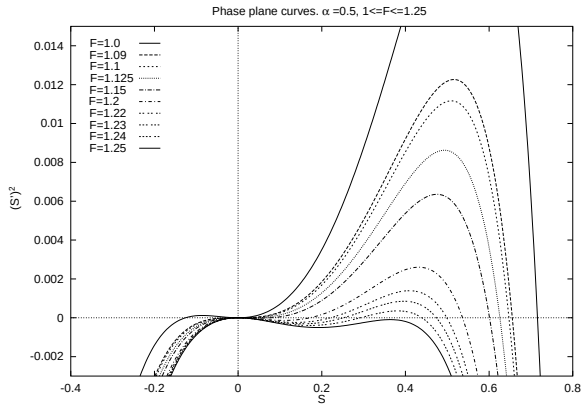

Figure 2.19 Phase plane curves for $\alpha = 0.5$, $1.0 \leq F \leq 1.25$.

$$W_t + 2(SW^2)_x = 0. \tag{2.96}$$

The following initial conditions are taken to coincide with those of numerical solutions presented later in Section 2.8:

$$S(x,0) = \varepsilon \sin x, \quad W(x,0) = 1 - \varepsilon \cos x, \tag{2.97}$$

where $\varepsilon > 0$ is the amplitude of an initial perturbation. The parity of solutions S and W for $t > 0$ remains the same as that for the initial conditions (2.97). This choice is not necessary either for theoretical or computational analysis but makes the presentation clearer.

Changing to $t' = 2t$ and then dropping prime $'$ in t removes the coefficient 2 from the second terms of the above equations, i.e.

$$S_t + (S^2W - W)_x = 0, \tag{2.98}$$

$$W_t + (SW^2)_x = 0. \tag{2.99}$$

This 2×2 system of conservation laws can be written in the matrix form as

$$\begin{pmatrix} S \\ W \end{pmatrix}_t + \begin{pmatrix} 2SW & S^2 - 1 \\ W^2 & 2SW \end{pmatrix} \begin{pmatrix} S \\ W \end{pmatrix}_x = \begin{pmatrix} 0 \\ 0 \end{pmatrix}. \tag{2.100}$$

The eigenvalues λ of the matrix $A = \begin{pmatrix} 2SW & S^2 - 1 \\ W^2 & 2SW \end{pmatrix}$ can be found from the characteristic equation

$$\det(A - \lambda I) = \begin{vmatrix} 2SW - \lambda & S^2 - 1 \\ W^2 & 2SW - \lambda \end{vmatrix} = (2SW - \lambda)^2 - W^2(S^2 - 1) = 0. \tag{2.101}$$

Since $S^2 - 1$ is negative, it follows that $(2SW - \lambda)^2 - W^2(S^2 - 1) > 0$, so the eigenvalues λ are complex and the system under consideration is elliptic. Since our nonlinear 2×2 system of conservation laws (2.100) is not hyperbolic, we cannot apply directly the theory of singularity formation developed by Lax [56]. If we extend the dependent and independent variables into the complex plane in such a way that the resulting system is a system of hyperbolic equations and then solve this system, at least implicitly, by the method of characteristics and Riemann invariants, then we obtain evidence of singularity formation for the system (2.100). We will investigate whether characteristics (or families of characteristics) cross on the real axis. This would imply, then, that a singularity is encountered by the physical solution on the real axis. These ideas were originated and successfully applied by Moore [67, 69] when he studied the singularity formation in vortex sheets. Here we adapt Moore's analysis to the present problem. We also use analytical results by Caflisch and Orellana [15, 16] who also studied vortex sheet singularities. The method presented here follows the ideas developed by Papageorgiou and Orellana in [71] where they studied analytically and numerically the cylindrical jet breakup using 2×2 system of conservation laws in

the complex plane. The material presented here also uses information from a private communication with Dr. Orellana.

We proceed, then, by analytically extending S and W into the complex plane through the change of variables

$$z = ix, \quad \eta(z,t) = iS(x,t)$$

so that the independent variables t and z, as well as the dependent variables $\eta(z,t)$ and $W(z,t)$ are real. Such a complexification now yields a hyperbolic system in the new variables which we analyze next.

In the new variables, system (2.98), (2.99) is

$$\eta_t + 2\eta W\eta_z + (1+\eta^2)W_z = 0, \tag{2.102}$$

$$W_t + W^2\eta_z + 2\eta W W_z = 0 \tag{2.103}$$

or in the matrix form

$$\begin{pmatrix} \eta \\ W \end{pmatrix}_t + \begin{pmatrix} 2\eta W & 1+\eta^2 \\ W^2 & 2\eta W \end{pmatrix} \begin{pmatrix} \eta \\ W \end{pmatrix}_z = \begin{pmatrix} 0 \\ 0 \end{pmatrix}. \tag{2.104}$$

The set of the initial conditions (2.97) transforms into the corresponding set of initial conditions for η and W as

$$\eta(z,0) = \varepsilon \sinh z, \tag{2.105}$$

$$W(z,0) = 1 - \varepsilon \cosh z. \tag{2.106}$$

It is seen that the new system has real eigenvalues and is therefore hyperbolic. Denote the eigenvalues by

$$\lambda^+ = 2\eta W + W(\eta^2+1)^{1/2}, \quad \lambda^- = 2\eta W - W(\eta^2+1)^{1/2}.$$

The Riemann invariants are the functionals of η and W, which are constant on the characteristics corresponding to the two distinct eigenvalues. To construct them, as

described in the paper by Lax [56], we need first to find the left eigenvectors. The left eigenvectors corresponding to λ^+ and λ^-, respectively, are

$$\vec{e}_+^{\,t} = (W(\eta^2+1)^{-1/2}, 1) \quad \text{and} \quad \vec{e}_-^{\,t} = (-W(\eta^2+1)^{-1/2}, 1).$$

Let

$$\tilde{A} = \begin{pmatrix} 2\eta W & 1+\eta^2 \\ W^2 & 2\eta W \end{pmatrix}.$$

Multiply equation (2.104) by the eigenvector $\vec{e}_+^{\,t}$ from the left (see, for example, [58] for more details) and use the fact that $\vec{e}_+^{\,t}\tilde{A} = \lambda^+ \vec{e}_+^{\,t}$. Factoring out $\vec{e}_+^{\,t}$ in the resulting equation, we obtain

$$\vec{e}_+^{\,t}\left[\begin{pmatrix} \eta \\ W \end{pmatrix}_t + \lambda^+ \begin{pmatrix} \eta \\ W \end{pmatrix}_z\right] = 0.$$

But this means that

$$\vec{e}_+^{\,t}\frac{d}{dt}\begin{pmatrix} \eta \\ W \end{pmatrix} = \vec{e}_+^{\,t}\left[\begin{pmatrix} \eta \\ W \end{pmatrix}_t + \frac{dz}{dt}\begin{pmatrix} \eta \\ W \end{pmatrix}_z\right] = 0,$$

where $\frac{dz}{dt} = \lambda^+$. Therefore, $\vec{e}_+^{\,t}\frac{d}{dt}\begin{pmatrix} \eta \\ W \end{pmatrix} = 0$ along $\frac{dz}{dt} = \lambda^+$ or

$$\vec{e}_+^{\,t}\begin{pmatrix} \frac{d\eta}{dt} \\ \frac{dW}{dt} \end{pmatrix} = 0 \quad \text{along} \quad \frac{dz}{dt} = \lambda^+. \tag{2.107}$$

Similarly, for the second eigenvalue λ^-, we obtain

$$\vec{e}_-^{\,t}\begin{pmatrix} \frac{d\eta}{dt} \\ \frac{dW}{dt} \end{pmatrix} = 0 \quad \text{along} \quad \frac{dz}{dt} = \lambda^-. \tag{2.108}$$

In component form, equation (2.107) can be written as

$$W(\eta^2+1)^{-1/2}\frac{d\eta}{dt} + 1 \cdot \frac{dW}{dt} = 0.$$

Separating variables in the above equation and integrating, we obtain

$$\int \frac{d\eta}{(\eta^2+1)^{1/2}} + \int \frac{dW}{W} = const.$$

Using the result

$$\int \frac{dx}{\sqrt{a^2+x^2}} = \sinh^{-1}\frac{x}{a} + C = \ln(x+\sqrt{a^2+x^2}) + C,$$

we obtain the first Riemann invariant, which we denote by

$$r(\eta, W) = \ln(\eta + \sqrt{\eta^2+1}) + \ln W = const \quad \text{along} \quad \frac{dz^+}{dt} = W(2\eta + \sqrt{\eta^2+1}).$$

Performing the above procedure with equation (2.108), we get the second Riemann invariant

$$s(\eta, W) = \ln(\eta + \sqrt{\eta^2+1}) - \ln W = const \quad \text{along} \quad \frac{dz^-}{dt} = W(2\eta - \sqrt{\eta^2+1}).$$

The superscripts $+$ and $-$ are used to denote the characteristics z^+ and z^-, respectively, due to their correspondence to the eigenvalues λ^+ and λ^-. We can convince ourselves that the functionals $r(\eta, W)$ and $s(\eta, W)$ are indeed the Riemann invariants. For that purpose, we have to check whether they are consistent with the evolution equations (2.102) and (2.103).

Since the functionals $r(\eta, W)$ and $s(\eta, W)$ are constant along the respective characteristics, we have

$$\frac{d}{dt}r(\eta, W) = 0 \quad \text{and} \quad \frac{d}{dt}s(\eta, W) = 0.$$

Differentiation of $r(\eta, W)$ with respect to t yields

$$\begin{aligned}\frac{d}{dt}r(\eta, W) &= \frac{1}{\eta + \sqrt{\eta^2+1}}\left(1 + \frac{2\eta}{2\sqrt{\eta^2+1}}\right)(\eta_z\frac{dz}{dt} + \eta_t) + \frac{1}{W}(W_z\frac{dz}{dt} + W_t) \\ &= \frac{1}{\sqrt{\eta^2+1}}\left(\eta_z W(2\eta + \sqrt{\eta^2+1}) + \eta_t\right) + \frac{1}{W}(W_z W(2\eta + \sqrt{\eta^2+1}) + W_t).\end{aligned}$$

Therefore,

$$\frac{1}{\sqrt{\eta^2+1}}\left(\eta_t W(2\eta + \sqrt{\eta^2+1}) + \eta_t\right) + W_z(2\eta + \sqrt{\eta^2+1}) + \frac{W_t}{W} = 0. \qquad (2.109)$$

Similarly, differentiating $s(\eta, W)$ with respect to t, we obtain

$$\frac{1}{\sqrt{\eta^2+1}}\left(\eta_t W(2\eta - \sqrt{\eta^2+1}) + \eta_t\right) - W_z(2\eta - \sqrt{\eta^2+1}) - \frac{W_t}{W} = 0. \qquad (2.110)$$

Addition of equations (2.109) and (2.110) gives

$$\frac{1}{\sqrt{\eta^2+1}}(4\eta W\eta_z + 2\eta_t) + 2W_z\sqrt{\eta^2+1} = 0.$$

Multiplying this equation by $\frac{\sqrt{\eta^2+1}}{2}$ we obtain equation (2.102). If we subtract equation (2.110) from equation (2.109) and then multiply the resulting equation by $W/2$, we will get equation (2.103). Thus, the consistency of the Riemann invariants with the system of conservation laws (2.102) and (2.103) is shown.

2.7.1 Asymptotic Calculation of Characteristics

The Riemann invariants $r(\eta, W)$ and $s(\eta, W)$ are not constant in time and considering the initial conditions (2.105), (2.106), we observe that the system is strictly nonlinear. Therefore, there is a possibility of singularity formation as we show next.

We assume that the initial perturbation is small, i.e., $\varepsilon \ll 1$. Denote by $(z_0, 0)$ an initial point in the (z, t) plane. Using the smallness of parameter ε, we approximate two characteristics emanating from the initial point, correct to order ε^2.

Initial conditions (2.105), (2.106) at the initial point $(z_0, 0)$ are

$$\eta(z_0, 0) = \varepsilon \sinh z_0 = \frac{\varepsilon}{2}(\mathrm{e}^{z_0} - \mathrm{e}^{-z_0}) = O(\varepsilon), \tag{2.111}$$

$$W(z_0, 0) = 1 - \varepsilon \cosh z_0 = 1 - \frac{\varepsilon}{2}(\mathrm{e}^{z_0} + \mathrm{e}^{-z_0}) = 1 + O(\varepsilon). \tag{2.112}$$

Notice that since η is of order ε, we have

$$(1+\eta^2)^{1/2} = \left(1 + \frac{\varepsilon^2}{4}(\mathrm{e}^{z_0} - \mathrm{e}^{-z_0})^2\right)^{1/2} = 1 + \frac{\varepsilon^2}{8}(\mathrm{e}^{z_0} - \mathrm{e}^{-z_0})^2 + O(\varepsilon^4). \tag{2.113}$$

First we approximate the characteristics near the initial point $(z_0, 0)$. Then with the leading order expressions of characteristics we can find values of the Riemann invariants $r(\eta, W)$ and $s(\eta, W)$. After that, we will be able to find approximations to solutions η and W. Once we have them, we can get higher corrections for characteristics.

For the z^+ characteristics, we have

$$\frac{dz^+}{dt} = W(2\eta + \sqrt{\eta^2+1}) = [1 + O(\varepsilon)] \cdot [2O(\varepsilon) + 1 + O(\varepsilon^2)].$$

Therefore,

$$\frac{dz^+}{dt} = 1 + O(\varepsilon). \tag{2.114}$$

Integrating (2.114) with respect to t and using the initial condition $z^+|_{t=0} = z_0$ we obtain

$$z^+ = z_0 + t + O(\varepsilon), \tag{2.115}$$

or

$$z_0 = z^+ - t + O(\varepsilon). \tag{2.116}$$

On the other hand, the Riemann invariant $r(\eta, W)$ may be written as

$$\begin{aligned} r(\eta, W) &= \ln(\eta + \sqrt{\eta^2+1}) + \ln W = \ln\left\{1 + \frac{\varepsilon}{2}(\mathrm{e}^{z_0} - \mathrm{e}^{-z_0}) + O(\varepsilon^2)\right\} \\ &+ \ln\left\{1 - \frac{\varepsilon}{2}(\mathrm{e}^{z_0} + \mathrm{e}^{-z_0})\right\} = \frac{\varepsilon}{2}(\mathrm{e}^{z_0} - \mathrm{e}^{-z_0}) - \frac{\varepsilon}{2}(\mathrm{e}^{z_0} + \mathrm{e}^{-z_0}) + O(\varepsilon^2) \\ &= -\varepsilon\,\mathrm{e}^{-z_0} + O(\varepsilon^2), \end{aligned}$$

where we used the smallness of the parameter ε. Therefore,

$$r(\eta, W) = \ln(\eta + \sqrt{\eta^2+1}) + \ln W = -\varepsilon\,\mathrm{e}^{-z_0} + O(\varepsilon^2). \tag{2.117}$$

But on z^+, we can express z_0 in terms of z^+ using relation (2.116). Then since ε is small, we have

$$\mathrm{e}^{-z_0} = \mathrm{e}^{-\left(z^+ - t + O(\varepsilon)\right)} = \mathrm{e}^{-(z^+ - t)} + O(\varepsilon)$$

and (2.117) yields the following relation

$$\ln(\eta + \sqrt{\eta^2+1}) + \ln W = -\varepsilon\,\mathrm{e}^{-(z^+ - t)} + O(\varepsilon^2).$$

Since for any z in the plane (z,t) there exists a characteristic z^+ passing through the point z, we can use z instead of z^+ in the above equation, i.e.,

$$\ln(\eta+\sqrt{\eta^2+1})+\ln W=-\varepsilon\,\mathrm{e}^{-(z-t)}+O(\varepsilon^2). \tag{2.118}$$

We proceed in an analogous way with the characteristic z^- and obtain

$$\frac{dz^-}{dt}=W(2\eta-\sqrt{\eta^2+1})=-1+O(\varepsilon)$$

that upon integration with respect to t and use of the initial condition $z^+|_{t=0}=z_0$ gives

$$z^-=-t+z_0+O(\varepsilon), \tag{2.119}$$

or

$$z_0=z^-+t+O(\varepsilon). \tag{2.120}$$

Then the Riemann invariant $s(\eta,W)$ may be written as

$$s(\eta,W)=\ln(\eta+\sqrt{\eta^2+1})-\ln W=\varepsilon\,\mathrm{e}^{z_0}+O(\varepsilon^2).$$

Expressing z_0 in terms of z^- by using (2.120), we obtain

$$\ln(\eta+\sqrt{\eta^2+1})-\ln W=\varepsilon\,\mathrm{e}^{z^-+t}+O(\varepsilon^2),$$

where again we can replace z^- with z since for any z in the plane, there exists a characteristic z^- passing through z. Hence we may write

$$\ln(\eta+\sqrt{\eta^2+1})-\ln W=\varepsilon\,\mathrm{e}^{z+t}+O(\varepsilon^2). \tag{2.121}$$

Adding equations (2.118) and (2.121) we get

$$\ln(\eta+\sqrt{\eta^2+1})=\frac{\varepsilon}{2}\left[\mathrm{e}^{z+t}-\mathrm{e}^{-(z-t)}\right]+O(\varepsilon^2).$$

Since $\ln(\eta + \sqrt{\eta^2+1}) = \sinh^{-1}\eta$, we can write

$$\eta = \sinh\left\{\frac{\varepsilon}{2}\left[\mathrm{e}^{z+t} - \mathrm{e}^{-(z-t)}\right] + O(\varepsilon^2)\right\}.$$

The argument of sinh in the above expression is of order ε, therefore, to the leading order

$$\eta = \frac{\varepsilon}{2}\left[\mathrm{e}^{z+t} - \mathrm{e}^{-(z-t)}\right] + O(\varepsilon^2).$$

Subtraction of equation (2.121) from (2.118) yields

$$\ln W = -\frac{\varepsilon}{2}\left[\mathrm{e}^{-(z-t)} + \mathrm{e}^{z+t}\right] + O(\varepsilon^2)$$

or

$$W = \exp\left\{-\frac{\varepsilon}{2}\left[\mathrm{e}^{-(z-t)} + \mathrm{e}^{z+t}\right] + O(\varepsilon^2)\right\}$$

and to the leading order

$$W = 1 - \frac{\varepsilon}{2}\left[\mathrm{e}^{-(z-t)} + \mathrm{e}^{z+t}\right] + O(\varepsilon^2).$$

Now as we have expressions for η and W, we can update the characteristics z^+ and z^-.

$$\frac{dz^+}{dt} = \left[1 - \frac{\varepsilon}{2}\left\{\mathrm{e}^{-(z-t)} + \mathrm{e}^{z+t}\right\} + O(\varepsilon^2)\right] \cdot \left[1 + \varepsilon\left\{\mathrm{e}^{z+t} - \mathrm{e}^{-(z-t)}\right\} + O(\varepsilon^2)\right].$$

Hence

$$\frac{dz^+}{dt} = 1 + \varepsilon\left\{\frac{1}{2}\,\mathrm{e}^{z+t} - \frac{3}{2}\,\mathrm{e}^{-(z-t)}\right\} + O(\varepsilon^2).$$

But on the characteristic z^+, we can express z in terms of z_0 using relation (2.115) and write

$$\frac{dz^+}{dt} = 1 + \varepsilon\left[\frac{1}{2}\exp\left\{2t + z_0 + \varepsilon t\left(\frac{1}{2}\,\mathrm{e}^{z_0} - \frac{3}{2}\,\mathrm{e}^{-z_0}\right) + O(\varepsilon^2)\right\}\right.$$

$$-\frac{3}{2}\exp\left\{-\left(z_0+\varepsilon t\left\{\frac{1}{2}\,\mathrm{e}^{z_0}-\frac{3}{2}\,\mathrm{e}^{-z_0}\right\}\right)+O(\varepsilon^2)\right\}\Bigg]$$

$$=1+\varepsilon\left[\frac{1}{2}\,\mathrm{e}^{2t}\,\mathrm{e}^{z_0}\left\{1+\varepsilon t\left(\frac{1}{2}\,\mathrm{e}^{z_0}-\frac{3}{2}\,\mathrm{e}^{-z_0}\right)+O(\varepsilon^2)\right\}\right.$$

$$\left.-\frac{3}{2}\,\mathrm{e}^{-z_0}\left\{1-\varepsilon t\left(\frac{1}{2}\,\mathrm{e}^{z_0}-\frac{3}{2}\,\mathrm{e}^{-z_0}\right)+O(\varepsilon^2)\right\}\right]+O(\varepsilon^2).$$

Therefore,

$$\frac{dz^+}{dt}=1+\varepsilon\left[\frac{1}{2}\,\mathrm{e}^{2t}\,\mathrm{e}^{z_0}-\frac{3}{2}\,\mathrm{e}^{-z_0}\right]+O(\varepsilon^2). \tag{2.122}$$

Integrating equation (2.122) with respect to t and using $z^+|_{t=0}=z_0$, we obtain

$$z^+=z_0+t+\varepsilon\left[\frac{1}{4}\,\mathrm{e}^{z_0}(\mathrm{e}^{2t}-1)-\frac{3}{2}t\,\mathrm{e}^{-z_0}\right]+O(\varepsilon^2).$$

Note that the condition $z^+|_{t=0}=z_0$ implies that the zero order constant of integration being z_0 while at the order ε we get $-\frac{1}{4}\,\mathrm{e}^{z_0}$.

Similarly, for characteristic z^- we have

$$\frac{dz^-}{dt}=-1+\varepsilon\left\{\frac{3}{2}\,\mathrm{e}^{z+t}-\frac{1}{2}\,\mathrm{e}^{-(z-t)}\right\}+O(\varepsilon^2).$$

Replacing z in the above expression with (2.119) gives

$$\frac{dz^-}{dt}=-1+\varepsilon\left[\frac{3}{2}\,\mathrm{e}^{z_0}-\frac{1}{2}\,\mathrm{e}^{-z_0}\,\mathrm{e}^{2t}\right]+O(\varepsilon^2).$$

Integration with respect to t yields

$$z^-=-t+z_0+\varepsilon\left[\frac{3}{2}t\,\mathrm{e}^{z_0}-\frac{1}{4}\,\mathrm{e}^{-z_0}(\mathrm{e}^{2t}-1)\right]+O(\varepsilon^2). \tag{2.123}$$

Proposition 1 *The following statement is true:*

$$z^+(z_0)=-z^-(-z_0)+O(\varepsilon^2).$$

Proof. Indeed, if we change z_0 to $-z_0$ into characteristic z^- written in (2.123), we obtain the following

$$z^-(-z_0) = -t - z_0 + \varepsilon\left[\frac{3}{2}t\,\mathrm{e}^{-z_0} - \frac{1}{4}\,\mathrm{e}^{z_0}(\mathrm{e}^{2t}-1)\right] + O(\varepsilon^2)$$
$$= -\left\{t + z_0 - \varepsilon\left[\frac{3}{2}t\,\mathrm{e}^{-z_0} - \frac{1}{4}\,\mathrm{e}^{z_0}(\mathrm{e}^{2t}-1)\right] + O(\varepsilon^2)\right\} = -z^+(z_0).$$

■

The symmetry established in Proposition 1 allows one to consider crossing of the z^+ characteristics alone since critical times, i.e., times of the shock formation, given by crossings of z^- characteristics are identical.

Let us introduce the following notations (they play a similar role in the paper by Papageorgiou and Orellana [71]).

$$f_1(t) = \frac{1}{4}(\mathrm{e}^{2t}-1), \quad f_2(t) = -\frac{3}{2}t. \tag{2.124}$$

Then characteristics z^+ and z^- may be written as

$$z^+ = z_0 + t + \varepsilon f_1(t)\,\mathrm{e}^{z_0} + \varepsilon f_2(t)\,\mathrm{e}^{-z_0} + O(\varepsilon^2). \tag{2.125}$$

$$z^- = z_0 - t - \varepsilon f_2(t)\,\mathrm{e}^{z_0} - \varepsilon f_1(t)\,\mathrm{e}^{-z_0} + O(\varepsilon^2). \tag{2.126}$$

Note that $f_1(t) > 0$ and $f_2(t) < 0$ for $t > 0$.

2.7.2 Crossing of Any z^+ Characteristics and Minimal Time when This Happens

Consider two initial points $(\alpha_1, 0)$ and $(\alpha_2, 0)$ in the (z, t) plane where without loss of generality we assume $\alpha_1 > \alpha_2$. We allow two z^+ characteristics to cross and we would like to find the minimum possible time when this happens. The z^+ characteristics emanating from these points cross after a time, correct to $O(\varepsilon^2)$, that may be found from the following equation

$$\alpha_1 + t + \varepsilon f_1(t)\,\mathrm{e}^{\alpha_1} + \varepsilon f_2(t)\,\mathrm{e}^{-\alpha_1} = \alpha_2 + t + \varepsilon f_1(t)\,\mathrm{e}^{\alpha_2} + \varepsilon f_2(t)\,\mathrm{e}^{-\alpha_2}$$

or after cancelling t

$$\alpha_1 + \varepsilon f_1(t)\,\mathrm{e}^{\alpha_1} + \varepsilon f_2(t)\,\mathrm{e}^{-\alpha_1} = \alpha_2 + \varepsilon f_1(t)\,\mathrm{e}^{\alpha_2} + \varepsilon f_2(t)\,\mathrm{e}^{-\alpha_2}\,. \tag{2.127}$$

Denote by t_c the minimum possible time over pairs (α_1, α_2). Equation (2.127) may be regarded as the equation for the function $t = t(\alpha_1, \alpha_2)$. The necessary condition of an extremum for the function $t(\alpha_1, \alpha_2)$ is that its partial derivatives $\frac{\partial t}{\partial \alpha_1}$ and $\frac{\partial t}{\partial \alpha_1}$ have to be zero. Differentiate equation (2.127) with respect to α_1 first to get

$$\begin{aligned} 1 \;+\; & \varepsilon f_1(t_c)\,\mathrm{e}^{\alpha_1} + \varepsilon \frac{\partial f_1(t_c)}{\partial \alpha_1}\,\mathrm{e}^{\alpha_1} - \varepsilon f_2(t_c)\,\mathrm{e}^{-\alpha_1} + \varepsilon \frac{\partial f_2(t_c)}{\partial \alpha_1}\,\mathrm{e}^{-\alpha_1} \\ = \;& \varepsilon \frac{\partial f_1(t_c)}{\partial \alpha_1}\,\mathrm{e}^{\alpha_2} + \varepsilon \frac{\partial f_2(t_c)}{\partial \alpha_1}\,\mathrm{e}^{-\alpha_2}\,. \end{aligned} \tag{2.128}$$

But

$$\frac{\partial f_1(t_c)}{\partial \alpha_1} = \frac{1}{2}\,\mathrm{e}^{2t_c}\,\frac{\partial t}{\partial \alpha_1} \quad \text{and} \quad \frac{\partial f_2(t_c)}{\partial \alpha_1} = -\frac{3}{2}\frac{\partial t}{\partial \alpha_1}$$

and setting $\frac{\partial t}{\partial \alpha_1} = 0$ in (2.128) we obtain

$$1 + \varepsilon f_1(t_c)\,\mathrm{e}^{\alpha_1} - \varepsilon f_2(t_c)\,\mathrm{e}^{-\alpha_1} = 0. \tag{2.129}$$

Similarly, if we differentiate equation (2.127) with respect to α_2 and then set $\frac{\partial t}{\partial \alpha_2}$ to be zero in the resulting equation, we get an equation exactly the same as (2.129) but with α_2, i.e.

$$1 + \varepsilon f_1(t_c)\,\mathrm{e}^{\alpha_2} - \varepsilon f_2(t_c)\,\mathrm{e}^{-\alpha_2} = 0. \tag{2.130}$$

Since equations (2.129) and (2.130) are of the same type, they may be written simultaneously as

$$1 + \varepsilon f_1(t_c)\,\mathrm{e}^{\alpha_{1,2}} - \varepsilon f_2(t_c)\,\mathrm{e}^{-\alpha_{1,2}} = 0. \tag{2.131}$$

If we multiply the above equation by $\mathrm{e}^{\alpha_{1,2}}$, then the resulting equation is quadratic with respect to $\mathrm{e}^{\alpha_{1,2}}$. The possible roots are

$$\mathrm{e}^{\alpha_1} = \frac{-1 + \sqrt{1 + 4\varepsilon^2 f_1(t_c) f_2(t_c)}}{2\varepsilon f_1(t_c)},$$

$$\mathrm{e}^{\alpha_2} = \frac{-1 - \sqrt{1 + 4\varepsilon^2 f_1(t_c) f_2(t_c)}}{2\varepsilon f_1(t_c)}.$$

Note that the expression under the square root sign is less than one for all $t > 0$, therefore, the right-hand side is negative for both roots $\mathrm{e}^{\alpha_{1,2}}$ for all $t > 0$. Hence, there are no real solutions which implies in turn that z^+ characteristics emanating from different initial points do not cross. However, we can show that at least to order ε^2 these characteristics may become tangent after some time. Two characteristics z^+ are tangent when $\frac{\partial z^+}{\partial z_0} = 0$ which gives the equation of an envelope of the one parameter family of characteristics z^+. This envelope is the curve along which singularities propagate.

2.7.3 Envelopes of Characteristics

As was mentioned in the previous subsection, the equation of the envelope of the characteristics is $\frac{\partial z^+}{\partial z_0} = 0$. Differentiating equation (2.125) with respect to z_0, we get

$$\frac{\partial z^+}{\partial z_0} = 1 + \varepsilon f_1(t_c)\,\mathrm{e}^{z_0} - \varepsilon f_2(t_c)\,\mathrm{e}^{-z_0} + O(\varepsilon^2) = 0$$

that implies

$$\varepsilon f_1(t_c)\,\mathrm{e}^{2z_0} + \mathrm{e}^{z_0} - \varepsilon f_2(t_c) = 0.$$

This is the same type of equation as in (2.131). The roots are

$$\mathrm{e}^{z_0} = \frac{-1 + \sqrt{1 + 4\varepsilon^2 f_1(t_c) f_2(t_c)}}{2\varepsilon f_1(t_c)} = \mathrm{e}^{\alpha_1}$$

and

$$\mathrm{e}^{z_0} = \frac{-1 - \sqrt{1 + 4\varepsilon^2 f_1(t_c) f_2(t_c)}}{2\varepsilon f_1(t_c)} = \mathrm{e}^{\alpha_2}\,.$$

We first use the root e^{α_1} in the equation of characteristics z^+ (2.125).

$$z^+ = \ln\left[\frac{-1 + \sqrt{1 + 4\varepsilon^2 f_1(t_c) f_2(t_c)}}{2\varepsilon f_1(t_c)}\right] + t_c + \varepsilon f_1(t_c)\frac{-1 + \sqrt{1 + 4\varepsilon^2 f_1(t_c) f_2(t_c)}}{2\varepsilon f_1(t_c)}$$

$$+\varepsilon f_2(t_c)\frac{2\varepsilon f_1(t_c)}{-1+\sqrt{1+4\varepsilon^2 f_1(t_c)f_2(t_c)}}+O(\varepsilon^2)$$

$$=\ln\left[\frac{-1+1+2\varepsilon^2 f_1(t_c)f_2(t_c)+O(\varepsilon^4)}{2\varepsilon f_1(t_c)}\right]+t_c+\varepsilon f_1(t_c)$$

$$*\,\frac{-1+1+2\varepsilon^2 f_1(t_c)f_2(t_c)+O(\varepsilon^4)}{2\varepsilon f_1(t_c)}+\frac{2\varepsilon^2 f_1(t_c)f_2(t_c)}{-1+1+2\varepsilon^2 f_1(t_c)f_2(t_c)+O(\varepsilon^4)}$$

$$+O(\varepsilon^2)=\ln(2\varepsilon f_2(t_c))+t_c+1+O(\varepsilon^2).$$

Therefore,

$$z^+=\ln(2\varepsilon f_2(t_c))+t_c+1+O(\varepsilon^2) \tag{2.132}$$

is the equation of the envelope of the family of z^+ characteristics. Setting $z^+=0$ gives the critical time t_c when the envelope reaches the real axis,

$$\ln(2\varepsilon f_2(t_c))=-(t_c+1),$$

hence solving for ε we obtain

$$\varepsilon=\frac{1}{2f_2(t_c)}\,\mathrm{e}^{-(t_c+1)}.$$

We observe that in order for the right-hand side to be of order ε, time t_c has to be large. Taking ln of both sides, we get

$$\ln\varepsilon=-(t_c+1)-\ln(2f_2(t_c))$$

but $f_2(t_c)=-\frac{3}{2}t_c$, therefore,

$$\ln\varepsilon=-(t_c+1)-\ln(-3t_c).$$

For large t_c, the dominant term in the right hand side of the above equation is $-t_c$ (the term $\ln(-3t_c)$ is of order $\ln t_c$ and therefore, for large t_c this term can be neglected). Therefore, to the leading order

$$\ln\varepsilon=-t_c,$$

whence we obtain the value for the critical time t_c to the leading order as $\varepsilon \to 0$, i.e.

$$t_c = \ln \frac{1}{\varepsilon} + O(\varepsilon^2). \tag{2.133}$$

The use of the other root e^{α_2} gives the same estimate of the critical time t_c. Indeed, substituting e^{α_2} into z^+ and using the smallness of ε, we obtain

$$\begin{aligned} z^+ &= \ln \left[\frac{-1 - \sqrt{1 + 4\varepsilon^2 f_1(t_c) f_2(t_c)}}{2\varepsilon f_1(t_c)} \right] + t_c + \varepsilon f_1(t_c) \frac{-1 - \sqrt{1 + 4\varepsilon^2 f_1(t_c) f_2(t_c)}}{2\varepsilon f_1(t_c)} \\ &\quad + \varepsilon f_2(t_c) \frac{2\varepsilon f_1(t_c)}{-1 - \sqrt{1 + 4\varepsilon^2 f_1(t_c) f_2(t_c)}} + O(\varepsilon^2) \\ &= \ln \left[-\frac{1}{\varepsilon f_1(t_c)} + O(\varepsilon) \right] + t_c - 1 + O(\varepsilon^2). \end{aligned}$$

Equating z_0 to zero yields

$$\ln \frac{1}{\varepsilon} + \ln \left(-\frac{4}{\mathrm{e}^{2t_c} - 1} \right) + t_c - 1 = 0$$

or

$$\ln \frac{1}{\varepsilon} + \ln(-4) - 2t_c - \ln(1 - \mathrm{e}^{-2t_c}) + t_c - 1 = 0.$$

Ignoring lower order terms for large t_c, we obtain

$$t_c \sim \ln \frac{1}{\varepsilon},$$

same as in (2.133).

2.7.4 Comparison of Singular Times between Theory and Numerics

The theory presented in the previous subsection can be used to estimate singular times once ε is given. In what follows we compare singular times obtained by numerical solution of the evolution equations (2.98), (2.99) and analytical prediction of the singular time given in (2.133). The numerical method described in Subsection 2.8.1

was used to obtain solutions of the governing equations. Computations were stopped when the maximum value of S_x or W_x reached a value of 10. The time when this happens is defined to be the critical time (or the singular time) t_c. Solutions were obtained for representative values of ε in the range $0.0001 \leq \varepsilon \leq 0.1$. As the numerical experiments show, the solution appears to develop an infinite-slope singularity both in the interface S and vortex sheet strength W. As opposed to the Subsection 2.8.2 where a relatively large initial perturbation $\varepsilon = 0.3$ was used and the vortex sheet strength W had the slope growing faster then the slope in the interface S, for smaller values of $\varepsilon < 0.1$, the function S develops the singularity faster than W. The experiment shows that a fixed time-step $t = 10^{-5}$ and $n = 512$ points were enough to produce numerical solutions, at least with graphical accuracy (in the next section we will need to use up to $n = 4096$ points as well as adjustable decreasing time step in order to achieve the maximum slopes in S_x or W_x being set to 50).

The evidence of the finite-time singularities may also be obtained by numerical evaluation of the analytical prediction of the critical times from (2.133). In Figure 2.20 we compare the critical times obtained by numerical solution of the evolution equations (2.98), (2.99) as was described above (solid line) and critical times calculated by using (2.133) (open circles). We plot critical times, t_c, versus initial amplitude ε. As it can be seen, the agreement is not very good, but the analytical prediction shows only the leading order behavior of t_c as the initial perturbation ε tends to 0.

In the paper by Papageorgiou and Orellana [71], the correction to the singular time t_c of the order $\ln(\ln \frac{1}{\varepsilon})$ is given. Even though, the problem of cylindrical jet breakup studied in that article is different, we observe some similarity with our problem in the system of conservation laws and analytical construction of the characteristics. In addition, when we obtained the leading order estimate of the critical time t_c, we ignored terms of order $\ln t_c$. This suggests that we also have in

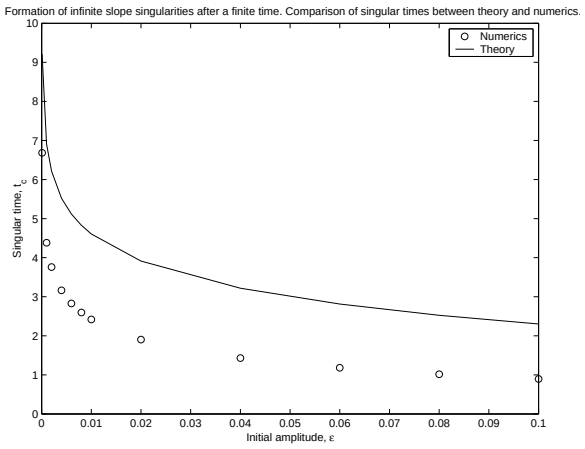

Figure 2.20 Comparison of singular times between theory and numerics.

our problem a correction term $A \cdot \ln(\ln \frac{1}{\varepsilon})$ where A is a constant. We empirically determine $A = 1.2$ as described below. Of course, more strict theoretical analysis is needed to justify such a correction term, but we are going to find this constant A by numerically fitting the difference between the numerical and analytical critical times presented on Figure 2.20.

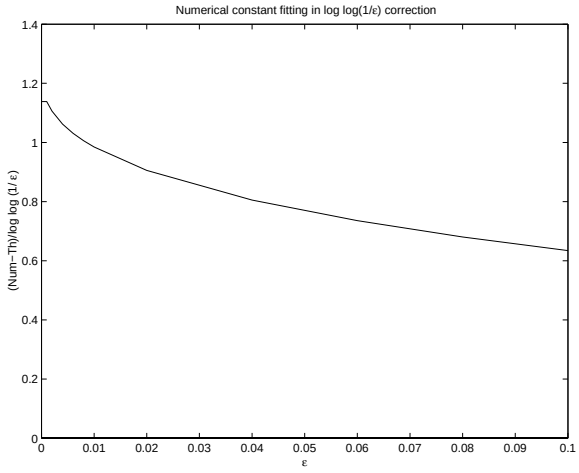

Figure 2.21 Numerical constant fitting in $O(\ln(\ln \frac{1}{\varepsilon}))$ term.

Figure 2.21 contains the graph of the difference of the numerical critical times and analytical ones divided by $\ln(\ln \frac{1}{\varepsilon})$ versus ε. As it is seen from the graph, we can

use $A = 1.0$ or $A = 1.2$. The latter choice produces the better correction term in t_c. Therefore, the estimation for the critical time is

$$t_c \approx \ln \frac{1}{\varepsilon} + (1.2) \ln \left(\ln \frac{1}{\varepsilon} \right). \tag{2.134}$$

The comparison of singular solutions obtained by numerical solution of the evolution equations with the corrected estimate of t_c in (2.134) is presented in Figure 2.22. The agreement is found to be very good.

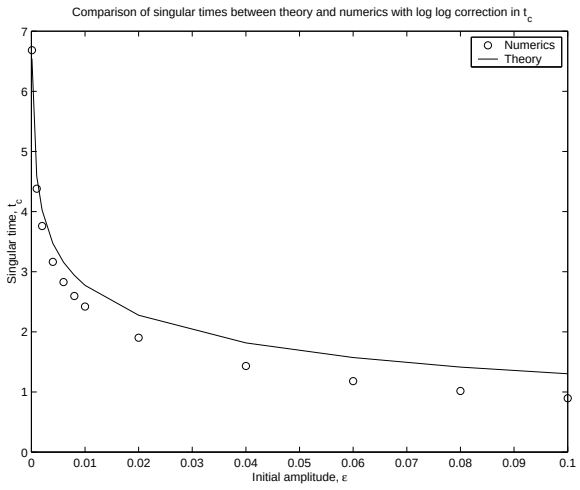

Figure 2.22 Comparison of singular times between corrected theoretical estimate and numerics.

Remark. For the case of $\alpha \neq 0$, i.e., when we have two immiscible fluids of different densities, the system of governing equations has regions where it is elliptic and where it is hyperbolic depending on values of the interface S and vortex sheet strength W. It would be possible to start from the initial condition of one type, let us say, elliptic, and then with time evolution to get a solution of the other type, hyperbolic. However, if the initial perturbation is small enough, following Lax' theory, [56] the solution will preserve its type with time. The analysis of this case is the subject of future work.

2.8 Numerical Solution of Evolution Equations

2.8.1 Numerical Method

In this section we solve the initial value problem (2.36) and (2.37) numerically. It follows from the linear stability results of Section 2.4 that the regularization of the system at high wavenumbers can at best be dispersive and is provided by surface tension. Physically this arises from the conservative nature of the governing equations We choose to solve (2.36), (2.37) subject to periodic boundary conditions

$$S(x+2\pi,t) = S(x,t), \quad W(x+2\pi,t) = W(x,t).$$

A pseudo-spectral scheme with time integration performed in Fourier space is used. This scheme is based on the ideas of Fornberg and Whitham (1978) [32] developed for the KdV equation. In view of the third derivative term in (2.37), a rough accuracy criterion is $k_{max}^3 dt < 1$ where dt is the time step. Such a criterion is quite severe in view of the fact that *twenty* fast fourier transforms (FFT's) per time-step are needed for a four level scheme, for example.

Using S and W as dependent variables in (2.36) and (2.37) implies that equation (2.37) will have the term with S_{xxx}, the highest derivative of S, present nonlinearly. We introduce a new dependent variable

$$Q = (1-\alpha S)W, \tag{2.135}$$

and rewrite the evolution equations (2.36) and (2.37) as

$$S_t = \frac{2}{(1-\alpha S)^2}\left[(1-\alpha S)(1-S^2)Q_x + (\alpha S^2 - 2S + \alpha)QS_x\right], \tag{2.136}$$

$$\begin{aligned} Q_t \;=\; & \frac{\alpha}{F}S_x - \gamma S_{xxx} + \frac{2Q}{(1-\alpha S)^3}\left[(\alpha^2-1)QS_x\right. \\ & + \left.(1-\alpha S)Q_x(\alpha S^2 - 2S + \alpha)\right]. \end{aligned} \tag{2.137}$$

This form of evolution equations is used for numerical solution of the initial value problem.

The case of equal densities ($\alpha = 0$) can be implemented efficiently by the split time-step scheme since in this case it is possible to split the linear and nonlinear operators and treat them separately.

We use a pseudo-spectral scheme (see also Fornberg and Whitham (1978) [32], Papageorgiou and Smith (1988) [72]). Time marching is done by a fourth order Runge-Kutta method.

Computational accuracy is checked throughout the evolution by monitoring the three conserved quantities we found. These are the total energy of the system, equation (2.46), and the integrals

$$\int_0^{2\pi} S dx \quad \text{and} \quad \int_0^{2\pi} (W - \alpha SW) dx = \int_0^{2\pi} Q dx.$$

which follow directly from (2.36), (2.37). For the computations reported here the error in the constancy of these quantities was of the order of machine precision (double precision is used throughout). If the accuracy criteria associated with the dispersive regularization of the equations are violated, however, the conserved quantities drift slightly and the error builds up as time increases. The conclusion after many numerical experiments is that 512 modes at early times and then up to 2048 or even 4096 modes at later times close to the time of any singularities, and provide an optimal spatial discretization in view of the time-step restrictions, and for the values of the surface tension coefficient studied here.

2.8.2 Computational Results

The initial conditions used are

$$S(t = 0, x) = a \sin(x), \quad W(t = 0, x) = W_0 - a \cos(x)$$

with the corresponding initial value of $Q(t, x)$. Here a, $|a| < 1$, is the amplitude of the perturbation, W_0 is initial vortex sheet strength and the range of x is $(0, 2\pi)$. These conditions represent a sinusoidal initial perturbation to a flat vortex sheet of strength W_0.

Numerical solutions presented in this subsection have the following parameters fixed

$$\alpha = 0,\ F = 1.0,\ W_0 = 1.0,\ a = 0.3.$$

The value $\alpha = 0$ models the situation of both fluids having the same density. The following set of results examines the effect of the surface tension γ on the interfacial evolution and corresponding vortex sheet strength.

The initial condition for the interface is an odd function of x whereas that for the vortex sheet strength is even. On the graphs, the symmetry is about $x = \pi$. Equations preserve this symmetry during the course of evolution. The parity of numerical solutions is preserved as well.

Calculations were run until the maximum of the absolute values of S_x and Q_x reached a preset value of 50. It is found numerically (see below) that a finite-time singularity is encountered. The time of the singularity is denoted by t_c. It is observed that the W_x (the derivative of the vortex sheet strength) is more singular than S_x as $t \to t_{c^-}$ for the initial perturbation of amplitude $a = 0.3$ reported here.

The results presented in this section have some similarity with those obtained by Siegel [84] where the author studied singularity formation in the Kelvin-Helmholtz instability with surface tension.

Case $\gamma = 0$. The initial condition for the vortex sheet strength has a single local maximum at $x = \pi$. As time evolves the slope of the vortex sheet in the vicinity of this maximum point grows (the value of the maximum remains bounded) developing a cusp singularity at the critical time t_c. The vortex sheet strength at $x = \pi$ at the critical time is 2.5. The interface exhibits bounded growth with time and develops an infinite slope at the critical time; the amplitude remains bounded and does not exceed a value of 0.45. The final computed time is $t_f = 0.206991735$.

The case of zero surface tension corresponds to $k_c \to \infty$ where k_c is cut-off number from the linearized theory investigated in Section 2.4.

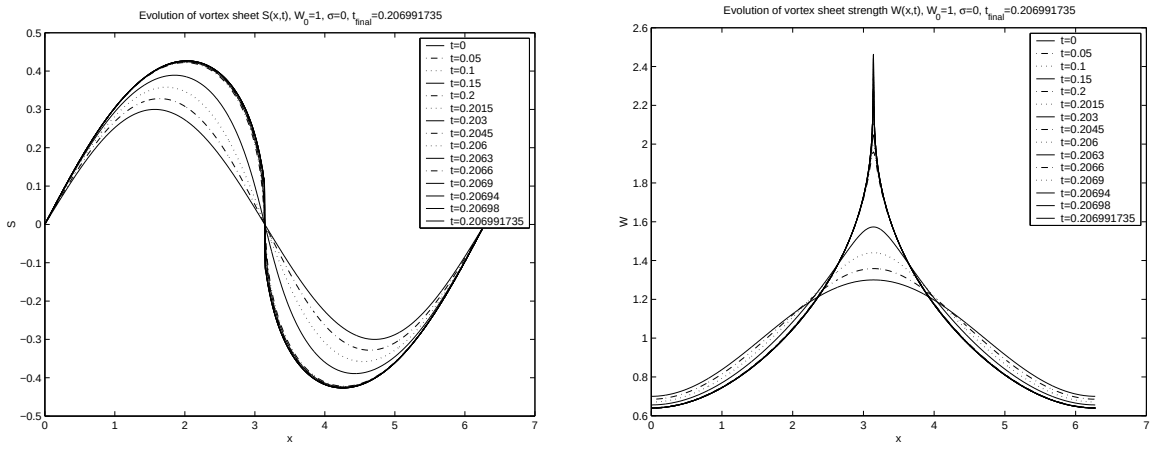

Figure 2.23 $\gamma = 0$, final time $t_f = 0.206991735$. Evolution of: (a) interface $S(x,t)$; (b) vortex sheet strength $W(x,t)$.

Theoretical analysis of the case with zero surface tension by using Riemann invariants is done in Section 2.7. It is shown there that characteristics cross and reach the real axis in finite time thus forming a singularity of the physical solution. The slope of the interface is infinite at the critical time but its amplitude remains finite and less then 1.

As surface tension assumes non-zero values, the situation changes. For some range of parameters γ we observe the finite time singularity formation. This range of γ corresponds to that when the system has at least one unstable mode that will grow to form the singularity. See Section 2.4 and stability diagram 2.3 for more details.

Case $\gamma = 0.01$. The interface at the time close to critical forms two symmetric corners located near the point of symmetry $x = \pi$. The amplitude does not exceed .45. The vortex sheet strength curve narrows down around $x = \pi$ but does not form a cusp at this point. It still has one single local maximum. This value is 2.4 which is slightly smaller than for $\gamma = 0.0$. The final computed time is $t_f = 0.22$.

The number of linearly unstable modes k_c can be calculated using formula (2.51). For $\gamma = 0.01$, this number is $k_c = 28$.

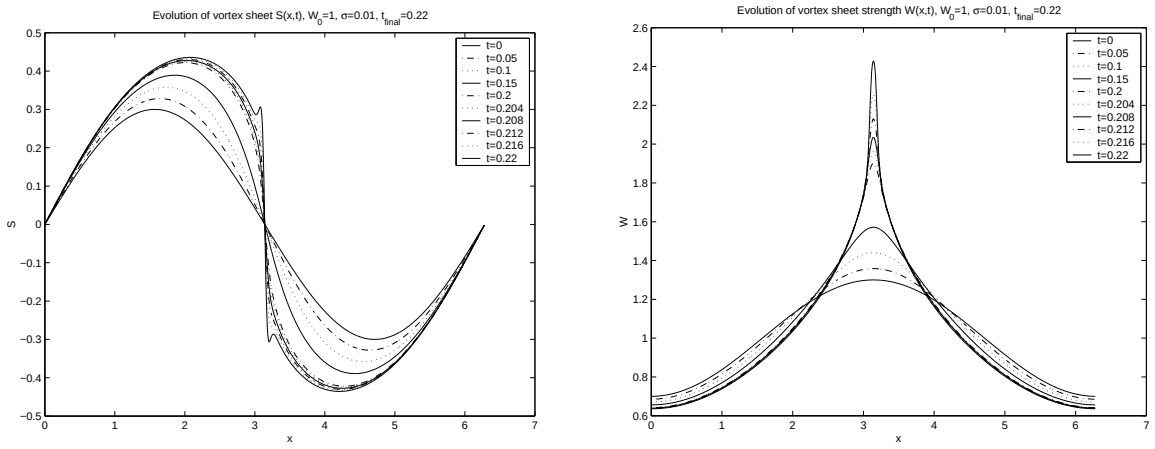

Figure 2.24 $\gamma = 0.01$, final time $t_f = 0.22$. Evolution of: (a) interface $S(x,t)$; (b) vortex sheet strength $W(x,t)$.

Case $\gamma = 0.1$. The two humps (a local maximum to the left of $x = \pi$ and local minimum to the right) on the interface that were observed for the previous case grow faster. As γ increases, they are more pronounced at times closer to $t = t_c$. The support of these humps is wider than for smaller value of γ. At later times the slope of the interface connecting these humps gets bigger. The interfacial amplitude at the final time reaches the value 0.8. The main difference for the vortex sheet is that now it has two local maxima formed. Comparing with the previous case when $\gamma = 0.01$ where we observed only one local maximum, for the case of $\gamma = 0.1$ shows that at the previous value of the surface tension, the support for the local maximum broadens as γ increases and splits to give two local maxima. The vortex sheet strength reaches the value 3.8 at the final computed time, $t_f = 0.26926337$.

The critical wave number is $k_c = 8$. Decreasing the critical wave number k_c, we decrease the number of unstable modes, and as a consequence, the singularity formation delays.

Case $\gamma = 1.0$. Interface grows and reached the value 0.95 which is close to 1 that is close to the walls. The distance between two vorticity maxima increases and

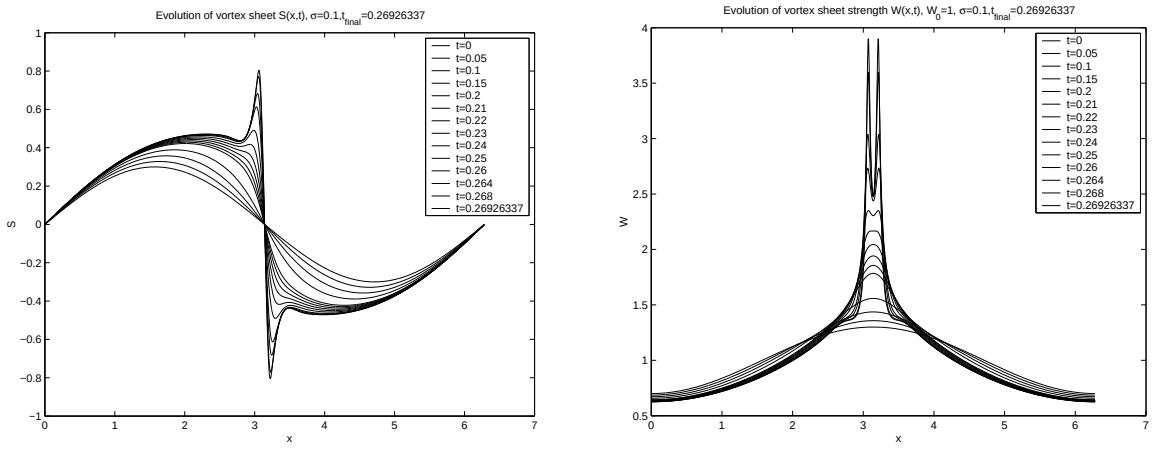

Figure 2.25 $\gamma = 0.1$, final time $t_f = 0.26926337$. Evolution of: (a) interface $S(x,t)$; (b) vortex sheet strength $W(x,t)$.

is about 0.7 at the critical time. These maxima have values 4.7. The final time is $t_f = 0.40707$. There are $k_c = 2$ linearly unstable modes in this case.

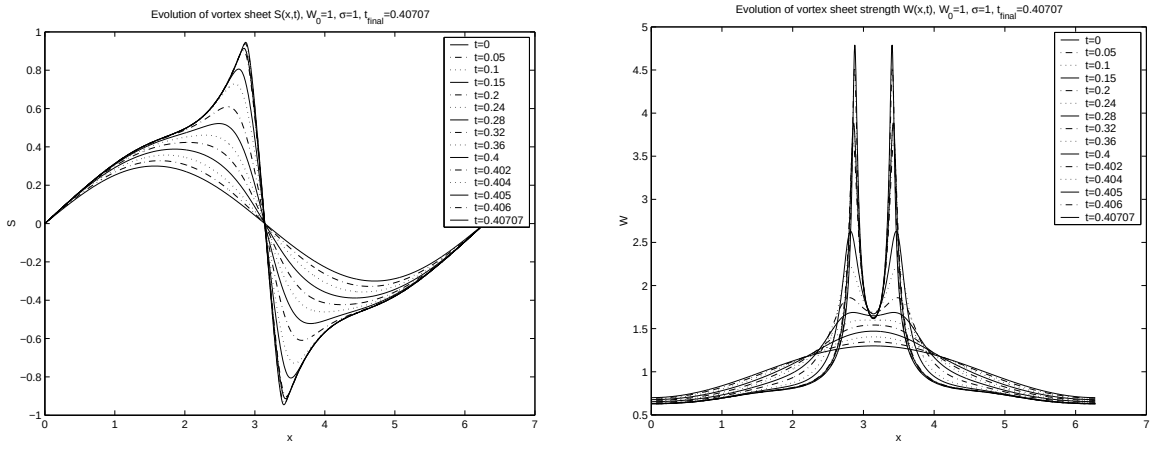

Figure 2.26 $\gamma = 1.0$, final time $t_f = 0.40707$. Evolution of: (a) interface $S(x,t)$; (b) vortex sheet strength $W(x,t)$.

Case $\gamma = 3.0$. The amplitude of the interface at the critical time is 0.96. The corners are wider than in the previous case. They affect almost the whole solution. The distance between vorticity maxima is about 1.2. Not only the distance with vortex sheet strength increases, these peaks themselves become wider. The final time is $t_f = 0.669217999$. In this case, we have only one linearly unstable mode since $k_c = 1$ for $\gamma = 3.0$.

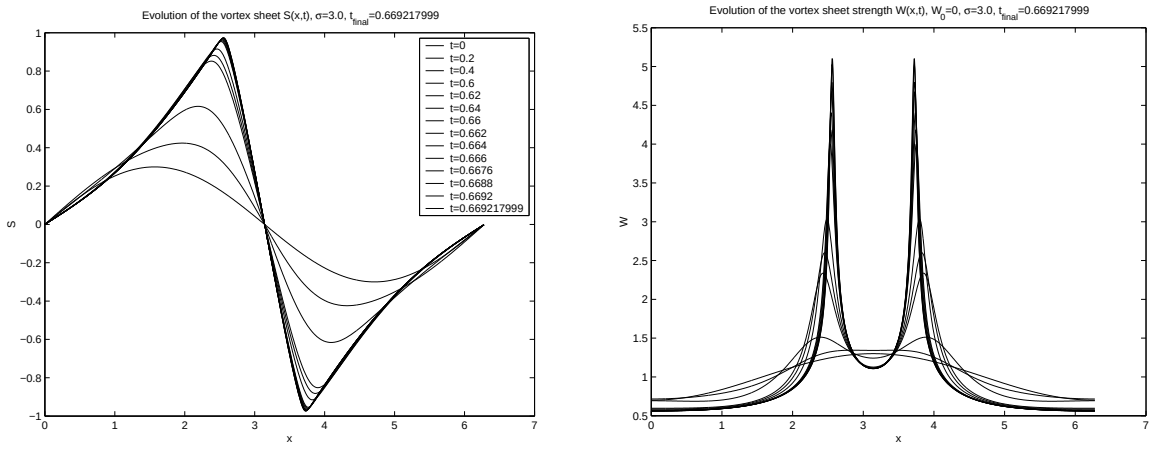

Figure 2.27 $\gamma = 3.0$, final time $t_f = 0.669217999$. Evolution of: (a) interface $S(x,t)$; (b) vortex sheet strength $W(x,t)$.

Case $\gamma = 5.0$. The sides of the corners on the interface are almost straight lines. The interface is very close to the walls. The amplitude is around 0.99. The vortex sheet strength has maxima vorticity peaks at the distance is about 2.0. The final time is $t_f = 1.244447$. We still have only one linearly unstable mode, i.e. $k_c = 1$.

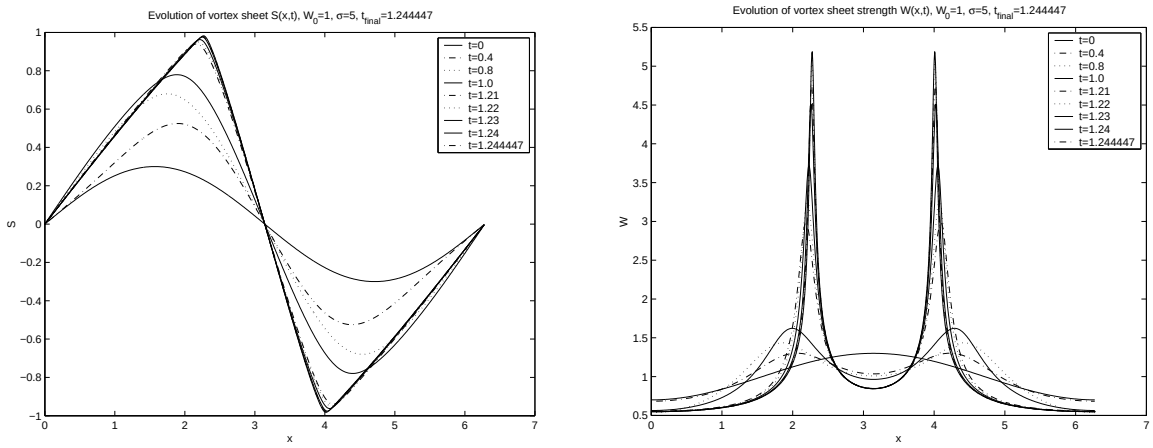

Figure 2.28 $\gamma = 5.0$, final time $t_f = 1.244447$. Evolution of: (a) interface $S(x,t)$; (b) vortex sheet strength $W(x,t)$.

For values of γ from 0.1 to 5.0, the vortex sheet strength curve first becomes dimple shaped. Then the lobes where vorticity has a maximum, narrow down and grow with the slope growing as well. As γ increases, lobes get higher values and the distance between these peaks increases as well. The slope of the vortex sheet strength

at the final time reaches the final preset tolerance and the solution has a cusp type shape. As γ increases but stays within the regime of unstable modes, the singularity forms later in time.

In all cases, the value of W remains bounded.

Case $\gamma = 13.0$. In this case there are no unstable modes, so the solution for both interface and vortex sheet strength just oscillate with time. The representative numerical solutions are constructed for final time $t_f = 5.0$.

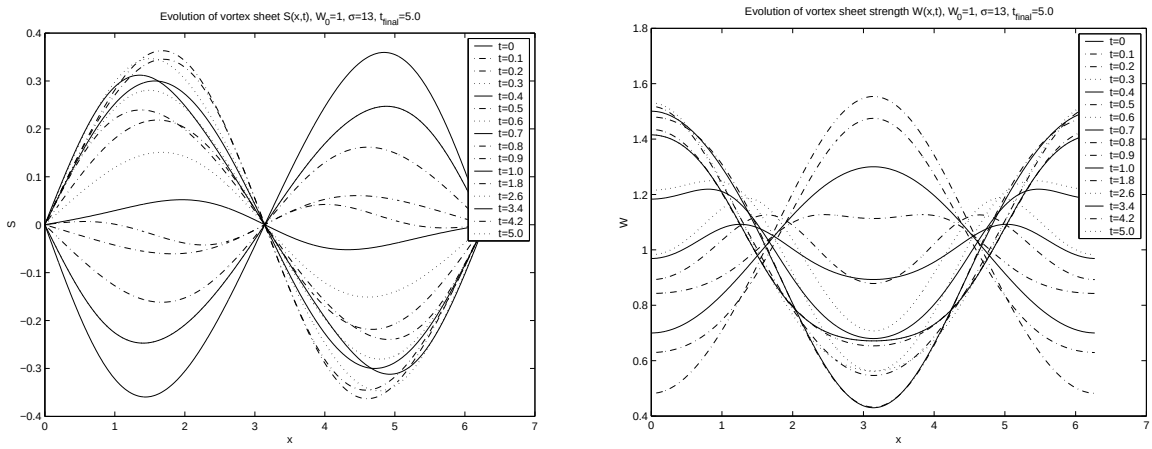

Figure 2.29 $\gamma = 5.0$, final time $t_f = 5.0$. Evolution of: (a) interface $S(x,t)$; (b) vortex sheet strength $W(x,t)$.

CHAPTER 3

THREE-DIMENSIONAL NONLINEAR WATER WAVES PROBLEM

In this chapter we generalize the problem of the interfacial evolution of two fluids to the three-dimensional case.

3.1 Formulation and Derivation of Governing Equations: Layers of Different Thicknesses

We consider a system of two incompressible, inviscid and immiscible fluids which are bounded between two parallel infinite plates. Denote the upper and lower fluids by subscripts 1 and 2, respectively. In dimensional variables, the height of the upper and lower walls of the channel are h_1 and h_2, respectively. The densities are assumed to be ρ_1 and ρ_2. Cartesian coordinates (x, y, z) will be used with the undisturbed interface at $z = 0$. At later times, the deformed interface is given by the function $z = S(x, y, t)$. The geometry of the problem is given in Figure 3.1.

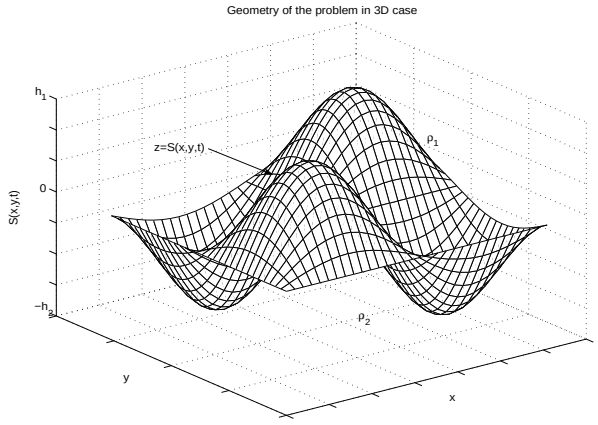

Figure 3.1 Geometry of the problem in 3D case. Interface between two fluids.

Assuming the flow of each fluid away from the interface to be irrotational, enables one to introduce the complex potential ϕ_i, $i = 1, 2$, for the upper and lower

fluids. The evolution equations are the following (see Appendix A for derivation details).

$$(\Delta + \partial_{zz})\,\phi_i = 0, \quad i = 1, 2, \tag{3.1}$$

$$\phi_{1z} = 0 \quad \text{at} \quad z = h_1, \tag{3.2}$$

$$\phi_{2z} = 0 \quad \text{at} \quad z = -h_2, \tag{3.3}$$

$$\phi_{1z} = S_t + (\nabla\phi_1 \cdot \nabla S) \quad \text{on} \quad z = S^+(\vec{x}, t), \tag{3.4}$$

$$\phi_{2z} = S_t + (\nabla\phi_2 \cdot \nabla S) \quad \text{on} \quad z = S^-(\vec{x}, t), \tag{3.5}$$

$$\begin{aligned} \rho_1 \left[\phi_{1t} \; + \; \frac{1}{2}(\Delta + \partial_{zz})\,\phi_1 + gz\right] - \rho_2 \left[\phi_{2t} + \frac{1}{2}(\Delta + \partial_{zz})\,\phi_2 + gz\right] \\ = \; -\frac{\sigma_0}{\left[1 + S_x^2 + S_y^2\right]^{3/2}} \left(S_{xx} + S_y^2 S_{xx} + S_{yy} + S_x^2 S_{yy} - 2S_x S_y S_{xy}\right). \end{aligned} \tag{3.6}$$

The approximations and physical assumptions made in deducing evolution equations become clear once the problem is non-dimensionalized. The long wave analysis is based on the smallness of the ratio of upper layer channel height h_1 (note that we assume $h_1 \sim h_2$) to a typical wavelength of the interface. Let l be a typical wavelength and c_0 a typical wavespeed. Non-dimensional variables with the superscript $*$ are introduced as follows

$$\begin{aligned} x^* &= \frac{x}{l}, \quad y^* = \frac{y}{l}, \quad z^* = \frac{z}{h_1}, \quad t^* = \frac{c_0}{2l}t, \quad S^* = \frac{S}{h_1}, \\ \phi_i^* &= \frac{1}{c_0 l}\phi_i, \quad p_i^* = \frac{2}{\rho_2 c_0^2}p_i, \quad i = 1, 2. \end{aligned} \tag{3.7}$$

Changing to dimensionless variables and dropping $*$, the governing equations become

$$\varepsilon^2\Delta\phi_1 + \phi_{1zz} = 0, \quad S < z < 1, \tag{3.8}$$

$$\varepsilon^2\Delta\phi_2 + \phi_{2zz} = 0, \quad -D < z < S, \tag{3.9}$$

$$\phi_{1z} = 0 \quad \text{on} \quad z = 1, \tag{3.10}$$

$$\phi_{2_z} = 0 \quad \text{on} \quad z = -D, \tag{3.11}$$

$$\varepsilon^2 \left(\frac{1}{2} S_t + \nabla \phi_i \cdot \nabla S \right) = \phi_{i_z} \quad \text{on} \quad z = S(x, y, t), \quad i = 1, 2, \tag{3.12}$$

$$\begin{aligned} \rho \left[\phi_{1t} \right. &+ \left. (\phi_{1x})^2 + \left(\phi_{1y} \right)^2 + \frac{1}{\varepsilon^2} (\phi_{1z})^2 + \frac{1}{F} S \right] \\ &- \left[\phi_{2t} + (\phi_{2x})^2 + \left(\phi_{2y} \right)^2 + \frac{1}{\varepsilon^2} (\phi_{2z})^2 + \frac{1}{F} S \right] \\ &= -\varepsilon \tilde{\sigma} \frac{\left\{ S_{xx} + S_{yy} + \varepsilon^2 \left[S_x^2 S_{yy} + S_y^2 S_{xx} \right] \right\}}{[1 + \varepsilon^2 (S_x^2 + S_y^2)]^{3/2}} \quad \text{on} \quad z = S. \end{aligned} \tag{3.13}$$

The parameters appearing above are the depth ratio D, the upper layer thickness to wavelength ratio ε, the upper to lower fluid density ratio ρ, the dimensionless surface tension coefficient $\tilde{\sigma}$ and the Froude number F of the flow based on the upper layer thickness, the latter being the ratio of the typical speed to the speed of small-amplitude surface waves in shallow water:

$$D = \frac{h_1}{h_2}, \quad \varepsilon = \frac{h_1}{l}, \quad \rho = \frac{\rho_1}{\rho_2}, \quad \tilde{\sigma} = \frac{2\sigma_0}{l c_0^2 \rho_2}, \quad F = \frac{c_0^2}{2 g h_1}. \tag{3.14}$$

In what follows canonical evolution equations are derived that describe the dynamics in the asymptotic limit $\varepsilon \to 0$. It is desirable to retain both gravity and surface tension forces in the canonical equations, which can then be used to analyze individual limits corresponding to different physical situations. Since the curvature of the interface is "small" in dimensional terms, it is not surprising to find that strong surface tension is required to make capillary effects comparable to those of gravity. From the equations above it is seen that the scaling

$$\tilde{\sigma} = \frac{\sigma}{\varepsilon}$$

is required with σ an order one parameter. Multiply both sides of the Bernoulli equation (3.13) by ε^2 and use the parameter σ as the dimensionless surface tension

coefficient to obtain the equation

$$\begin{aligned}\rho\varepsilon^2\left[\phi_{1t}\right. &+ \left.(\phi_{1x})^2+\left(\phi_{1y}\right)^2+\frac{1}{\varepsilon^2}(\phi_{1z})^2+\frac{1}{F}S\right]\\ &- \varepsilon^2\left[\phi_{2t}+(\phi_{2x})^2+\left(\phi_{2y}\right)^2+\frac{1}{\varepsilon^2}(\phi_{2z})^2+\frac{1}{F}S\right]\\ &= -\frac{\sigma\varepsilon^2\left\{S_{xx}+S_{yy}+\varepsilon^2\left[S_x^2S_{yy}+S_y^2S_{xx}\right]\right\}}{[1+\varepsilon^2(S_x^2+S_y^2)]^{3/2}} \quad \text{on} \quad z=S. \end{aligned} \tag{3.15}$$

The problem stated above is exact and results from the chosen non-dimensionalization, for example, setting $\varepsilon = 1$, (3.8)–(3.12), (3.15) are the equations for a non-slender two fluid-system. In what follows we study nonlinear solutions valid in the limit $\varepsilon \to 0$.

In the limit $\varepsilon \to 0$, the only small parameter appearing in the governing equations (3.8)–(3.12), (3.15) is ε^2, and we assume the following asymptotic expansions

$$S = S^{(0)}+\varepsilon^2 S^{(1)}+\varepsilon^4 S^{(2)}+\ldots, \quad \phi_i = \phi_i^{(0)}+\varepsilon^2\phi_i^{(1)}+\varepsilon^4\phi_i^{(2)}+\ldots, \quad i=1,2. \tag{3.16}$$

At leading order, we have the following problem

$$\phi_{1\,zz}^{(0)} = 0, \quad S^{(0)} < z < 1, \tag{3.17}$$

$$\phi_{2\,zz}^{(0)} = 0, \quad -D < z < S^{(0)}, \tag{3.18}$$

$$\phi_{1\,z}^{(0)} = 0 \quad \text{on} \quad z=1 \quad \text{and} \quad z=S^{(0)}, \tag{3.19}$$

$$\phi_{2\,z}^{(0)} = 0 \quad \text{on} \quad z=-D \quad \text{and} \quad z=S^{(0)}, \tag{3.20}$$

$$\rho\left(\phi_{1\,z}^{(0)}\right)^2-\left(\phi_{2\,z}^{(0)}\right)^2 = 0 \quad \text{on} \quad z=S^{(0)}.$$

As we see from the last equation, the Bernoulli equation is satisfied automatically at order ε^0. Since $\phi_{1\,zz}^{(0)} = 0$ by (3.17), it follows that $\phi_{1\,z}^{(0)} = f(x,y,t)$ where $f(x,y,t)$ is some function of integration. But $\phi_{1\,z}^{(0)} = 0$ on $z=1$ from (3.19). Hence $f(x,y,t)\equiv 0$. Therefore $\phi_{1\,z}^{(0)} \equiv 0$ and ϕ_1 does not depend on z. Denote it by

$$\phi_1^{(0)} \equiv \Phi_1(x,y,t). \tag{3.21}$$

Similarly, we deduce that ϕ_2 also does not depend on z, and we call this function

$$\phi_2^{(0)} \equiv \Phi_2(x, y, t). \tag{3.22}$$

At the next order, we have

$$\phi_{1\,zz}^{(1)} = -\Delta\phi_1^{(0)}, \quad S^{(0)} < z < 1, \tag{3.23}$$

$$\phi_{2\,zz}^{(1)} = -\Delta\phi_2^{(0)}, \quad -D < z < S^{(0)}, \tag{3.24}$$

$$\phi_{1\,z}^{(1)} = 0 \quad \text{on} \quad z = 1, \tag{3.25}$$

$$\phi_{2\,z}^{(1)} = 0 \quad \text{on} \quad z = -D, \tag{3.26}$$

$$\phi_{i\,z}^{(1)} = \frac{1}{2}S_t^{(0)} + \nabla\phi_i^{(0)} \cdot \nabla S^{(0)} \quad \text{on} \quad z = S^{(0)}, \quad i = 1, 2, \tag{3.27}$$

$$\begin{aligned} \rho\Big[\phi_{1\,t}^{(0)} \;&+\; \left(\phi_{1\,x}^{(0)}\right)^2 + \left(\phi_{1\,y}^{(0)}\right)^2 + \frac{1}{F}S^{(0)}\Big] - \Big[\phi_{2\,t}^{(0)} \\ &+\; \left(\phi_{2\,x}^{(0)}\right)^2 + \left(\phi_{2\,y}^{(0)}\right)^2 + \frac{1}{F}S^{(0)}\Big] = -\sigma\left(S_{xx}^{(0)} + S_{yy}^{(0)}\right). \end{aligned} \tag{3.28}$$

The problem above has the following compatibility conditions

$$\frac{1}{2}S_t^{(0)} + \nabla\phi_1^{(0)} \cdot \nabla S^{(0)} = -(S^{(0)} - 1)\Delta\phi_1^{(0)} \quad \text{on} \quad z = S^{(0)}(x, y, t) \tag{3.29}$$

and

$$\frac{1}{2}S_t^{(0)} + \nabla\phi_2^{(0)} \cdot \nabla S^{(0)} = -(S^{(0)} + D)\Delta\phi_2^{(0)} \quad \text{on} \quad z = S^{(0)}(x, y, t). \tag{3.30}$$

The above conditions may be obtained as follows. Integration of equation (3.23) gives $\phi_{1\,z}^{(1)} = -z\Delta\phi_1^{(0)} + B_1(x, y, t)$, since $\Delta\phi_1^{(0)}$ is a function of x, y and t alone. At $z = 1$, $\phi_{1\,z}^{(1)} = 0$ from equation (3.25), and so $B_1(x, y, t) = \Delta\phi_1^{(0)}$. Hence $\phi_{1\,z}^{(1)} = -(z-1)\Delta\phi_1^{(0)}$. Similarly we obtain that $\phi_{2\,z}^{(1)} = -(z + D)\Delta\phi_2^{(0)}$.

Substitute these expressions for $\phi_{1\,z}^{(1)}$ and $\phi_{2\,z}^{(1)}$ into equations (3.27) for $i = 1$ and $i = 2$, respectively, to obtain

$$\frac{1}{2}S_t^{(0)} + \phi_{1\,x}^{(0)}S_x^{(0)} + \phi_{1\,y}^{(0)}S_y^{(0)} = -(S^{(0)} - 1)\Delta\phi_1^{(0)} \quad \text{on} \quad z = S^{(0)}, \tag{3.31}$$

$$\frac{1}{2}S_t^{(0)} + \phi_{2\,x}^{(0)} S_x^{(0)} + \phi_{2\,y}^{(0)} S_y^{(0)} = -(S^{(0)} + D)\Delta\phi_2^{(0)} \quad \text{on} \quad z = S^{(0)}, \tag{3.32}$$

as given earlier. Equations (3.31) and (3.32) may be written in the shorter form

$$\frac{1}{2}S_t^{(0)} + \nabla\left\{\nabla\phi_1^{(0)}(S^{(0)} - 1)\right\} = 0 \quad \text{on} \quad z = S^{(0)},$$

$$\frac{1}{2}S_t^{(0)} + \nabla\left\{\nabla\phi_2^{(0)}(S^{(0)} + D)\right\} = 0 \quad \text{on} \quad z = S^{(0)}.$$

Adding equations (3.31) and (3.32) gives

$$S_t^{(0)} + \left(S^{(0)}(\phi_1^{(0)} + \phi_2^{(0)})_x\right)_x + \left(S^{(0)}(\phi_1^{(0)} + \phi_2^{(0)})_y\right)_y + D\Delta\phi_2^{(0)} - \Delta\phi_1^{(0)} = 0, \tag{3.33}$$

while subtraction of equations (3.31) and (3.32) yields

$$\left(S^{(0)}(\phi_1^{(0)} - \phi_2^{(0)})_x\right)_x + \left(S^{(0)}(\phi_1^{(0)} - \phi_2^{(0)})_y\right)_y = \Delta\phi_1^{(0)} + D\Delta\phi_2^{(0)}. \tag{3.34}$$

Equation (3.34) is crucial in the reduction of dependent variables as we discuss next.

3.2 Layers of the Equal Thicknesses

When the undisturbed upper and lower fluid thicknesses are equal ($h_1 = h_2$, i.e., $D = 1$) we can reduce the number of dependent variables as shown below. Let

$$\Phi = \frac{1}{2}(\phi_1^{(0)} + \phi_2^{(0)}), \quad \Lambda = \frac{1}{2}(\phi_1^{(0)} - \phi_2^{(0)}), \tag{3.35}$$

so that $\phi_1^{(0)} = \Phi + \Lambda$ and $\phi_2^{(0)} = \Phi - \Lambda$. Equations (3.28), (3.33) and (3.34) can be written in terms of the functions S, Φ and Λ, where we denote $S^{(0)}$ by S

$$\frac{1}{2}S_t + (S\Phi_x)_x + (S\Phi_y)_y - \Delta\Lambda = 0, \tag{3.36}$$

$$(S\Lambda_x)_x + (S\Lambda_y)_y = \Delta\Phi, \tag{3.37}$$

$$\begin{aligned}(\rho - 1)\Phi_t \;&+\; (\rho + 1)\Lambda_t + \rho(\Phi_x + \Lambda_x)^2 + \rho(\Phi_y + \Lambda_y)^2 - (\Phi_x - \Lambda_x)^2 \\ &-\; (\Phi_y - \Lambda_y)^2 + \frac{\rho - 1}{F}S = -\sigma\Delta S.\end{aligned} \tag{3.38}$$

Introducing the Atwood ratio $\alpha = \frac{1-\rho}{1+\rho}$ and a scaled surface tension coefficient $\gamma = \frac{\sigma}{1+\rho}$, we can write equation (3.38) as

$$(\Lambda - \alpha\Phi)_t - (\alpha\Phi_x^2 - 2\Phi_x\Lambda_x + \alpha\Lambda_x^2) - (\alpha\Phi_y^2 - 2\Phi_y\Lambda_y + \alpha\Lambda_y^2) - \frac{\alpha}{F}S = -\gamma\Delta S. \quad (3.39)$$

Equations (3.36) and (3.37) can be also rewritten in the shorter vector form

$$\frac{1}{2}S_t + \nabla \cdot (S\nabla\Phi) - \Delta\Lambda = 0, \quad (3.40)$$

$$\nabla \cdot (S\nabla\Lambda) = \Delta\Phi. \quad (3.41)$$

Integrating equation (3.41) gives $S\nabla\Lambda = \nabla\Phi - \vec{\chi}(t)$, hence $\nabla\Phi = S\nabla\Lambda + \vec{\chi}(t)$. The vector $\chi(t)$ can be found by considering the unperturbed flow at large $|x|$ and $|y|$. Assuming that far away the interface is flat, gives $\lim_{x\to\pm\infty} S(x,y,t) = 0$ and $\lim_{y\to\pm\infty} S(x,y,t) = 0$. The components of $\nabla\Phi$ are the averages of the undisturbed fluid velocities in the two layers in the x- and y-directions, respectively, and if the fluids are at rest far away, it follows that $\vec{\chi}(t) = \vec{0}$. The general case has $\nabla\Phi \neq \vec{0}$ and thus $\vec{\chi}$ may be a vector function of t. The case $\vec{\chi} = \vec{const}$ corresponds to a flow having uniform inviscid stream components in the x- and y-directions, while any time oscillatory far fields, for example, give rise to a time dependence. Eliminating $\nabla\Phi$ from equation (3.40) we obtain

$$S_t + 2\nabla \cdot (S\chi(t)) + 2\nabla \cdot (S^2\nabla\Lambda) = 2\Delta\Lambda. \quad (3.42)$$

Another vector equation is obtained by taking the gradient of (3.39) and eliminating $\nabla\Phi$:

$$\begin{aligned} ([1-\alpha S]\nabla\Lambda)_t &- \alpha\vec{\chi}_t + 2\nabla[(1-\alpha S)\nabla\Lambda\vec{\chi}] - \nabla([\alpha S^2 - 2S + \alpha]\Delta\Lambda) \\ &- \frac{\alpha}{F}\nabla S = -\gamma\nabla(\Delta S). \end{aligned} \quad (3.43)$$

If $\vec{\chi} = \vec{const}$ (corresponding to uniform flow at infinity), we can change to the inertial frame

$$x \to x - 2\int^t \chi_1(\tau)d\tau = x - 2\chi_1 t, \quad y \to y - 2\int^t \chi_2(\tau)d\tau = y - 2\chi_2 t, \quad t \to t$$

and remove $\vec{\chi}$ from the problem. This gives

$$S\nabla\Lambda = \nabla\Phi$$

or in component form

$$S\Lambda_x = \Phi_x \quad \text{and} \quad S\Lambda_y = \Phi_y. \tag{3.44}$$

Equation (3.40) now becomes

$$\frac{1}{2}S_t + \nabla\cdot\Big((S^2-1)\nabla\Lambda\Big) = 0, \tag{3.45}$$

and the Bernoulli equation (3.38) changes to

$$\begin{aligned}(\rho-1)\Phi_t &+ (\rho+1)\Lambda_t + \rho(S+1)^2(\Lambda_x^2+\Lambda_y^2) - (S-1)^2(\Lambda_x^2+\Lambda_y^2)\\ &+ \frac{\rho-1}{F}S = -\sigma\Delta S.\end{aligned} \tag{3.46}$$

Let

$$u = \Lambda_x, \quad v = \Lambda_y, \quad \text{so} \quad \nabla\Lambda = (\Lambda_x,\Lambda_y) = (u,v). \tag{3.47}$$

Physically u and v are velocity jumps across the interface in the x and y directions, respectively.

Differentiate equation (3.46) with respect to x to obtain

$$\begin{aligned}(\rho-1)(Su)_t &+ (\rho+1)u_t + \rho\Big\{(S+1)^2(u^2+v^2)\Big\}_x\\ &- \Big\{(S-1)^2(u^2+v^2)\Big\}_x + \frac{\rho-1}{F}S_x = -\sigma\Delta S_x,\end{aligned} \tag{3.48}$$

while differentiation of equation (3.46) with respect to y gives

$$\begin{aligned}(\rho-1)(Sv)_t &+ (\rho+1)v_t + \rho\Big\{(S+1)^2(u^2+v^2)\Big\}_y\\ &- \Big\{(S-1)^2(u^2+v^2)\Big\}_y + \frac{\rho-1}{F}S_y = -\sigma\Delta S_y.\end{aligned} \tag{3.49}$$

The system of equations (3.45), (3.48) and (3.49) provides the evolution of the unknowns S, u and v, the interfacial shape and the velocity jumps across it in the x and y directions, respectively.

Introduce a vector $\vec{q} = \nabla\Lambda = (u, v)$ with $|\vec{q}|^2 = u^2 + v^2$. Then equations (3.45), (3.48) and (3.49) can be written in the more compact form

$$\frac{1}{2}S_t + \nabla \cdot \left[(S^2-1)\vec{q}\right] = 0, \tag{3.50}$$

$$\begin{aligned}(\rho-1)(S\vec{q})_t &+ (\rho+1)\vec{q}_t + \nabla\left\{\left[\rho(S+1)^2 - (S-1)^2\right]|\vec{q}|^2\right\} \\ &+ \frac{\rho-1}{F}\nabla S = -\sigma\nabla(\Delta S).\end{aligned} \tag{3.51}$$

Using the notation of (3.47), we can rewrite equations (3.51), (3.50) as

$$S_t = -2\left[\{u(S^2-1)\}_x + \{v(S^2-1)\}_y\right], \tag{3.52}$$

$$\begin{aligned}(\rho-1)(Su)_t &+ (\rho+1)u_t + \frac{\rho-1}{F}S_x + \Big[(u^2+v^2)\left\{\rho(S+1)^2\right. \\ &- \left.(S-1)^2\right\}\Big]_x = -\sigma(S_{xx}+S_{yy})_x,\end{aligned} \tag{3.53}$$

$$\begin{aligned}(\rho-1)(Sv)_t &+ (\rho+1)v_t + \frac{\rho-1}{F}S_y + \Big[(u^2+v^2)\left\{\rho(S+1)^2\right. \\ &- \left.(S-1)^2\right\}\Big]_y = -\sigma(S_{xx}+S_{yy})_y.\end{aligned} \tag{3.54}$$

Substituting the expression for S_t from (3.52) into (3.53) and (3.54) we derive the following system of equations given in form:

$$S_t = -2\left[(u_x+v_y)(S^2-1) + 2S(uS_x+vS_y)\right], \tag{3.55}$$

$$\begin{aligned}u_t &= \frac{1}{(\rho-1)S+\rho+1}\Big\{2(\rho-1)u[(u_x+v_y)(S^2-1)+2S(uS_x+vS_y)] \\ &- \frac{\rho-1}{F}S_x - 2(uu_x+vv_x)\{\rho(S+1)^2-(S-1)^2\} \\ &- 2(u^2+v^2)S_x(\rho(S+1)-(S-1)) - \sigma(S_{xxx}+S_{xyy})\Big\},\end{aligned} \tag{3.56}$$

$$\begin{aligned}v_t &= \frac{1}{(\rho-1)S+\rho+1}\{2(\rho-1)v[(u_x+v_y)(S^2-1)+2S(uS_x+vS_y)] \\ &- \frac{\rho-1}{F}S_y - 2(uu_y+vv_y)\{\rho(S+1)^2-(S-1)^2\} \\ &- 2(u^2+v^2)S_y(\rho(S+1)-(S-1)) - \sigma(S_{xxy}+S_{yyy})\}.\end{aligned} \tag{3.57}$$

In terms of the Atwood ratio α defined by $\alpha = \frac{1-\rho}{1+\rho}$ and the scaled surface tension $\gamma = \frac{\sigma}{1+\rho}$, equations (3.56), (3.57) are finally written as

$$\begin{aligned} u_t &= \frac{1}{1-\alpha S}\{-2\alpha u[(u_x+v_y)(S^2-1)+2S(uS_x+vS_y)] \\ &+ \frac{\alpha}{F}S_x - 2(uu_x+vv_x)(-\alpha S^2+2S-\alpha) \\ &- 2(u^2+v^2)S_x(1-\alpha S)-\gamma(S_{xxx}+S_{xyy})\}, \end{aligned} \tag{3.58}$$

$$\begin{aligned} v_t &= \frac{1}{1-\alpha S}\{-2\alpha v[(u_x+v_y)(S^2-1)+2S(uS_x+vS_y)] \\ &+ \frac{\alpha}{F}S_y - 2(uu_y+vv_y)(-\alpha S^2+2S-\alpha) \\ &- 2(u^2+v^2)S_y(1-\alpha S)-\gamma(S_{xxy}+S_{yyy})\}. \end{aligned} \tag{3.59}$$

From equations (3.58) and (3.59), we observe that terms with highest derivative of S, i.e. S_{xxx}, S_{xxy}, S_{xyy}, S_{yyy} appear with nonlinear coefficients. Such terms can cause problems in numerical calculations (i.e., time-step restrictions for stability). In the present problem, the nonlinear coefficients of the highest derivatives of S can be removed by introducing the new dependent variables U and V defined as follows.

$$U = (1-\alpha S)u, \quad V = (1-\alpha S)v. \tag{3.60}$$

The evolution system (3.55), (3.58) and (3.59) changes to

$$\begin{aligned} S_t &= \frac{2}{(1-\alpha S)^2}\Big[(S^2-1)(\alpha S-1)(U_x+V_y) \\ &+ (\alpha S^2-2S+\alpha)(S_xU+S_yV)\Big], \end{aligned} \tag{3.61}$$

$$\begin{aligned} U_t &= \frac{2}{(1-\alpha S)^3}\Big[(\alpha^2-1)S_x(U^2+V^2) \\ &+ (\alpha S^2-2S+\alpha)(1-\alpha S)(UU_x+VV_x)\Big] + \frac{\alpha}{F}S_x - \gamma(S_{xxx}+S_{xyy}), \end{aligned} \tag{3.62}$$

$$\begin{aligned} V_t &= \frac{2}{(1-\alpha S)^3}\Big[(\alpha^2-1)S_y(U^2+V^2) \\ &+ (\alpha S^2-2S+\alpha)(1-\alpha S)(UU_y+VV_y)\Big] + \frac{\alpha}{F}S_y - \gamma(S_{xxy}+S_{yyy}). \end{aligned} \tag{3.63}$$

This form of equations is used in the numerical calculations described in Section 3.5.

3.2.1 Special Cases: $\alpha = 0$ and $\alpha = 1$

We consider some special cases when the Atwood ratio is $\alpha = 0$ or $\alpha = 1$. The first corresponds to the case when both fluids have the same density, whereas the second it when the upper fluid is absent, i.e. has vanishing density.

Case $\alpha = 0$: fluids of the same density

In this case, equations (3.51) and (3.50) can be written as

$$\vec{q}_t + \nabla\left\{2S|\vec{q}|^2\right\} = -\frac{\sigma}{2}\nabla(\Delta S), \tag{3.64}$$

$$\frac{1}{2}S_t + \nabla.\left[(S^2-1)\vec{q}\right] = 0, \tag{3.65}$$

or in component form using equations (3.61)–(3.63)

$$S_t = -2\left[(S^2-1)(U_x+V_y) + 2S(S_xU + S_yV)\right], \tag{3.66}$$

$$U_t = -2\left[S_x(U^2+V^2) + 2S(UU_x + VV_x)\right] - \gamma(S_{xxx} + S_{xyy}), \tag{3.67}$$

$$V_t = -2\left[S_y(U^2+V^2) + 2S(UU_y + VV_y)\right] - \gamma(S_{xxy} + S_{yyy}). \tag{3.68}$$

Case $\alpha = 1$: upper fluid is absent

For upper fluid having zero density, parameter $\rho = 0$ implies $\alpha = 1$. In this case, equations (3.61)–(3.63) become

$$S_t = 2\left[(S+1)(U_x+V_y) + (S_xU + S_yV)\right], \tag{3.69}$$

$$U_t = 2(UU_x + VV_x) + \frac{1}{F}S_x - \gamma(S_{xxx} + S_{xyy}), \tag{3.70}$$

$$V_t = 2(UU_y + VV_y) + \frac{1}{F}S_y - \gamma(S_{xxy} + S_{yyy}). \tag{3.71}$$

3.2.2 Problem in Polar Coordinates

In this section, we reformulate the system (3.45), (3.48) and (3.49) to polar coordinates with the aim of considering interfacial waves which are axisymmetric. Such disturbances could arise, for example, from a localized pressure disturbance at a point.

Let $u_r(r,\theta,t)$, $u_\theta(r,\theta,t)$ be components of the velocity vector in the r and θ directions, respectively. The components $u(x,y,t)$ and $v(x,y,t)$ of velocity in the x and y directions, respectively, can be written in terms of u_r, u_θ as follows

$$u = u_r\cos\theta - u_\theta\sin\theta, \quad v = u_r\sin\theta + u_\theta\cos\theta.$$

The change of variables from the Cartesian system to the polar one is achieved by the transformations

$$x = r\cos\theta, \quad y = r\sin\theta \quad \text{with} \quad r^2 = x^2+y^2 \quad \text{and} \quad \tan\theta = \frac{y}{x}.$$

$$\frac{\partial r}{\partial x} = \cos\theta, \quad \frac{\partial r}{\partial y} = \sin\theta, \quad \frac{\partial\theta}{\partial x} = -\frac{\sin\theta}{r}, \quad \frac{\partial\theta}{\partial y} = \frac{\cos\theta}{r}.$$

Partial derivatives transform according to

$$\frac{\partial}{\partial x} = \cos\theta\frac{\partial}{\partial r} - \frac{\sin\theta}{r}\frac{\partial}{\partial\theta}, \quad \frac{\partial}{\partial y} = \sin\theta\frac{\partial}{\partial r} + \frac{\cos\theta}{r}\frac{\partial}{\partial\theta},$$

$$\Delta = \frac{\partial^2}{\partial x^2} + \frac{\partial^2}{\partial y^2} = \frac{\partial^2}{\partial r^2} + \frac{1}{r}\frac{\partial}{\partial r} + \frac{1}{r^2}\frac{\partial^2}{\partial\theta^2}.$$

Using these expressions we change variables in the Cartesian evolution equations (3.45), (3.48) and (3.49) to obtain them in polar coordinates. Since $\nabla\Lambda = (\Lambda_x, \Lambda_y) = (u,v)$, equation (3.45) becomes

$$\begin{aligned}\frac{1}{2}\frac{\partial S}{\partial t} &+ \left(\cos\theta\frac{\partial}{\partial r} - \frac{\sin\theta}{r}\frac{\partial}{\partial\theta}\right)\Big\{(S^2-1)(u_r\cos\theta - u_\theta\sin\theta)\Big\} \\ &+ \left(\sin\theta\frac{\partial}{\partial r} + \frac{\cos\theta}{r}\frac{\partial}{\partial\theta}\right)\Big\{(S^2-1)(u_r\sin\theta + u_\theta\cos\theta)\Big\} = 0. \qquad (3.72)\end{aligned}$$

Equation (3.48) transforms to

$$
\begin{aligned}
&[(\rho-1)S+(\rho+1)]_t(u_r\cos\theta-u_\theta\sin\theta)+[(\rho-1)S+(\rho+1)](u_r\cos\theta\\
&-u_\theta\sin\theta)_t+\rho\left(\cos\theta\frac{\partial}{\partial r}-\frac{\sin\theta}{r}\frac{\partial}{\partial\theta}\right)\left\{(S+1)^2(u_r^2+u_\theta^2)\right\}\\
&-\left(\cos\theta\frac{\partial}{\partial r}-\frac{\sin\theta}{r}\frac{\partial}{\partial\theta}\right)\left\{(S-1)^2(u_r^2+u_\theta^2)\right\}\\
&+\frac{\rho-1}{F}\left(\cos\theta\frac{\partial}{\partial r}-\frac{\sin\theta}{r}\frac{\partial}{\partial\theta}\right)S=-\sigma\left(\cos\theta\frac{\partial}{\partial r}-\frac{\sin\theta}{r}\frac{\partial}{\partial\theta}\right)\Delta S.
\end{aligned}
$$

This equation can be simplified further to

$$
\begin{aligned}
(\rho\ -\ 1)&\frac{\partial S}{\partial t}(u_r\cos\theta-u_\theta\sin\theta)+[(\rho-1)S+(\rho+1)]\left(\frac{\partial u_r}{\partial t}\cos\theta-\frac{\partial u_\theta}{\partial t}\sin\theta\right)\\
+\ &\left(\cos\theta\frac{\partial}{\partial r}-\frac{\sin\theta}{r}\frac{\partial}{\partial\theta}\right)\left\{[\rho(S+1)^2-(S-1)^2](u_r^2+u_\theta^2)\right\}\\
+\ &\frac{\rho-1}{F}\left\{\cos\theta\frac{\partial S}{\partial r}-\frac{\sin\theta}{r}\frac{\partial S}{\partial\theta}\right\}=-\sigma\left(\cos\theta\frac{\partial}{\partial r}-\frac{\sin\theta}{r}\frac{\partial}{\partial\theta}\right)\Delta S. \qquad (3.73)
\end{aligned}
$$

Similarly equation (3.49) transforms to

$$
\begin{aligned}
(\rho\ -\ 1)&\frac{\partial S}{\partial t}(u_r\sin\theta+u_\theta\cos\theta)+[(\rho-1)S+(\rho+1)]\left(\frac{\partial u_r}{\partial t}\sin\theta+\frac{\partial u_\theta}{\partial t}\cos\theta\right)\\
+\ &\left(\sin\theta\frac{\partial}{\partial r}+\frac{\cos\theta}{r}\frac{\partial}{\partial\theta}\right)\left\{[\rho(S+1)^2-(S-1)^2](u_r^2+u_\theta^2)\right\}\\
+\ &\frac{\rho-1}{F}\left\{\sin\theta\frac{\partial S}{\partial r}+\frac{\cos\theta}{r}\frac{\partial S}{\partial\theta}\right\}=-\sigma\left(\sin\theta\frac{\partial}{\partial r}+\frac{\cos\theta}{r}\frac{\partial}{\partial\theta}\right)\Delta S. \qquad (3.74)
\end{aligned}
$$

Inspection of equation (3.72) shows that it can be written in more useful conservative form

$$
\frac{1}{2}\frac{\partial S}{\partial t}+\frac{\partial}{\partial r}\left\{(S^2-1)u_r\right\}+\frac{1}{r}\frac{\partial}{\partial\theta}\left\{(S^2-1)u_\theta\right\}=0. \qquad (3.75)
$$

Multiply equation (3.73) by $\cos\theta$, equation (3.74) by $\sin\theta$ and then add the resulting equations to obtain

$$
\begin{aligned}
(\rho\ -\ 1)&\frac{\partial S}{\partial t}u_r+[(\rho-1)S+(\rho+1)]\frac{\partial u_r}{\partial t}+\frac{\partial}{\partial r}\left\{[\rho(S+1)^2\right.\\
-\ &\left.(S-1)^2](u_r^2+u_\theta^2)\right\}+\frac{\rho-1}{F}\frac{\partial S}{\partial r}=-\sigma\frac{\partial}{\partial r}(\Delta S). \qquad (3.76)
\end{aligned}
$$

Multiplication of equation (3.74) by $\cos\theta$, equation (3.73) by $\sin\theta$ and then subtraction of the resulting equations gives

$$(\rho - 1)\frac{\partial S}{\partial t}u_\theta + [(\rho-1)S + (\rho+1)]\frac{\partial u_\theta}{\partial t} + \frac{1}{r}\frac{\partial}{\partial\theta}\Big\{[\rho(S+1)^2 - (S-1)^2](u_r^2+u_\theta^2)\Big\} + \frac{\rho-1}{F}\frac{1}{r}\frac{\partial S}{\partial\theta} = -\sigma\frac{1}{r}\frac{\partial}{\partial\theta}(\Delta S). \tag{3.77}$$

In terms of the Atwood ratio $\alpha = \frac{1-\rho}{1+\rho}$ and $\gamma = \frac{\sigma}{1+\rho}$, the system of evolution equations becomes

$$\frac{1}{2}\frac{\partial S}{\partial t} + \frac{\partial}{\partial r}\Big\{(S^2-1)u_r\Big\} + \frac{1}{r}\frac{\partial}{\partial\theta}\Big\{(S^2-1)u_\theta\Big\} = 0, \tag{3.78}$$

$$\alpha\frac{\partial S}{\partial t}u_r + (\alpha S - 1)\frac{\partial u_r}{\partial t} + \frac{\partial}{\partial r}\Big\{(\alpha S^2 - 2S + \alpha)(u_r^2+u_\theta^2)\Big\} + \frac{\alpha}{F}\frac{\partial S}{\partial r} = \gamma\frac{\partial}{\partial r}(\Delta S), \tag{3.79}$$

$$\alpha\frac{\partial S}{\partial t}u_\theta + (\alpha S - 1)\frac{\partial u_\theta}{\partial t} + \frac{1}{r}\frac{\partial}{\partial\theta}\Big\{(\alpha S^2 - 2S + \alpha)(u_r^2+u_\theta^2)\Big\} + \frac{\alpha}{Fr}\frac{\partial S}{\partial\theta} = \gamma\frac{1}{r}\frac{\partial}{\partial\theta}(\Delta S). \tag{3.80}$$

Note that S_t can be eliminated from (3.79), (3.80) by use of (3.78) as was done in the Cartesian case.

3.2.3 Axisymmetric Case: $\frac{\partial}{\partial\theta} = 0$

In the axisymmetric case, the system of equations (3.78)–(3.80) reduces to

$$\frac{1}{2}\frac{\partial S}{\partial t} + \frac{\partial}{\partial r}\Big\{(S^2-1)u_r\Big\} = 0, \tag{3.81}$$

$$\alpha\frac{\partial S}{\partial t}u_r + (\alpha S - 1)\frac{\partial u_r}{\partial t} + \frac{\partial}{\partial r}\Big\{(\alpha S^2 - 2S + \alpha)(u_r^2+u_\theta^2)\Big\} + \frac{\alpha}{F}\frac{\partial S}{\partial r} = \gamma\frac{\partial}{\partial r}(\Delta S), \tag{3.82}$$

$$\alpha\frac{\partial S}{\partial t}u_\theta + (\alpha S - 1)\frac{\partial u_\theta}{\partial t} = 0, \tag{3.83}$$

where the operator $\Delta \equiv \frac{\partial^2}{\partial r^2} + \frac{1}{r}\frac{\partial}{\partial r}$ now.

It follows from the last equation that

$$\frac{\partial}{\partial t}[(\alpha S-1)u_\theta]=0,$$

i.e., $(\alpha S-1)u_\theta$ does not depend on t, so $(\alpha S-1)u_\theta = G(r)$, where G is some function of r. Equation (3.83) shows also that $u_\theta \equiv const.$ yields trivial solutions since $S_t = 0$ then.

As a partial case, we can consider flows in which the component $u_\theta = 0$. Then the system of three equations (3.81)–(3.83) reduces to two equations for the unknowns S and u_r.

$$\frac{1}{2}\frac{\partial S}{\partial t}+\frac{\partial}{\partial r}\left\{(S^2-1)u_r\right\}=0, \tag{3.84}$$

$$\begin{aligned}\alpha\frac{\partial S}{\partial t}u_r &+ (\alpha S-1)\frac{\partial u_r}{\partial t}+\frac{\partial}{\partial r}\left\{(\alpha S^2-2S+\alpha)u_r^2\right\}\\ &+ \frac{\alpha}{F}\frac{\partial S}{\partial r}=\gamma\frac{\partial}{\partial r}\left(\frac{\partial^2 S}{\partial r^2}+\frac{1}{r}\frac{\partial S}{\partial r}\right).\end{aligned} \tag{3.85}$$

Note that equation (3.83) in this particular case is satisfied identically.

When the densities are equal, $\alpha = 0$, equation (3.85) simplifies, and we have the following system of governing equations

$$\frac{1}{2}\frac{\partial S}{\partial t}+\frac{\partial}{\partial r}\left\{(S^2-1)u_r\right\}=0, \tag{3.86}$$

$$\frac{\partial u_r}{\partial t}+2\frac{\partial}{\partial r}\left\{Su_r^2\right\}=-\frac{\sigma}{2}\frac{\partial}{\partial r}\left(\frac{\partial^2 S}{\partial r^2}+\frac{1}{r}\frac{\partial S}{\partial r}\right). \tag{3.87}$$

3.3 Linear Stability Analysis

Consider next, the evolution of the infinitesimal wavy disturbances at the interface according to the model (3.55), (3.58) and (3.59). The undisturbed flow is described by a flat interface separating two fluids which flow at uniform velocities having components in the x and y-directions with velocity jumps v_0 and v_0 across the

interface, respectively. This undisturbed flow is a weak solution of the three-dimensional Euler equations. The appropriate perturbations are

$$S(x,y,t) = \delta\tilde{S}\,\mathrm{e}^{i(k_1x+k_2y)+\hat{\omega}t}, \quad (u,v) = (u_0,v_0) + \delta(\tilde{u},\tilde{v})\,\mathrm{e}^{i(k_1x+k_2y)+\hat{\omega}t}. \tag{3.88}$$

Here $\tilde{S}$, $\tilde{u}$, $\tilde{v}$ are constants and u_0 and v_0 are components of the constant strength of the unperturbed vortex sheet in the x and y-directions, respectively, and δ is the linearization parameter assumed to be infinitesimally small.

We substitute expressions (3.88) into equations (3.55), (3.58) and(3.59), and multiply equations (3.58) and (3.59) by $1-\alpha S$. After collecting terms of the order $O(\delta)$, we obtain the following linear homogeneous system

$$\tilde{S}\hat{\omega} = 2i(k_1\tilde{u}+k_2\tilde{v}), \tag{3.89}$$

$$\begin{aligned}\tilde{u}\hat{\omega} &= 2i\alpha u_0(k_1\tilde{u}+k_2\tilde{v}) + 2i\alpha k_1(u_0\tilde{u}+v_0\tilde{v}) \\ &+ ik_1\tilde{S}\left[\frac{\alpha}{F} - 2(u_0^2+v_0^2) + \gamma(k_1^2+k_2^2)\right],\end{aligned} \tag{3.90}$$

$$\begin{aligned}\tilde{v}\hat{\omega} &= 2i\alpha v_0(k_1\tilde{u}+k_2\tilde{v}) + 2i\alpha k_2(u_0\tilde{u}+v_0\tilde{v}) \\ &+ ik_2\tilde{S}\left[\frac{\alpha}{F} - 2(u_0^2+v_0^2) + \gamma(k_1^2+k_2^2)\right].\end{aligned} \tag{3.91}$$

Define

$$Q = \frac{\alpha}{F} - 2(u_0^2+v_0^2) + \gamma(k_1^2+k_2^2).$$

We need to eliminate $\tilde{S}$, $\tilde{u}$ and $\tilde{v}$ in order to get a dispersion relation. It follows from equation (3.89) that

$$\tilde{S} = \frac{2i}{\hat{\omega}}(\tilde{u}k_1+\tilde{v}k_2). \tag{3.92}$$

Substitute $\tilde{S}$ from (3.92) into (3.90) and (3.91). Equations (3.90) and (3.91) are linear equations for the unknowns $\tilde{u}$ and $\tilde{v}$ with the matrix

$$A = \begin{pmatrix} \hat{\omega} - 4i\alpha k_1u_0 + \frac{2k_1^2}{\hat{\omega}}Q & -2i\alpha(k_2u_0+k_1v_0) + \frac{2k_1k_2}{\hat{\omega}}Q \\ -2i\alpha(k_1v_0+k_2u_0) + \frac{2k_1k_2}{\hat{\omega}}Q & \hat{\omega} - 4i\alpha k_2v_0 + \frac{2k_2^2}{\hat{\omega}}Q \end{pmatrix}.$$

For non-trivial solution $(\tilde{u}, \tilde{v})$, we require $\det A = 0$, i.e.,

$$\begin{aligned} \det A &= \hat{\omega}^2 - 4i\alpha(k_1u_0 + k_2v_0)\hat{\omega} + \Big(2(k_1^2 + k_2^2)Q \\ &- 16\alpha^2 k_1k_2u_0v_0 + 4\alpha^2(k_1v_0 + k_2u_0)\Big) = 0, \end{aligned} \tag{3.93}$$

which is the quadratic equation for $\hat{\omega}$. Note that terms in $\det A = 0$ of order $O(\frac{1}{\hat{\omega}})$ and $O(\frac{1}{\hat{\omega}^2})$ cancel. The discriminant of equation(3.93) is

$$\mathcal{D} = -16\alpha^2(k_1u_0 + k_2v_0)^2 - 4\left(2(k_1^2 + k_2^2)Q - 16\alpha^2 k_1k_2u_0v_0\right.$$

$$\left.+4\alpha^2(k_1v_0 + k_2u_0)^2\right) = 8(k_1^2 + k_2^2)\left[-\frac{\alpha}{F} - \gamma(k_1^2 + k_2^2) + 2(1-\alpha^2)(u_0^2 + v_0^2)\right].$$

Then, the dispersion relation is

$$\hat{\omega} = 2i\alpha(k_1u_0 + k_2v_0) \pm \sqrt{2}(k_1^2 + k_2^2)^{1/2}\Big[-\frac{\alpha}{F} - \gamma(k_1^2 + k_2^2)$$

$$+ 2(1-\alpha^2)(u_0^2 + v_0^2)\Big]^{1/2}$$

where $k = (k_1^2 + k_2^2)^{1/2}$ is called the *total wave number*. Instability occurs when the real part of $\hat{\omega}$ is positive, i.e., when

$$-\frac{\alpha}{F} - \gamma(k_1^2 + k_2^2) + 2(1-\alpha^2)(u_0^2 + v_0^2) > 0.$$

This inequality is quadratic in α and can be written as

$$-2(u_0^2 + v_0^2)\alpha^2 - \frac{\alpha}{F} + 2(u_0^2 + v_0^2) - \gamma(k_1^2 + k_2^2) > 0. \tag{3.94}$$

It is clear from (3.94) that for $\gamma \neq 0$, short waves $(k_1, k_2 \gg 1)$ are linearly neutrally stable. The discriminant for inequality (3.94) is

$$\mathcal{D}_1 = \frac{1}{F^2} + 8(u_0^2 + v_0^2)\left(2(u_0^2 + v_0^2) - \gamma(k_1^2 + k_2^2)\right).$$

If surface tension is absent, i.e. $\gamma = 0$, then

$$\mathcal{D}_1 = 16\left(\frac{1}{16F^2} + (u_0^2 + v_0^2)\right) > 0 \quad \text{for all values of} \quad F,\ u_0 \text{ and } v_0$$

and values for α are the following:

$$\alpha_1 = \frac{\frac{1}{F} + 4\left(\frac{1}{16F^2} + (u_0^2+v_0^2)^2\right)^{1/2}}{-4(u_0^2+v_0^2)}$$

$$= -\frac{1}{4F(u_0^2+v_0^2)} - \left(\frac{1}{16F^2(u_0^2+v_0^2)^2}+1\right)^{1/2},$$

$$\alpha_2 = -\frac{1}{4F(u_0^2+v_0^2)} + \left(\frac{1}{16F^2(u_0^2+v_0^2)^2}+1\right)^{1/2}.$$

Clearly $\alpha_1 < -1$, and the admissible values of α are

$$-1 < \alpha < \alpha_2. \tag{3.95}$$

Condition (3.95) implies that flow is unstable for all negative values of α. This case corresponds to that of a heavier fluid on the top. In addition, the range $0 \leq \alpha < \alpha_2$ is linearly unstable — surface tension acts to stabilize sufficiently short waves. Representative graphs of the growth rate $\mathrm{Re}\,\hat{\omega}$ for $\gamma \neq 0$ and $\gamma = 0$ are shown in Figure 3.2.

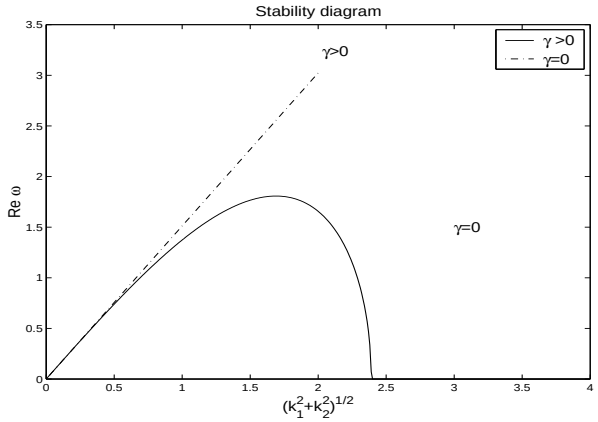

Figure 3.2 Representative graphs of growth rate $\mathrm{Re}\,\hat{\omega}$ for $\alpha = 0.5$, $F = 1, 4$, $\gamma = 0.2$ and $\gamma = 0$.

3.4 Conserved Integrals

The system of the evolution equations (3.61)–(3.63) has the following constants of motion that corresponds to mass, total circulation in the x- and y-direction, respectively, and energy

$$\mathcal{I}_1 = \int\int S dxdy, \quad \mathcal{I}_2 = \int\int (1-\alpha S) u dxdy, \quad \mathcal{I}_3 = \int\int (1-\alpha S) v dxdy, \tag{3.96}$$

$$\begin{aligned} \mathcal{I}_4 &= \int\int \left[\frac{1}{2}(1-\alpha S)(1-S^2)(u^2+v^2) - \frac{\alpha}{4F}(1-S^2) \right. \\ &+ \left. \frac{\gamma}{4}(S_x^2 + S_y^2) \right] dxdy. \end{aligned} \tag{3.97}$$

These constants of motion are analogues of the corresponding ones (2.39), (2.40) from the two-dimensional problem considered in Chapter 2. Since these quantities do not change during the course of the evolution, they have been used in monitoring the accuracy during numerical calculations of the evolution equations (3.61)–(3.63).

Derivation of the integrals of motion (3.96), (3.97) is similar to that of their two-dimensional analogues.

3.4.1 Mass Conservation

We use the dimensional notation of Section 3.1. We assume without loss of generality that the flow is periodic with period l in the x- and y-directions. The total mass contained in one periodic cell is

$$M = \rho_1 \int_S^h \int_0^l \int_0^l dxdydz + \rho_2 \int_{-h}^S \int_0^l \int_0^l dxdydz.$$

Changing to dimensionless variables by using (3.7) and then subsequently dropping the superscript $*$, we obtain

$$M = \rho_2 lh \left\{ \frac{\rho_1}{\rho_2} \int_S^1 \int_0^1 \int_0^1 dxdydz + \int_{-1}^S \int_0^1 \int_0^1 dxdydz \right\}.$$

Integration with respect to z and use of the density ratio $\rho = \frac{\rho_1}{\rho_2}$ yields

$$M = \rho_2 lh \int_0^1 \int_0^1 \{\rho(1-S) + (S+1)\} dxdy = \rho_2 lh \int_0^1 \int_0^1 \{(\rho+1)$$

$$+(1-\rho)S\}\,dxdy = \rho_2 lh(1+\rho)\int_0^1\int_0^1 (1+\alpha S)dxdy,$$

where we used the definition of the Atwood ratio $\alpha = \frac{1-\rho}{1-\rho}$. Then the dimensionless mass

$$\tilde{M} = \frac{M}{\rho_2 lh} = (1+\rho)\int_0^1\int_0^1 (1+\alpha S)dxdx$$

is the conserved density, i.e.,

$$\int_0^1\int_0^1 S(x,y,t)dxdy = const_1,$$

thus giving the constant of motion $\mathcal{I}_1$.

Note that we could also derive the conserved quantity $\mathcal{I}_1$ using the conservative form of equation (3.50) and the periodicity of the boundary conditions.

3.4.2 Total Circulation Conservation

To derive the constants of motion $\mathcal{I}_2$ and $\mathcal{I}_3$, we observe that evolution equations (3.61)–(3.63) or their vector equivalent in unknown functions u and v, i.e., equation (3.50), may be written in the conservative form

$$[(1-\alpha S)\vec{q}]_t + \nabla\left\{[-\alpha S^2 + 2S - \alpha]|\vec{q}|^2 - \frac{\alpha}{F}S + \gamma\nabla S\right\} = 0$$

and we conclude that $(1-\alpha S)\vec{q}$ is the vector conserved density. Hence,

$$\int_0^1\int_0^1 (1-\alpha S)\vec{q}dxdy = \vec{const}.$$

Recalling that $\vec{q} = (u, v)$, we obtain

$$\int_0^1\int_0^1 (1-\alpha S)udxdy = const_2 \quad \text{and} \quad \int_0^1\int_0^1 (1-\alpha S)vdxdy = const_3.$$

But from (3.60) we have $U = (1-\alpha S)u$ and $V = (1-\alpha S)v$. Therefore,

$$\int_0^1\int_0^1 Udxdy = const_2 \quad \text{and} \quad \int_0^1\int_0^1 Vdxdy = const_3.$$

as desired. The quantities $\mathcal{I}_2$ and $\mathcal{I}_3$ are long wave analogues of the total circulation in the x- and y-directions, respectively, as can be shown in a similar fashion as in Section 2.3.2. Total circulation appears to be conserved due to the assumption that the flows are irrotational.

3.4.3 Energy Conservation

The derivation of the energy integral is similar to the corresponding one for the two-dimensional case. The dimensional notation of Section 3.1 is used to obtain the total energy of the system at any time. The total energy has contributions from (i) kinetic energy, (ii) potential energy due to density differences, (iii) interfacial energy due to surface tension. Without loss of generality we take the flow to be periodic with period l in the x- and y-directions. Then the total energy in a single square periodic cell is

$$\begin{aligned} E &= \frac{1}{2}\rho_1 \int_S^h \int_0^l \int_0^l ((\phi_{1x})^2 + (\phi_{1y})^2 + \phi_{1z})^2) dxdydz \\ &+ \frac{1}{2}\rho_2 \int_{-h}^S \int_0^l \int_0^l ((\phi_{2x})^2 + (\phi_{2y})^2 + (\phi_{2z})^2) dxdydz \\ &+ \rho_1 g \int_S^h \int_0^l \int_0^l z dxdydz + \rho_2 g \int_{-h}^S \int_0^l \int_0^l z dxdydz \\ &+ \sigma_0 \int_0^l \int_0^l (1 + S_x^2 + S_y^2)^{1/2} dxdy. \end{aligned} \tag{3.98}$$

Changing to dimensionless variables in (3.98) via (3.7) and subsequently dropping superscript $*$ yields

$$\begin{aligned} E &= \frac{1}{2}\rho \int_S^1 \int_0^1 \int_0^1 ((\phi_{1x})^2 + (\phi_{1y})^2 + \frac{1}{\varepsilon^2}(\phi_{1z})^2) dxdydz \\ &+ \frac{1}{2} \int_{-1}^S \int_0^1 \int_0^1 ((\phi_{2x})^2 + (\phi_{2y})^2 + \frac{1}{\varepsilon^2}(\phi_{2z})^2) dxdydz \\ &+ \frac{1}{4F}(\rho - 1) \int_0^1 \int_0^1 (1 - S^2) dx + \frac{\tilde{\sigma}}{2\varepsilon} \int_0^1 \int_0^1 (1 + \varepsilon^2 S_x^2 + \varepsilon^2 S_y^2)^{1/2} dxdy. \end{aligned} \tag{3.99}$$

Expanding functions ϕ_1, ϕ_2 and S into power series in ε^2 as was done in (3.16) and using the solutions (3.21) and (3.22) of the leading order problem, we obtain the

following functional

$$\begin{aligned} E &= \frac{1}{2}\rho\int_S^1\int_0^1\int_0^1 \left((\Phi_{1x})^2+(\Phi_{1y})^2\right)dxdydz \\ &+ \frac{1}{2}\int_{-1}^S\int_0^1\int_0^1 \left((\Phi_{2x})^2+(\Phi_{2y})^2\right)dxdydz \\ &+ \int_0^1\int_0^1\left[\frac{1}{4F}(\rho-1)(1-S^2)+\frac{\varepsilon\tilde{\sigma}}{4}(S_x^2+S_y^2)\right]dxdy. \end{aligned} \tag{3.100}$$

It follows from (3.100) that strong surface tension of order ε^{-1} is required in order to compete with the effects of gravity and inertia.

Using the notation

$$\Phi=\frac{1}{2}\left(\Phi_1+\Phi_2\right),\quad \Lambda=\frac{1}{2}\left(\Phi_2-\Phi_1\right),\quad \alpha=\frac{1-\rho}{1+\rho},\quad \gamma=\frac{\sigma}{1+\rho},\quad \tilde{\sigma}=\frac{\sigma}{\varepsilon},$$

equation (3.100) gives

$$\begin{aligned} \tilde{E}=\frac{E_0}{1+\rho} &= \int_0^1\int_0^1\left[\frac{1}{2}(1-\alpha S)(1-S^2)(\Lambda_x^2+\Lambda_y^2)\right. \\ &- \left.\frac{\alpha}{4F}(1-S^2)+\frac{\gamma}{4}(S_x^2+S_y^2)\right]dxdy \end{aligned} \tag{3.101}$$

where $\tilde{E}$ is a constant since energy is conserved at each level of the expansion.

The expression (3.101) is a conserved quantity for the system. Next we show that this is consistent with the governing equations (3.55), (3.58) and (3.59).

Using notation $\vec{q}=\nabla\Lambda=(\Lambda_x,\Lambda_y)=(u,v)$ recasts equation (3.101) into

$$\begin{aligned} \tilde{E}=\frac{E_0}{1+\rho} &= \int_0^1\int_0^1\left[\frac{1}{2}(1-\alpha S)(1-S^2)(u^2+v^2)\right. \\ &- \left.\frac{\alpha}{4F}(1-S^2)+\frac{\gamma}{4}(S_x^2+S_y^2)\right]dxdy, \end{aligned} \tag{3.102}$$

that is the required conserved energy. Next we check the consistency of the obtained expression for the energy with the evolution equation. For that purpose, differentiate equation (3.102) with respect to t.

$$\begin{aligned} \frac{\partial\tilde{E}}{\partial t} &= \int_0^1\int_0^1\left[-\frac{1}{2}S_t(u^2+v^2)(\alpha+2S-3\alpha S^2)\right. \\ &+ (1-\alpha S)(1-S^2)(uu_t+vv_t) \\ &+ \left.\frac{\alpha}{2F}SS_t+\frac{\gamma}{2}(S_xS_{xt}+S_yS_{yt})\right]dxdy. \end{aligned} \tag{3.103}$$

Eliminate S_t, u_t and v_t using equations (3.55), (3.58) and (3.59) to obtain

$$\begin{aligned}\frac{\partial \tilde{E}}{\partial t} &= \int_0^1\int_0^1 \left(\frac{\partial}{\partial x}\left[u(S^2-1)(u^2+v^2)(-\alpha S^2+2S-\alpha)+\frac{\alpha}{F}S(1-S^2)u\right.\right.\\ &+ \left.\gamma\left\{u(S^2-1)(S_{xx}+S_{yy})-S_x\left[\frac{\partial}{\partial x}(u(S^2-1))+\frac{\partial}{\partial y}(v(S^2-1))\right]\right\}\right]\\ &+ \frac{\partial}{\partial y}\left[v(S^2-1)(u^2+v^2)(-\alpha S^2+2S-\alpha)+\frac{\alpha}{F}S(1-S^2)v+\gamma\left\{v(S^2\right.\right.\\ &- \left.\left.1)(S_{xx}+S_{yy})-S_y\left[\frac{\partial}{\partial x}(u(S^2-1))+\frac{\partial}{\partial y}(v(S^2-1))\right]\right\}\right]\Bigg)\,dxdy \quad (3.104)\end{aligned}$$

Since $\Delta S = S_{xx}+S_{yy}$ and $\vec{q}=(u,v)$, equation (3.104) can be written as

$$\begin{aligned}\frac{\partial \tilde{E}}{\partial t} &= \int_0^1\int_0^1 \left(\frac{\partial}{\partial x}\left[u(S^2-1)(u^2+v^2)(-\alpha S^2+2S-\alpha)+\frac{\alpha}{F}S(1-S^2)u\right.\right.\\ &+ \left.\left.\gamma\left\{u(S^2-1)\Delta S-S_x\,\mathrm{div}((S^2-1)\vec{q})\right\}\right]\right.\\ &+ \frac{\partial}{\partial y}\left[v(S^2-1)(u^2+v^2)(-\alpha S^2+2S-\alpha)+\frac{\alpha}{F}S(1-S^2)v\right.\\ &+ \left.\left.\gamma\left\{v(S^2-1)\Delta S-S_y\,\mathrm{div}((S^2-1)\vec{q})\right\}\right]\right)dxdy. \quad (3.105)\end{aligned}$$

The integrand in (3.105) is a sum of two partial derivatives with respect to x and y, respectively. Therefore, the integral is a constant. Since the functions S, u and v are periodic with period 1 in both x and y, the double integral on the right-hand side is zero. Thus, the consistency of the energy equation (3.101) with evolution equations (3.61)–(3.63) is verified.

3.5 Numerical Solution of Evolution Equations

In this section, the initial value problem for the system of evolution equations (3.61)–(3.63) is addressed numerically.

3.5.1 Numerical Method

Numerical solutions are constructed on periodic domains for given periodic initial conditions

$$S(x+2\pi, y+2\pi, t) = S(x,y,t),$$

$$U(x+2\pi, y+2\pi, t) = U(x,y,t), \quad V(x+2\pi, y+2\pi, t) = V(x,y,t), \quad (3.106)$$

$$S = a\sin x + \varepsilon \sin y, \quad U = U_0, \quad V = V_0 - \varepsilon \cos y. \quad (3.107)$$

Conserved quantities $\mathcal{I}_i$, $i = 1, 2, 3, 4$, derived in Section 3.4 provide a useful accuracy check for the numerics.

A pseudo-spectral scheme was used, computing derivatives by use of FFTs, and the time integrations are done in the real space by fourth-order Runge-Kutta method. A stability requirement for this method restricts the size of Δt as the number of active Fourier modes increases. The reason of this is the dispersive nature of the regularization provided by surface tension.

As can be seen from the evolution equations ((3.61)–(3.63), i.e., equations using the unknown functions U and V, terms with the highest order derivatives present linearly as opposed to the formulation in terms of the unknown functions u and v, i.e. equations (3.55), (3.58) and (3.59). The first formulation allows to use the bigger time step than the second one.

The computation is stopped when the value of any of the derivatives S_x, S_y, U_x, U_y, V_x or V_y reaches the value of 5. The number of points used for numerical solutions presented in the next section is $n = 512$, and the time step is 10^{-5} towards the end of the computation. The results presented show that the number n of points should be bigger, ranging between $n = 1024$ and $n = 4096$. Then it would be possible to set a higher value for the slopes in the interface and the vortex sheet. This in turn requires much more space and memory to use, decreases the time step due to the stability criterium and makes calculations to be very lengthy.

The figures obtained at the last time computed indicate that another scheme, possibly, implicit should be used in order to follow further the singularity formation and remove numerical instability.

In what follows, we report on results from the above method.

3.5.2 Computational Results: Solutions of Initial Value Problem

The following initial conditions were used,

$$S = a\sin x + \varepsilon \sin y, \quad U = U_0, \quad V = V_0 - \varepsilon \cos y \tag{3.108}$$

with $a = 0.3$, $\varepsilon = 0.1$, $U_0 = 0$ (initially velocity jump in x-direction is absent), $V_0 = 1.0$ (we have initial velocity jump in y-direction). These initial conditions impose disturbances which produce a three-dimensional flow. Note that the initial amplitude $a = 0.3$ is relatively large. Smaller disturbances require much longer runs.

Numerical solutions presented in this section have surface tension coefficient $\gamma = 0$ and $\gamma = 3$.

No Surface Tension: $\gamma = 0$.

Evolution of the interface $S(x, y, t)$ for $n = 512$ is presented below. Figure 3.3 is initial shape of the interface. In this case, the number of linearly instable modes is infinite.

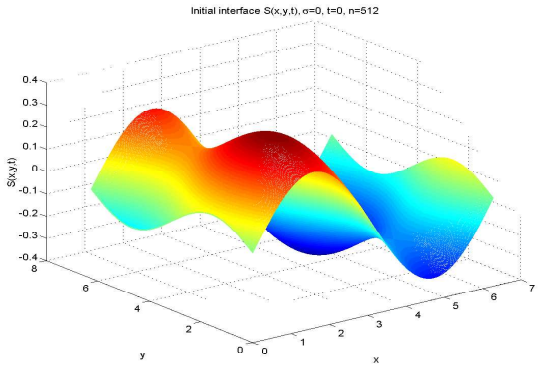

Figure 3.3 Initial interface $S(x, y, t)$, $t = 0$, $\gamma = 0$, $n = 512$.

In the next four figures 3.4 (a), (b) and 3.5 (a), (b), we show the interface at $t = 0.1$, $t = 0.2$, $t = 0.3$ and $t = 0.34672$, respectively. The computations stopped at $t = 0.34672$ according to a criterion that any of the derivatives S_x, S_y, U_x, U_v, V_x, V_y reached the preset value of 5.

To see the details better, we present two-dimensional "slices" of the three-dimensional interfacial shape for some values of x and y where we observed interesting

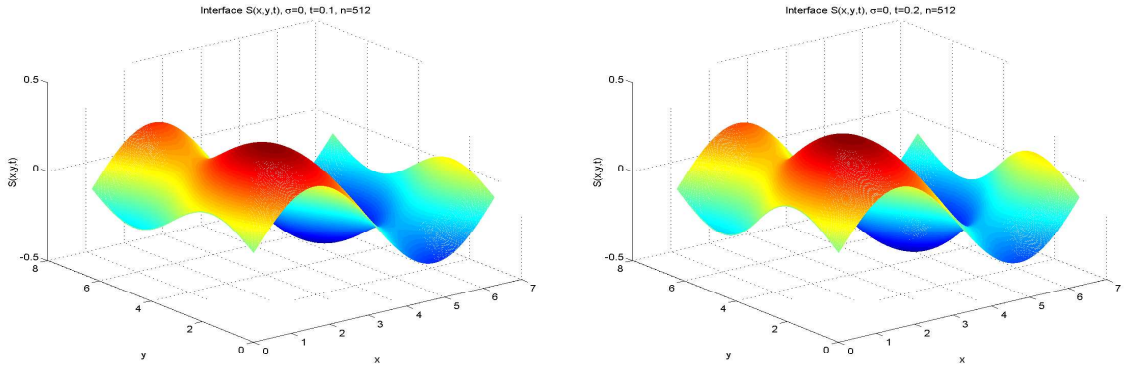

Figure 3.4 Interface $S(x, y, t)$, $\gamma = 0$, $n = 512$ at time: (a) $t = 0.1$; (b) $t = 0.2$.

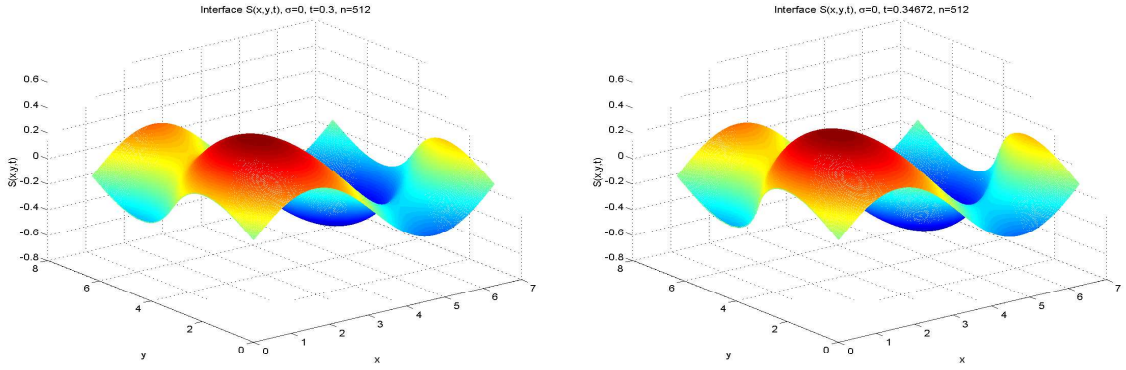

Figure 3.5 Interface $S(x, y, t)$, $\gamma = 0$, $n = 512$ at time: (a) $t = 0.3$; $t = 0.34672$.

behavior. The first series of graphs (see Figure 3.6) represents the evolution of S at fixed position $x = 0$ and $x = \pi$ while y varies.

In Figures 3.7 (a) and (b), the evolution of slices of the interface with fixed $y = 0$, $y = \pi$ and varying x is presented.

Evolution of the vortex sheet strength in x-direction $U(x, y, t)$ is presented next. Figure 3.8 shows the initial shape for U which is flat since we initially impose no velocity jump in the x-direction.

Its evolution for times $t = 0.1$, $t = 0.2$, $t = 0.3$ and $t = 0.34672$ is in Figures 3.9 (a), (b) and 3.10 (a), (b)

Cross-sections of U at $x = 0$ and $x = \pi$ are shown on Figures 3.11 (a) and (b), respectively.

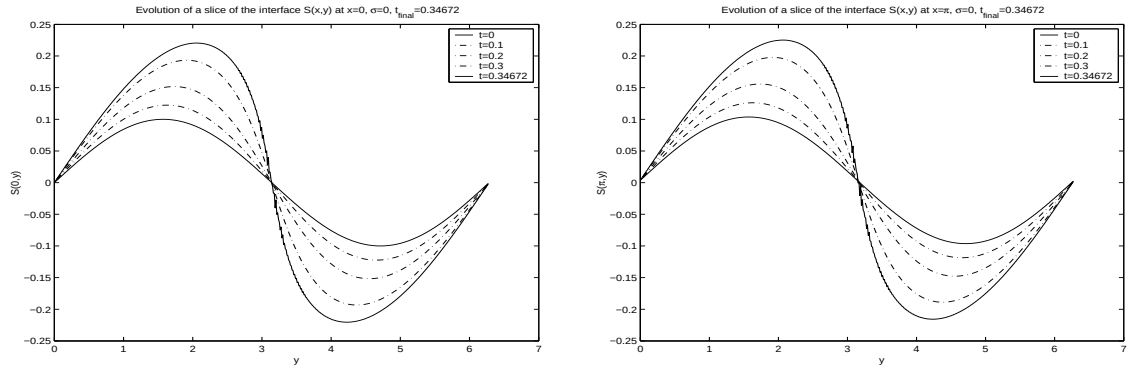

Figure 3.6 Slices of the interface $S(x, y, t)$, $\gamma = 0$, $n = 512$ at: (a) $x = 0$; (b) $x = \pi$.

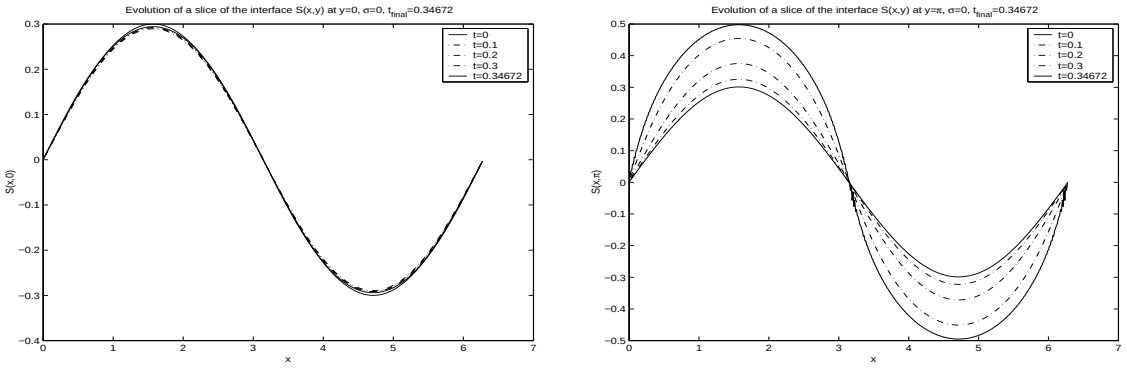

Figure 3.7 Slice of the interface $S(x, y, t)$, $\gamma = 0$, $n = 512$ at: (a) $y = 0$; (b) $y = \pi$.

At $y = 0$, $y = \pi$ and x varying, the slices of U are presented in Figures 3.12 (a) and (b).

The evolution of the vortex sheet strength in the y-direction, $V(x, y, t)$, is shown next. Figure 3.13 has the initial shape of V.

In the next four figures 3.14 (a), (b) and 3.15 (a), (b) we present graphs of V for times $t = 0.1$, $t = 0.2$, $t = 0.3$ and $t = 0.34672$.

Slices of V at $x = 0$ and $x = \pi$ are given in Figures 3.16 (a) and (b), respectively.

At $y = 0$, $y = \pi$ and x varying, the slices of V are presented in Figures 3.17 (a) and (b), respectively.

It should be noted that while the vortex sheet strength components appear to grow, the interface remains bounded.

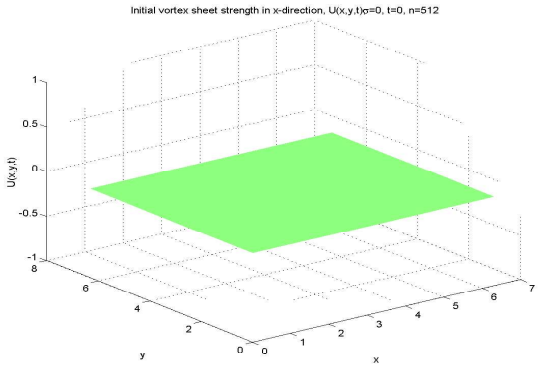

Figure 3.8 Initial vortex sheet strength in x-direction, $U(x, y, t)$, $\gamma = 0$, $t = 0$, $n = 512$.

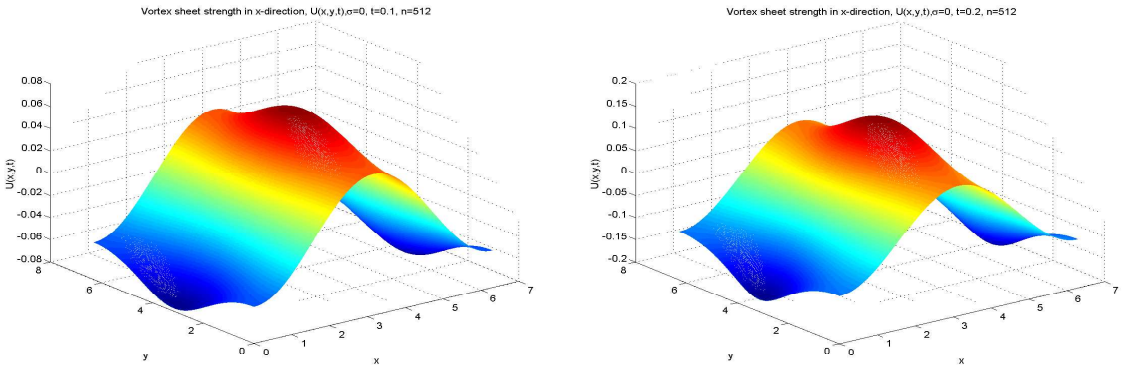

Figure 3.9 Vortex sheet strength in x-direction, $U(x, y, t)$, $\gamma = 0$, $n = 512$ at time: (a) $t = 0.1$; (b) $t = 0.2$.

Some graphs exhibit numerical instability at the last time $t = 0.34672$. This instability is due to the fact that solution becomes more singular as the time evolves and more points are needed to resolve this instability since higher wavenumbers begin to play more important role, and we cannot neglect them. In this particular case, we would need to work with $n = 1024$ at least in order to get solutions with higher slopes.

More extensive computations are needed to pinpoint the singularity but our results indicate that the solution becomes singular at a single point (x_0, y_0), say, after a finite time. These findings are consistent with the calculations by Hou & Hu[40] who considered three-dimensional vortex sheet evolution in unbounded domains and

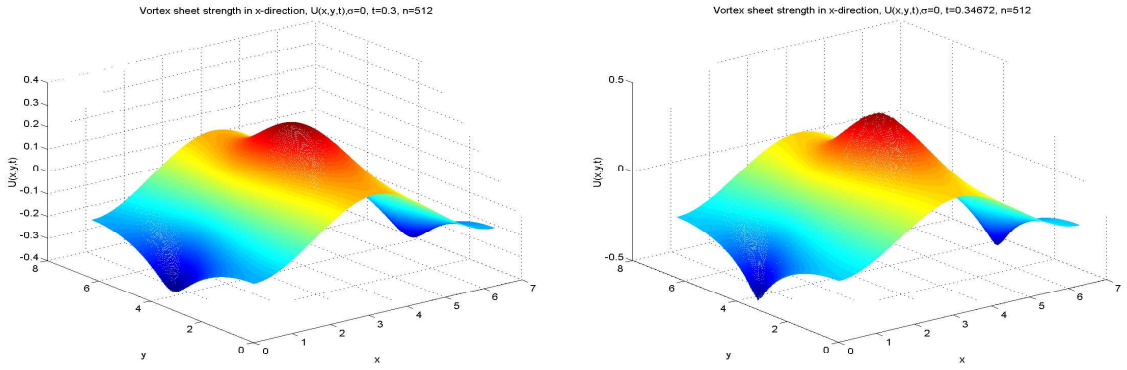

Figure 3.10 Vortex sheet strength in x-direction, $U(x, y, t)$, $\gamma = 0$, $n = 512$ at time: (a) $t = 0.3$; (b) $t = 0.34672$.

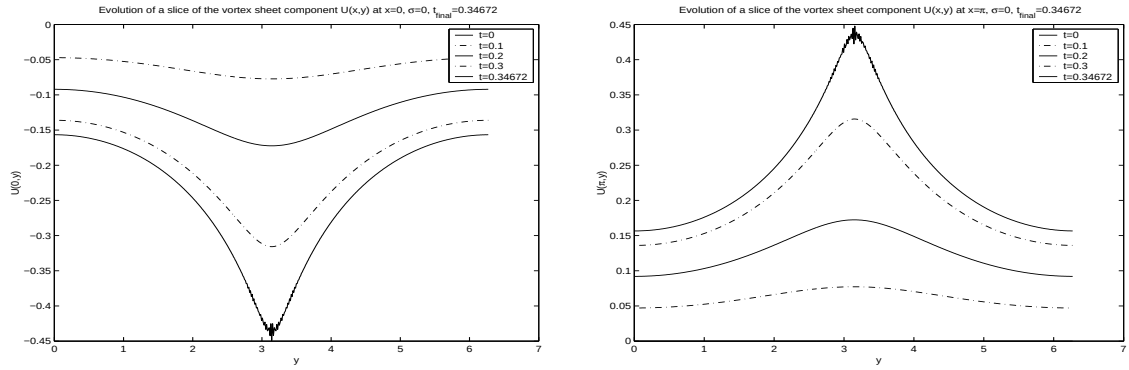

Figure 3.11 Slices of the vortex sheet component $U(x, y, t)$, $\gamma = 0$, $n = 512$ at: (a) $x = 0$; (b) $x = \pi$.

came to the conclusion that singularity may appear at isolated points or along the entire one-dimensional line but not along the segment.

`Surface tension coefficient` $\gamma = 3.0$.

Using the same initial conditions (3.108) as for the case $\gamma = 0$, we obtain the solution at $t = 0.4$ for the interface $S(x, y, t)$, given in Figure 3.18.

The corresponding graphs for vortex sheet strength components $U(x, y, t)$ and $V(x, y, t)$, components in x and y directions, respectively, are presented in Figure 3.19.

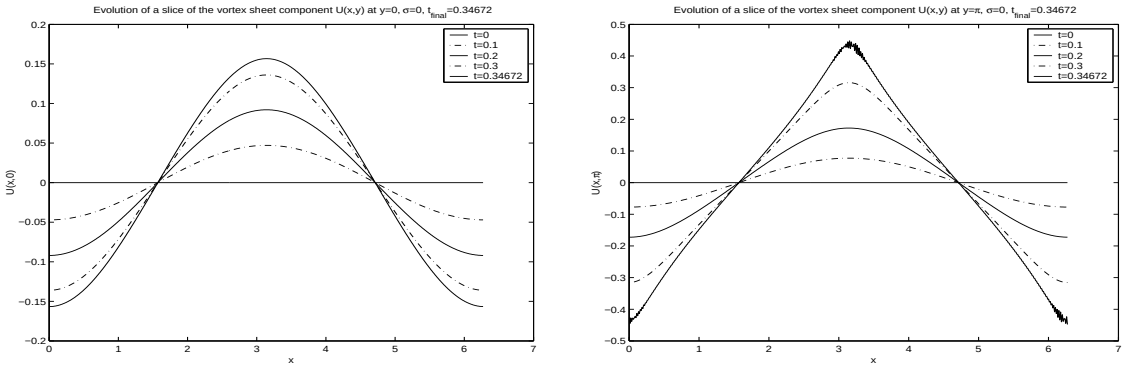

Figure 3.12 Slice of the vortex sheet component $U(x, y, t)$, $\gamma = 0$, $n = 512$ at: (a) $y = 0$; (b) $y = \pi$.

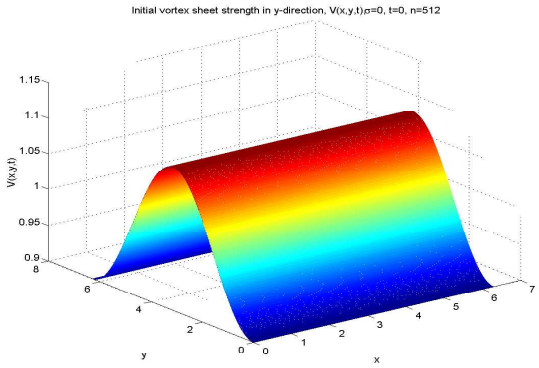

Figure 3.13 Initial vortex sheet strength in y-direction, $V(x, y, t)$, $\gamma = 0$, $t = 0$, $n = 512$.

In the program, the limit for the maximum derivative of S, U and V is set to 5. More extensive numerical calculations are needed to better resolve the singular solution.

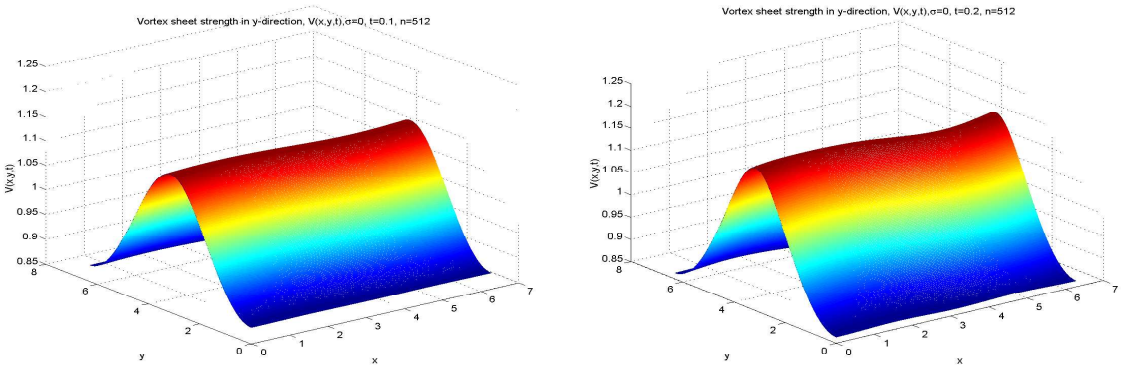

Figure 3.14 Vortex sheet strength in y-direction, $V(x, y, t)$, $\gamma = 0$, $n = 512$ at time: (a) $t = 0.1$; (b) $t = 0.2$.

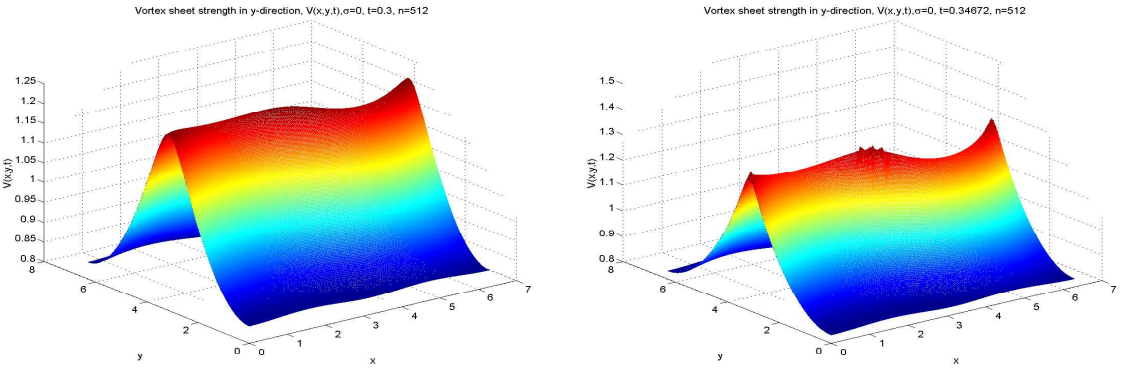

Figure 3.15 Vortex sheet strength in y-direction, $V(x, y, t)$, $\gamma = 0$, $n = 512$ at time: (a) $t = 0.3$; (b) $t = 0.34672$.

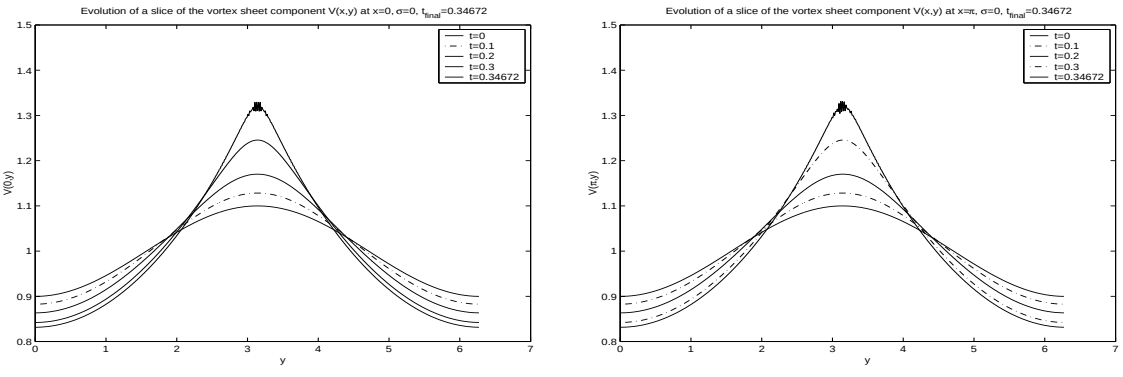

Figure 3.16 Slices of the vortex sheet component $V(x, y, t)$, $\gamma = 0$, $n = 512$ at: (a) $x = 0$; (b) $x = \pi$.

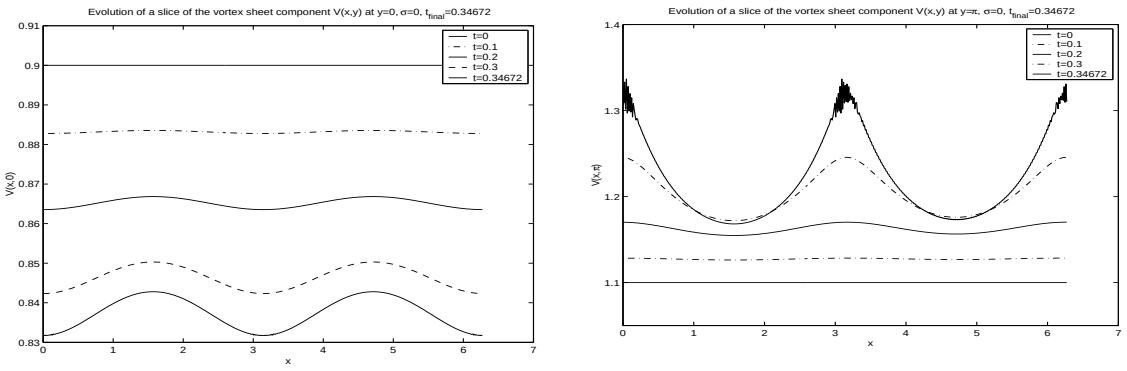

Figure 3.17 Slice of the vortex sheet component $V(x, y, t)$, $\gamma = 0$, $n = 512$ at: (a) $y = 0$; (b) $y = \pi$.

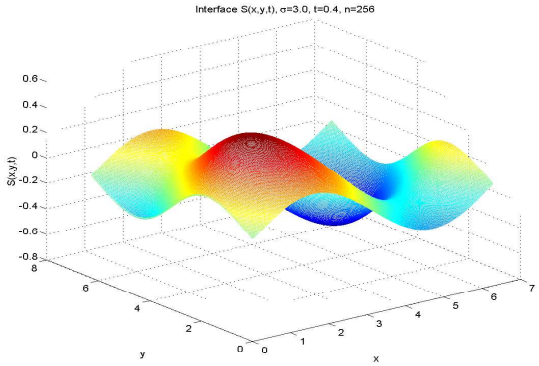

Figure 3.18 Interface $S(x, y, t)$, $\gamma = 3.0$, $n = 256$ at time $t = 0.4$.

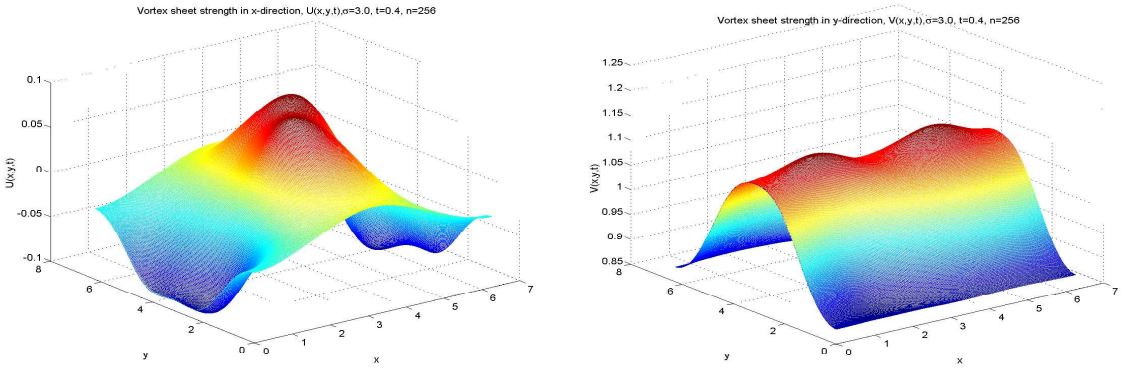

Figure 3.19 Vortex sheet strength component $\gamma = 3.0$, $n = 256$ at time $t = 0.4$. (a) $U(x, y, t)$, component in x-direction; (b) $V(x, y, t)$, component in y-direction.

CHAPTER 4

DERIVATION OF GOVERNING EQUATIONS IN INTEGRO-DIFFERENTIAL FORM

In this chapter we will derive a Birkhoff-Rott type integral equation that describes the evolution of the shape of a vortex sheet as well as the evolution equation for the unnormalized vortex sheet strength. We do this for a general configuration in a channel of arbitrary width and for vortex sheet amplitudes of arbitrary size. The main objective is to study the effect of the presence of walls at a finite distance, on singularity formation, for example. We also consider two limiting cases of the derived Birkhoff-Rott type equation for validation purposes where we compare our results with established ones for vortex sheets in unbounded domains and which are spatially periodic.

4.1 The Birkhoff-Rott Type Equation

Consider a two-dimensional velocity field $\mathbf{u}(x, y) = (u, v)$. The vorticity $\boldsymbol{\omega}(x, y)$ is defined by

$$\boldsymbol{\omega} = \nabla \times \mathbf{u}.$$

To begin with, we consider vorticity distributions $\boldsymbol{\omega}(x, y)$ which are smooth. Assuming that the flow is incompressible, i.e., $\nabla \cdot \mathbf{u} = 0$ or $u_x + v_y = 0$, there exists a scalar function $\psi(x, y)$, called the *stream function*, such that

$$u = \frac{\partial \psi}{\partial y}; \quad v = -\frac{\partial \psi}{\partial x}.$$

Then the vorticity is

$$\boldsymbol{\omega} = (-\nabla^2 \psi)\mathbf{k} = (v_x - u_y)\mathbf{k} = \omega(x, y)\mathbf{k},$$

and it follows that the stream function ψ satisfies the Poisson equations with the vorticity as a source function

$$\nabla^2\psi = -\omega. \tag{4.1}$$

The domain of consideration is the 2-D strip $\mathcal{D} = \{(x, y) : x \in \mathbb{R},\ 0 \le y \le D\}$, where D is the dimensional height of the channel. The geometry is shown in Figure 4.1 (a).

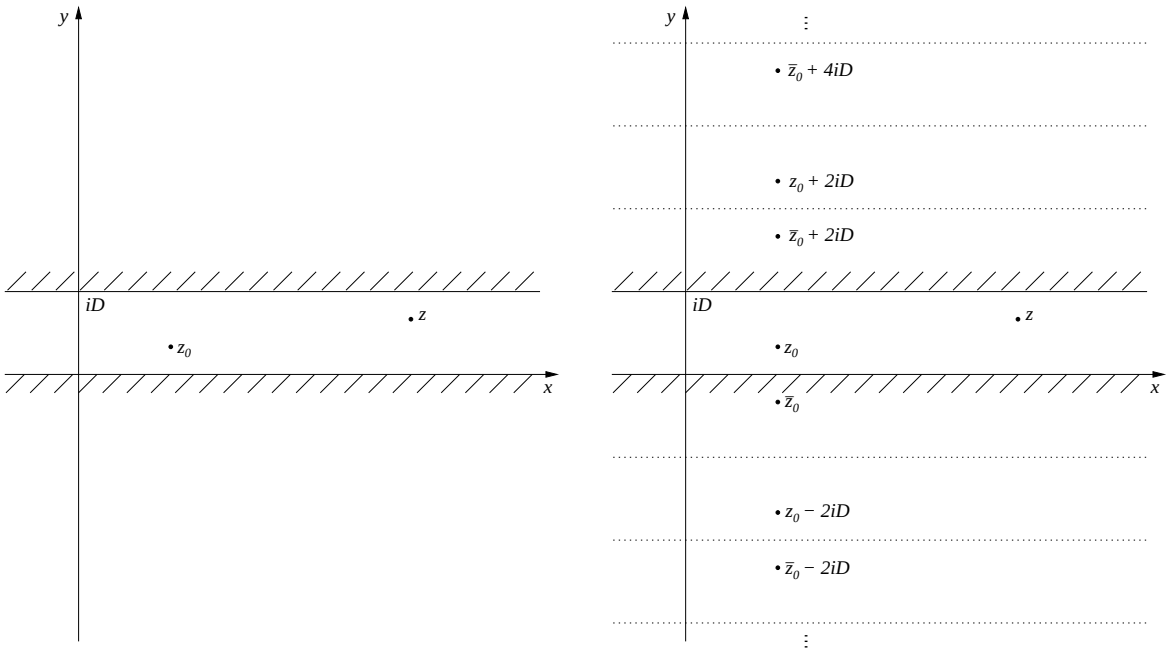

Figure 4.1 (a) Channel of height D; (b) infinite system of images.

A solution of equation (4.1) is obtained by solving the Poisson equation (4.1), and it gives

$$\psi(x, y) = -\iint_{\mathcal{D}} \omega(\xi, \eta) G(x, y; \xi, \eta) d\xi d\eta \tag{4.2}$$

where $G(x, y; \xi, \eta)$ is the Green's function for the Laplacian in $\mathcal{D}$. The boundary conditions along the top and bottom of the channel are zero normal flow

$$v(x, 0) = v(x, D) = 0 \quad \Rightarrow \quad \psi(x, 0) = \psi(x, D) = 0.$$

In order to derive the Green's function $G(x, y; \xi, \eta)$, we suppose that a source of unit strength is located inside the channel at (ξ, η) and that (x, y) is a second point

inside the channel with $(x, y) \neq (\xi, \eta)$. In order to satisfy the zero normal condition along the top and bottom of the channel, we introduce the infinite system of images shown in 4.1 (b). This system solves the Dirichlet Green's function problem we are interested in.

The images of positive strength are located at $(\xi, \eta + 2Dj)$ $(j = -\infty, \ldots, \infty)$ whereas images of negative strength have location at $(\xi, -\eta + 2Dj)$ $(j = -\infty, \ldots, \infty)$.

The free space Green's function is given by

$$G_F(x, y; \xi, \eta) = \frac{1}{2\pi} \ln \left((x - \xi)^2 + (y - \eta)^2 \right)^{1/2} = \frac{1}{4\pi} \ln \left((x - \xi)^2 + (y - \eta)^2 \right).$$

Therefore, the required Green's function for the strip $\mathcal{D}$ is

$$\begin{aligned} G(x, y; \xi, \eta) &= \sum_{j=-\infty}^{\infty} \frac{1}{4\pi} \left[\ln \left((x - \xi)^2 + (y - \eta - 2jD)^2 \right) \right. \\ &- \left. \ln \left((x - \xi)^2 + (y + \eta - 2jD)^2 \right) \right]. \end{aligned}$$

The velocity components u and v may be found by differentiating the stream function solution given in equation (4.2) with respect to y and x, respectively, i.e.

$$u = \frac{\partial \psi}{\partial y} = - \iint_{\mathcal{D}} \omega(\xi, \eta) \frac{\partial G}{\partial y} d\xi d\eta,$$

$$v = -\frac{\partial \psi}{\partial x} = \iint_{\mathcal{D}} \omega(\xi, \eta) \frac{\partial G}{\partial x} d\xi d\eta,$$

where

$$\frac{\partial G}{\partial x} = \sum_{j=-\infty}^{\infty} \frac{1}{2\pi} \left[\frac{x - \xi}{(x - \xi)^2 + (y - \eta - 2jD)^2} - \frac{x - \xi}{(x - \xi)^2 + (y + \eta - 2jD)^2} \right],$$

$$\frac{\partial G}{\partial y} = \sum_{j=-\infty}^{\infty} \frac{1}{2\pi} \left[\frac{y - \eta - 2jD}{(x - \xi)^2 + (y - \eta - 2jD)^2} - \frac{y + \eta - 2jD}{(x - \xi)^2 + (y + \eta - 2jD)^2} \right].$$

Then

$$\begin{aligned} u(x, y) &= - \iint_{\mathcal{D}} \omega(\xi, \eta) \sum_{j=-\infty}^{\infty} \frac{1}{2\pi} \left[\frac{y - \eta - 2jD}{(x - \xi)^2 + (y - \eta - 2jD)^2} \right. \\ &- \left. \frac{y + \eta - 2jD}{(x - \xi)^2 + (y + \eta - 2jD)^2} \right] d\xi d\eta, \end{aligned}$$

$$v(x,y) = \iint_{\mathcal{D}} \omega(\xi,\eta) \sum_{j=-\infty}^{\infty} \frac{1}{2\pi} \left[\frac{x-\xi}{(x-\xi)^2+(y-\eta-2jD)^2} - \frac{x-\xi}{(x-\xi)^2+(y+\eta-2jD)^2} \right] d\xi d\eta.$$

We can use these expressions to write a complex velocity,

$$(u-iv)(x,y) = -\frac{1}{2\pi} \iint_{\mathcal{D}} \omega(\xi,\eta) \sum_{j=-\infty}^{\infty} \left[\frac{y-\eta-2jD}{(x-\xi)^2+(y-\eta-2jD)^2} - \frac{y+\eta-2jD}{(x-\xi)^2+(y+\eta-2jD)^2} + i\frac{x-\xi}{(x-\xi)^2+(y-\eta-2jD)^2} - i\frac{x-\xi}{(x-\xi)^2+(y+\eta-2jD)^2} \right] d\xi d\eta$$

$$= -\frac{i}{2\pi} \iint_{\mathcal{D}} \omega(\xi,\eta) \sum_{j=-\infty}^{\infty} \left[\frac{x-\xi-i(y-\eta-2jD)}{(x-\xi)^2+(y-\eta-2jD)^2} - \frac{x-\xi-i(y+\eta-2jD)}{(x-\xi)^2+(y+\eta-2jD)^2} \right] d\xi d\eta.$$

Using complex notation

$$z = x+iy, \quad \tilde{z} = \xi+i\eta,$$

we obtain

$$(u-iv)(z) = \frac{1}{2\pi i} \iint_{\mathcal{D}} \omega(\tilde{z}) \sum_{j=-\infty}^{\infty} \left[\frac{\overline{z-(\tilde{z}+2jDi)}}{(z-(\tilde{z}+2jDi))\overline{(z-(\tilde{z}+2jDi))}} - \frac{\overline{z-(\bar{\tilde{z}}+2jDi)}}{(z-(\bar{\tilde{z}}+2jDi))\overline{(z-(\bar{\tilde{z}}+2jDi))}} \right] d\xi d\eta,$$

where the bar $^-$ indicates complex conjugation, and after simplification we have

$$(u-iv)(z) = \frac{1}{2\pi i} \iint_{\mathcal{D}} \omega(\tilde{z}) \sum_{j=-\infty}^{\infty} \left[\frac{1}{z-(\tilde{z}+2jDi)} - \frac{1}{z-(\bar{\tilde{z}}+2jDi)} \right] d\xi d\eta. \quad (4.3)$$

We now consider the case in which the vorticity is concentrated in a region of size ε about the curve $c(s)$ parametrized by $(x(s), y(s))$, where the parameter s is arc length. Define the function

$$\sigma(s) = \int_{-\varepsilon/2}^{\varepsilon/2} \omega(\nu(s)) d\nu(s) \quad (4.4)$$

where $\nu(s)$ is the distance normal to the curve at s. If we now suppose that $\varepsilon \to 0$ and $\max|\omega| \to \infty$ (i.e., the support of vorticity narrows and the vorticity becomes unbounded) so that $\sigma(s)$ remains constant, we arrive at the concept of a vortex sheet characterized locally by the vorticity density $\sigma(s)$.

Hence, when the vorticity is zero everywhere except on a given vortex sheet, equation (4.3) for the velocity is transformed into a line integral

$$\begin{aligned}(u-iv)(z) &= \frac{1}{2\pi i}\int_{-\infty}^{\infty}\sigma(s)\sum_{j=-\infty}^{\infty}\left[\frac{1}{z-(z(s)+2jDi)}\right. \\ &- \left.\frac{1}{z-(\overline{z(s)}+2jDi)}\right]ds \end{aligned} \tag{4.5}$$

where $\tilde{z} = z(s)$ and $z \in \mathbb{R}^2 \setminus c$.

Now, introduce a complex potential $\Omega = \phi + i\psi$, where ϕ is the potential of the flow ($\mathbf{u} = \nabla\phi$), and $q = u + iv$ is the complex velocity. Then $\bar{q} = \frac{d\Omega}{dz} = (u-iv)(z)$. Note that the complex potential corresponding to the velocity distribution (4.5) is

$$\begin{aligned}\Omega(z) &= \frac{1}{2\pi i}\int_{-\infty}^{\infty}\sigma(s)\sum_{j=-\infty}^{\infty}[\ln(z-(z(s)+2jDi)) \\ &- \ln(z-(\overline{z(s)}+2jDi))\Big]ds. \end{aligned} \tag{4.6}$$

Next we evaluate the infinite series in (4.5) using ideas presented in the paper by Greengard [35].

Denote by $\tilde{\mathbf{u}}_1(z)$ the velocity field induced by images of positive unit strength (more precisely, the velocity field is $\frac{1}{2\pi i}\tilde{\mathbf{u}}_1(z)$)

$$\begin{aligned}\tilde{\mathbf{u}}_1(z) &= \sum_{j=-\infty}^{\infty}\frac{1}{z-(z(s)+2jDi)} = \frac{1}{z-z(s)} + \sum_{j=1}^{\infty}\left(\frac{1}{z-z(s)-2jDi}\right. \\ &\left.+\frac{1}{z-z(s)+2jDi}\right) = \frac{1}{z-z(s)} + \sum_{j=1}^{\infty}\frac{2(z-z(s))}{(z-z(s))^2+4j^2D^2} \\ &= \frac{1}{z-z(s)} + \frac{2(z-z(s))}{4D^2}\sum_{j=1}^{\infty}\frac{1}{\left(\frac{z-z(s)}{2D}\right)^2+j^2} = \frac{1}{z-z(s)} + 2\frac{z-z(s)}{2D}\frac{1}{2D} \\ &* \sum_{j=1}^{\infty}\frac{1}{\left(\frac{z-z(s)}{2D}\right)^2+j^2} = \frac{\pi}{2D}\left\{\frac{2D}{\pi(z-z(s))} + 2\frac{z-z(s)}{2D\pi}\sum_{j=1}^{\infty}\frac{1}{\left(\frac{z-z(s)}{2D}\right)^2+j^2}\right\}. \end{aligned}$$

From ([34], p.36)

$$\coth(\pi z) = \frac{1}{\pi z} + \frac{2z}{\pi}\sum_{k=1}^{\infty}\frac{1}{z^2+k^2}, \tag{4.7}$$

and with $z = \frac{z-z(s)}{2D}$, we obtain

$$\tilde{\mathbf{u}}_1(z) = \frac{\pi}{2D}\coth\Big(\frac{\pi}{2D}(z-z(s))\Big). \tag{4.8}$$

Similarly, the velocity induced by images of negative strength

$$\tilde{\mathbf{u}}_2(z) = -\frac{\pi}{2D}\coth\Big(\frac{\pi}{2D}(z-\overline{z(s)})\Big). \tag{4.9}$$

The net velocity field is, therefore

$$\tilde{\mathbf{u}}(z) = \frac{\pi}{2D}\left[\coth\Big(\frac{\pi}{2D}(z-z(s))\Big) - \coth\Big(\frac{\pi}{2D}(z-\overline{z(s)})\Big)\right]. \tag{4.10}$$

Hence the velocity field equation (4.5) induced by vorticity distributed along the vortex sheet may be written as

$$\begin{aligned}(u-iv)(z) &= \frac{1}{2\pi i}\int_{-\infty}^{\infty}\sigma(s)\frac{\pi}{2D}\left[\coth\Big(\frac{\pi}{2D}(z-z(s))\Big)\right.\\ &- \left.\coth\Big(\frac{\pi}{2D}(z-\overline{z(s)})\Big)\right]ds\end{aligned} \tag{4.11}$$

where $z \in \mathbb{R}^2 \setminus c$. The last equation is the expression of the complex velocity of points z not on the vortex sheet.

If gravity and surface tension are absent, then we obtain the Kelvin-Helmholtz type problem and in this case we can make a change of variables replacing the variable of integration s by a variable Γ defined by

$$\Gamma(s) = \int_0^s \sigma(\tau)d\tau. \tag{4.12}$$

Then equation (4.11) becomes

$$\begin{aligned}(u-iv)(z) &= \frac{1}{2\pi i}\int_{-\infty}^{\infty}\frac{\pi}{2D}\left[\coth\Big(\frac{\pi}{2D}(z-z(\Gamma'))\Big)\right.\\ &- \left.\coth\Big(\frac{\pi}{2D}(z-\overline{z(\Gamma')})\Big)\right]d\Gamma'\end{aligned} \tag{4.13}$$

where $z \in \mathbb{R}^2 \setminus c$.

The variable $\Gamma(s)$ is the total vortex sheet strength between the point $s = 0$ and an arbitrary point s, and physically this is the circulation about a curve whose end points are $s = 0$ and s. The advantage of the variable Γ is that if an arbitrary point on the interface is defined to move with a velocity equal to the average of the flow velocities at the two sides of the sheet, then the quantity Γ remains constant in time at that point. This is a consequence of Kelvin's circulation theorem [79], which says that the circulation about any contour composed of the same fluid particles (a fluid line) is constant in an inviscid fluid and if the external forces are conservative.

When external forces, for example, gravity, are present, then it is more difficult to define the velocity of the interface in such a way that the quantity $\Gamma(s)$ would remain constant on the sheet. This is due to the creation of vorticity on the interface caused by the presence of external forces. Therefore, we cannot use equation (4.13). Instead, it is useful to rewrite equation (4.11) using the Lagrangian variable (Lagrangian marker) e. In terms of e, equation (4.11) becomes

$$\begin{aligned}(u - iv)(z) &= \frac{1}{2\pi i}\int_{-\infty}^{\infty} \sigma(e) s_e \frac{\pi}{2D}\left[\coth\left(\frac{\pi}{2D}(z - z(e))\right)\right. \\ &- \left.\coth\left(\frac{\pi}{2D}(z - \overline{z(e)})\right)\right] de \end{aligned} \tag{4.14}$$

where $z \in \mathbb{R}^2 \setminus c$. Introducing the unnormalized vortex sheet strength $\gamma(e, t)$ given by

$$\gamma(e, t) = \sigma(e, t)\frac{\partial s}{\partial e}, \tag{4.15}$$

equation (4.14) may be written as

$$\begin{aligned}(u - iv)(z) &= \frac{1}{2\pi i}\int_{-\infty}^{\infty} \gamma(e, t) \frac{\pi}{2D}\left[\coth\left(\frac{\pi}{2D}(z - z(e))\right)\right. \\ &- \left.\coth\left(\frac{\pi}{2D}(z - \overline{z(e)})\right)\right] de. \end{aligned} \tag{4.16}$$

We note that the vortex sheet strength γ depends on time t, which stresses that γ changes with time due to creation of vorticity as a consequence of action of gravity, for example.

Equation (4.16) defines the velocity field induced by the vortex sheet at any point z of the plane except at points on the sheet c. The velocity at the interface may be determined as the average of those just above and below the interface (this is more conventional) or may be defined as a weighted average of the velocities across the interface. The latter definition of the velocity of the vortex sheet was first used in [4] in order to improve the accuracy of numerical calculations. Later, this approach was shown to be convenient and useful in a theoretical analysis of the Rayleigh-Taylor problem in [83]. In this work, we choose the average speed approach. The choice of the tangential velocity of a point on the interface to be the arithmetic average (or weighted average) of the tangential components of the fluid velocity on either side corresponds to the so-called *Lagrangian formulation* [42] of the problem.

Let us define

$$
\begin{aligned}
B[z](e) &= \lim_{\varepsilon\to 0}\frac{1}{2\pi i}\left\{\int_{-1/\varepsilon}^{e-\varepsilon}\gamma(e,t)\frac{\pi}{2D}\left[\coth(\frac{\pi}{2D}(z-z(e)))-\coth(\frac{\pi}{2D}(z-\overline{z(e)}))\right]de\right. \\
&\left.+\int_{e+\varepsilon}^{1/\varepsilon}\gamma(e,t)\frac{\pi}{2D}\left[\coth(\frac{\pi}{2D}(z-z(e)))-\coth(\frac{\pi}{2D}(z-\overline{z(e)}))\right]de\right\} \\
&= \frac{1}{2\pi i}\fint_{-\infty}^{\infty}\gamma(e,t)\frac{\pi}{2D}\left[\coth(\frac{\pi}{2D}(z-z(e)))-\coth(\frac{\pi}{2D}(z-\overline{z(e)}))\right]de,
\end{aligned}
$$

$$
B[z]^{+}(e) = (u_1 - iv_1)(e) = \lim_{\substack{z\to z(e)^{+} \\ z\in \text{ upper fluid}}} (u-iv)(z), \tag{4.17}
$$

$$
B[z]^{-}(e) = (u_2 - iv_2)(e) = \lim_{\substack{z\to z(e)^{-} \\ z\in \text{ lower fluid}}} (u-iv)(z), \tag{4.18}
$$

where the limit in the last two expressions is taken over a path contained in the upper/lower part of the channel determined by the vortex sheet. The line through the integral sign in the first equation signifies Cauchy's principal value (for definition, see Appendix D). Using the Sokhotski-Plemelj formulae (see, for example, [61, 17], [55] and Appendix D), we obtain

$$
B[z](e) = \frac{1}{2}\left\{B[z]^{+}(e) + B[z]^{-}(e)\right\}. \tag{4.19}
$$

Since we defined the velocity at a point of the vortex sheet as the average of the limiting velocities just above and below the vortex sheet, respectively, i.e. $(u+iv)(\text{sheet}) = \frac{1}{2}\{(u_1+iv_1)+(u_2+iv_2)\}$, the desired equation for the complex velocity of a point on the vortex sheet follows from equation (4.19) as

$$\begin{aligned}\frac{d\bar{z}}{dt}(e,t) &= \frac{1}{2\pi i}\fint_{-\infty}^{\infty}\gamma(e,t)\frac{\pi}{2D}\left[\coth(\frac{\pi}{2D}(z-z(e)))\right.\\ &- \left.\coth(\frac{\pi}{2D}(z-\overline{z(e)}))\right]de. \end{aligned} \tag{4.20}$$

The integral on the right-hand side of (4.20) is the Birkhoff-Rott type integral for the case of a bounded vortex sheet, and it is analogous to the corresponding case of an unbounded vortex sheet. In order to complete the description of the motion, we need an additional equation that describes the evolution for $\gamma(t)$. We will derive this equation in the following section.

Note that the complex potential corresponding to the complex velocity (4.20) may be written as

$$\begin{aligned}\Omega(z) &= \frac{1}{2\pi i}\fint_{-\infty}^{\infty}\gamma(e,t)\frac{\pi}{2D}\left[\ln\sinh(\frac{\pi}{2D}(z-z(e)))\right.\\ &- \left.\ln\sinh(\frac{\pi}{2D}(z-\overline{z(e)}))\right]de. \end{aligned} \tag{4.21}$$

4.1.1 Limiting Case for the Complex Potential for $D \gg 1$ — Unbounded Vortex Sheet

We show next that as $D \to \infty$, we recover the Birkhoff-Rott equation for an unbounded vortex sheet [12], namely,

$$\frac{\partial}{\partial t}\bar{z}(e,t) = \frac{1}{2\pi i}\fint_{-\infty}^{\infty}\gamma(e,t)\frac{de}{z-z(e,t)}. \tag{4.22}$$

Equation (4.22) was first derived using the Biot-Savart law by Birkhoff [12] and then in a more mathematically rigorous way by Sulem et al. [86].

First make the change of variables

$$\zeta = z - \frac{iD}{2}, \quad \zeta(e) = z(e) - \frac{iD}{2}$$

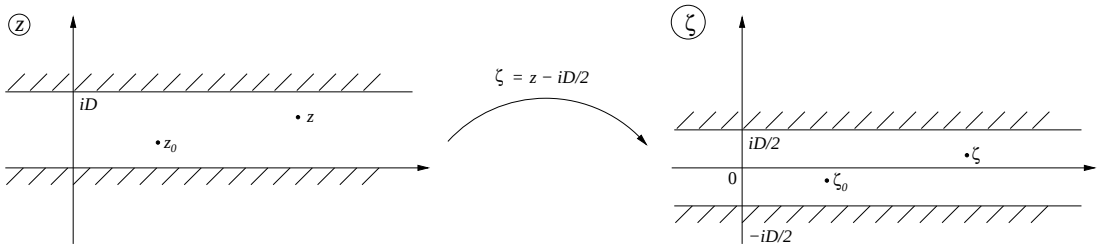

Figure 4.2 (a) Channel in z-plane; (b) shifted channel in ζ-plane.

that shifts the x-axis to the horizontal centerline of the strip (see Figure 4.2). Then

$$z - z(e) = \zeta - \zeta(e) \quad \text{and} \quad z - \overline{z(e)} = \zeta - \overline{\zeta(e)} + iD.$$

Consider the difference under the sign of the integral in (4.11),

$$\frac{\pi}{2D}\left[\coth\left(\frac{\pi}{2D}(z - z(e))\right) - \coth\left(\frac{\pi}{2D}(z - \overline{z(e)})\right)\right]$$
$$= \frac{\pi}{2D}\left[\coth\left(\frac{\pi}{2D}(\zeta - \zeta(e))\right) - \coth\left(\frac{\pi}{2D}(\zeta - \overline{\zeta(e)} + iD)\right)\right].$$

As $D \to \infty$, the upper wall will tend to plus infinity while the lower wall to minus infinity and the strip will cover the whole of $\mathbb{R}^2$. Observe that for fixed $\zeta - \zeta(e)$

$$\frac{\pi}{2D}(\zeta - \zeta(e)) \to 0,$$
$$\frac{\pi}{2D}(\zeta - \zeta(e) + iD) = \frac{\pi}{2D}(\zeta - \zeta(e)) + i\frac{\pi}{2} \to i\frac{\pi}{2} \text{ as } D \to \infty.$$

For $\frac{\pi}{2D}(\zeta - \zeta(e)) \ll 1$,

$$\coth\frac{\pi}{2D}(\zeta - \zeta(e)) = \frac{\cosh\frac{\pi}{2D}(\zeta - \zeta(e))}{\sinh\frac{\pi}{2D}(\zeta - \zeta(e))} \sim \frac{1}{\frac{\pi}{2D}(\zeta - \zeta(e))},$$
$$\coth\frac{\pi}{2D}(\zeta - \zeta(e) + iD) \sim \coth(i\frac{\pi}{2}) = \frac{\cosh(i\frac{\pi}{2})}{\sinh(i\frac{\pi}{2})} = \frac{\cos\frac{\pi}{2}}{i\sin\frac{\pi}{2}} = 0.$$

Hence,

$$\frac{\pi}{2D}\left[\coth\left(\frac{\pi}{2D}(\zeta - \zeta(e))\right) - \coth\left(\frac{\pi}{2D}(\zeta - \overline{\zeta(e)} + iD)\right)\right]$$

$$\sim \frac{\pi}{2D}\left[\frac{1}{\frac{\pi}{2D}(\zeta-\zeta(e))}-0\right]=\frac{1}{\zeta-\zeta(e)},$$

and we recover the equation for the unbounded vortex sheet (4.22) in terms of variables ζ and $\zeta(e)$,

$$\frac{\partial}{\partial t}\bar{\zeta}(e,t)=\frac{1}{2\pi i}\fint \gamma(e,t)\frac{de}{\zeta-\zeta(e,t)}.$$

4.1.2 The Periodic Bounded Vortex Sheet

We now give a formal derivation of the periodic bounded vortex sheet equation with period $P = 2L$. We will use a method modified from that proposed by Choi and Humphrey in [24] where the authors derived an expression for the stream function due to a single vortex for the potential flow in a rectangular domain.

Consider the complex potential (4.6) before summing the contributions of the doubly infinite image system. Using a Lagrangian representation, we have,

$$\begin{aligned}\Omega(z) &= \frac{1}{2\pi i}\int_{-\infty}^{\infty}\gamma(e)\left[\ln\prod_{j=-\infty}^{\infty}(z-z(e)-2jDi)\right.\\ &- \left.\ln\prod_{j=-\infty}^{\infty}(z-\overline{z(e)}-2jDi)\right]de. \qquad (4.23)\end{aligned}$$

Due to periodicity we can write $z(e,t) = e + s(e,t)$ where $s(e+2L,t) = s(e,t)$ and $\gamma(e+2L,t) = \gamma(e,t)$. Then the integral in (4.23) can be written as an infinite sum over a finite interval as follows

$$\begin{aligned}\Omega(z) = \frac{1}{2\pi i}\sum_{n=-\infty}^{\infty}\int_{2Ln}^{2L(n+1)}\gamma(e,t)\left\{\ln\prod_{j=-\infty}^{\infty}(z-z(e)-2jDi)\right.\\ \left.-\ln\prod_{j=-\infty}^{\infty}(z-\overline{z(e)}-2jDi)\right\}de.\end{aligned}$$

Changing the variable of integration e to $p = e - 2Ln$ we obtain

$$\begin{aligned}\Omega(z) &= \frac{1}{2\pi i}\sum_{n=-\infty}^{\infty}\int_{0}^{2L}\gamma(p+2Ln,t)\left\{\ln\prod_{j=-\infty}^{\infty}(z-[p+2Ln+s(p+2Ln,t)]\right.\\ &- \left.2jDi)-\ln\prod_{j=-\infty}^{\infty}(z-[p+2Ln+\overline{s(p+2Ln)}]-2jDi)\right\}dp.\end{aligned}$$

Periodicity of s and γ in variable p gives

$$\Omega(z) = \frac{1}{2\pi i}\sum_{n=-\infty}^{\infty}\int_0^{2L}\gamma(p,t)\left\{\ln\prod_{j=-\infty}^{\infty}(z-z(p,t)-2Ln-2jDi)\right.$$

$$\left.-\ln\prod_{j=-\infty}^{\infty}(z-\overline{z(p,t)}-2Ln-2jDi)\right\}dp$$

$$=\frac{1}{2\pi i}\int_0^{2L}\gamma(p,t)\left\{\ln\prod_{n=-\infty}^{\infty}\prod_{j=-\infty}^{\infty}(z-z(p,t)-2Ln-2jDi)\right.$$

$$\left.-\ln\prod_{n=-\infty}^{\infty}\prod_{j=-\infty}^{\infty}(z-\overline{z(p,t)}-2Ln-2jDi)\right\}dp.$$

Introduce

$$\mathcal{F}(z)=\gamma(p,t)\ln\prod_{n=-\infty}^{\infty}\prod_{j=-\infty}^{\infty}(z-2Ln-2jDi).$$

Then the complex potential may be written as

$$\Omega(z)=\frac{1}{2\pi i}\int_0^{2L}[\mathcal{F}(z-z(p,t))-\mathcal{F}(z-\overline{z(p,t)})]dp.$$

Consider the function $\mathcal{F}$ next. Changing the order of multiplication in both infinite products, $\mathcal{F}$ may be written as

$$\begin{aligned}\mathcal{F} &= \gamma(p,t)\ln\prod_{n=\infty}^{-\infty}\prod_{j=\infty}^{-\infty}(z+2Ln+2jDi)\\ &= \gamma(p,t)\ln\left[z\cdot\prod_{\substack{n\neq 0\\ \text{simult.}}}\prod_{j\neq 0}(z+2Ln+2jDi)\right].\end{aligned}\tag{4.24}$$

Note that in the last doubly infinite product, the simultaneous values of $n=0$, $j=0$ are to be omitted. We can rewrite $\mathcal{F}$ as

$$\mathcal{F}=\gamma(p,t)\ln\left[z\cdot\prod_{\substack{n\neq 0\\ \text{simult.}}}\prod_{j\neq 0}(2Ln+2jDi)\left(1+\frac{z}{2Ln+2jDi}\right)\right].$$

Proposition 2 *The following identity is true*

$$\ln\left(\prod_n\prod_m a_{nm}b_{nm}\right)=\ln\left(\prod_n\prod_m a_{nm}\cdot\prod_n\prod_m b_{nm}\right).\tag{4.25}$$

Proof. Indeed,

$$\ln\left(\prod_n\prod_m a_{nm}b_{nm}\right)=\sum_n\sum_m\ln(a_{nm}b_{nm})=\sum_n\sum_m\ln(a_{nm}+\ln b_{nm})$$

$$=\sum_n\sum_m\ln a_{nm}+\sum_n\sum_m\ln b_{nm}=\ln\prod_n\prod_m a_{nm}+\ln\prod_n\prod_m b_{nm}$$

$$=\ln\left(\prod_n\prod_m a_{nm}\cdot\prod_n\prod_m b_{nm}\right).$$

■

Using (4.25) we get

$$\mathcal{F}=\gamma(p,t)\ln\left[z\prod_{\substack{n\neq0\\ \text{simult.}}}\prod_{j\neq0}\left(1+\frac{z}{2Ln+2jDi}\right)\cdot\prod_{\substack{n\neq0\\ \text{simult.}}}\prod_{j\neq0}(2Ln+2jDi)\right]$$

$$=\gamma(p,t)\ln\left[z\prod_{\substack{n\neq0\\ \text{simult.}}}\prod_{j\neq0}\left(1+\frac{z}{2Ln+2jDi}\right)\right]+\gamma(p,t)\ln\left[\prod_{\substack{n\neq0\\ \text{simult.}}}\prod_{j\neq0}(2Ln+2jDi)\right].$$

Denote

$$G_1(n,j)=\gamma(p,t)\ln\left[\prod_{\substack{n\neq0\\ \text{simult.}}}\prod_{j\neq0}(2Ln+2jDi)\right].$$

Then

$$\mathcal{F}=\gamma(p,t)\ln\left[z\prod_{\substack{n\neq0\\ \text{simult.}}}\prod_{j\neq0}\left(1+\frac{z}{2Ln+2jDi}\right)\right]+G_1(n,j).$$

The Jacobi's function $H(u,k)$ is defined as ([18], p.303)

$$H(u,k)=\sqrt{\frac{2kk'K}{\pi}}u\prod_{\substack{n\neq0\\ \text{simult.}}}\prod_{j\neq0}\left[1+\frac{u}{2nK+2jK'i}\right] \tag{4.26}$$

where k is the modulus, $K=\int_0^{\pi/2}\frac{d\phi}{\sqrt{1-k^2\sin^2\phi}}$, and $k'=\sqrt{1-k^2}$ is the complimentary modulus, and $K'=\int_0^{\pi/2}\frac{d\phi}{\sqrt{1-k'^2\sin^2\phi}}$. For more information about Jacobi's functions and their relations to elliptic integrals and elliptic functions, see Appendix C as well

as Cayley [18] and Milne-Thomson in [1], Chapters 16 and 17. Using (4.26), we can write

$$z \prod_{\substack{n\neq 0\\ \text{simult.}}} \prod_{j\neq 0} \left(1+\frac{z}{2Ln+2jDi}\right) = z \prod_{\substack{n\neq 0\\ \text{simult.}}} \prod_{j\neq 0} \left(1+\frac{z}{\frac{L}{K}(2nK+2jD\frac{K}{L}i)}\right)$$

$$= z \prod_{\substack{n\neq 0\\ \text{simult.}}} \prod_{j\neq 0} \left(1+\frac{\frac{K}{L}z}{2nK+2jK'i}\right) = \frac{L}{K}\cdot\frac{K}{L} z \prod_{\substack{n\neq 0\\ \text{simult.}}} \prod_{j\neq 0} \left(1+\frac{\frac{K}{L}z}{2nK+2jK'i}\right)$$

$$= \frac{L}{K}\sqrt{\frac{\pi}{2kk'K}} H\left(\frac{K}{L}z,k\right)$$

where $\frac{DK}{L}=K'$ or $\frac{L}{D}=\frac{K}{K'}$. Hence

$$z \prod_{\substack{n\neq 0\\ \text{simult.}}} \prod_{j\neq 0} \left(1+\frac{z}{2Ln+2jDi}\right) = \frac{L}{K}\sqrt{\frac{\pi}{2kk'K}} H\left(\frac{K}{L}z,k\right).$$

This is really a function of L and D since the relation $\frac{DK}{L}=K'$ picks any k (see Figure C.1 in Appendix C). Then

$$\begin{aligned}\mathcal{F} &= \gamma(p,t)\ln\left[\frac{L}{K}\sqrt{\frac{\pi}{2kk'K}} H\left(\frac{K}{L}z,k\right)\right] + G_1(n,j)\\ &= \gamma(p,t)\ln\left[\frac{L}{K}\sqrt{\frac{\pi}{2kk'K}}\right] + \gamma(p,t)\ln H\left(\frac{K}{L}z,k\right) + G_1(n,j),\end{aligned}$$

whence

$$\mathcal{F}(z-z(p,t)) - \mathcal{F}(z-\overline{z(p,t)}) = \gamma(p,t)\ln H\left(\frac{K}{L}(z-z(p,t)),k\right)$$

$$-\gamma(p,t)\ln H\left(\frac{K}{L}(z-\overline{z(p,t)}),k\right).$$

Hence we can write the complex potential as

$$\begin{aligned}\Omega(z) &= \frac{1}{2\pi i}\int_0^{2L}\gamma(p,t)\left[\ln H\left(\frac{K}{L}(z-z(p,t)),k\right)\right.\\ &- \left.\ln H\left(\frac{K}{L}(z-\overline{z(p,t)}),k\right)\right]dp. \qquad (4.27)\end{aligned}$$

Differentiating formally the complex potential Ω in (4.27) with respect to z, we get

$$(u-iv)(z)=\frac{d\Omega}{dz}=\frac{1}{2\pi i}\int_0^{2L}\gamma(p,t)\frac{d}{dz}\left[\ln H\left(\frac{K}{L}(z-z(p,t)),k\right)\right.$$
$$\left.-\ln H\left(\frac{K}{L}(z-\overline{z(p,t)}),k\right)\right]dp.$$

From ([18], pp.155 and 143)

$$H(u,k)=-i\,\mathrm{e}^{-\frac{\pi}{4K}(K'-2iu)}\,\Theta(u+iK',k),\quad \frac{d}{du}\Theta(u,k)=\Theta(u,k)\cdot Z(u,k)$$

where $\Theta(u,k)$ and $Z(u,k)$ are Theta and Zeta Jacobi's functions (see Appendix C). We derive, therefore,

$$\frac{d}{du}H(u,k)=H(u,k)\cdot\left[\frac{\pi i}{2K}+Z(u+iK',k)\right]. \tag{4.28}$$

Using (4.28) we obtain

$$(u-iv)(z)=\frac{1}{2\pi i}\int_0^{2L}\gamma(p,t)\left[\frac{\frac{K}{L}}{H(\frac{K}{L}(z-z(p,t)),k)}H\Big(\frac{K}{L}(z-z(p,t)),k\Big)\right.$$
$$*\left(\frac{\pi i}{2K}+Z\Big(\frac{K}{L}(z-z(p,t))+iK',k\Big)\right)-\frac{\frac{K}{L}}{H(\frac{K}{L}(z-\overline{z(p,t)}),k)}$$
$$\left.*H\Big(\frac{K}{L}(z-\overline{z(p,t)}),k\Big)\left(\frac{\pi i}{2K}+Z\Big(\frac{K}{L}(z-\overline{z(p,t)})+iK',k\Big)\right)\right]dp.$$

Hence

$$(u-iv)(z)=\frac{1}{2\pi i}\int_0^{2L}\gamma(p,t)\frac{K}{L}\left[Z\Big(\frac{K}{L}(z-z(p,t))+iK',k\Big)\right.$$
$$\left.-Z\Big(\frac{K}{L}(z-\overline{z(p,t)})+iK',k\Big)\right]dp. \tag{4.29}$$

Equation (4.29) is the required periodic extension of the bounded vortex sheet.

4.1.3 Limiting Case for the Complex Potential $L \gg 1$, D is Finite

Consider the complex potential (4.27). We can show that as the aspect ratio $\frac{L}{D} \to \infty$, i.e., the period becomes infinite, we recover the expression for the complex potential without periodic extension (4.21). Indeed, as $\frac{L}{D} \to \infty$, the values of k, k', K and K' become

$$k = 1, \quad k' = 0, \quad K = \infty, \quad K' = \frac{\pi}{2}.$$

We also have $\frac{L}{D} = \frac{K}{K'}$, hence $\frac{K}{L} = \frac{K'}{D}$ and as $K \to \infty$, the ratio $\frac{K'}{D} = \frac{\pi/2}{D} = \frac{\pi}{2D}$ remains finite.

It follows from ([18], p.156)

$$H(u,k) = \sqrt{k}\,\mathrm{sn}(u,k)\Theta(u,k), \tag{4.30}$$

where $\Theta(u,k)$ is the Jacobi's function defined as ([18], p.143)

$$\Theta(u,k) = \sqrt{\frac{2k'K}{\pi}}\,\mathrm{e}^{\int_0 Z(u,k)du}. \tag{4.31}$$

Denote the difference of logarithms in (4.27) as

$$\Lambda(z,k) = \ln H\left(\frac{K}{L}(z - z(p,t)), k\right) - \ln H\left(\frac{K}{L}(z - \overline{z(p,t)}), k\right)$$

and let

$$u = \frac{K}{L}(z - z(p,t)) = \frac{K'}{D}(z - z(p,t)), \quad v = \frac{K}{L}(z - \overline{z(p,t)}) = \frac{K'}{D}(z - \overline{z(p,t)})$$

for brevity.

Then using (4.30) we obtain

$$\Lambda(z,k) = \ln\frac{H(u,k)}{H(v,k)} = \ln\frac{\sqrt{\frac{2kk'K}{\pi}}\,\mathrm{sn}(u,k)\,\mathrm{e}^{\int_0 Z(u,k)du}}{\sqrt{\frac{2kk'K}{\pi}}\,\mathrm{sn}(v,k)\,\mathrm{e}^{\int_0 Z(v,k)dv}} = \ln\frac{\mathrm{sn}(u,k)\,\mathrm{e}^{\int_0 Z(u,k)du}}{\mathrm{sn}(v,k)\,\mathrm{e}^{\int_0 Z(v,k)dv}}.$$

As $k = 1$, $Z(u,1) = \tanh u$. Therefore,

$$\int_0 Z(u,1)du = \int_0 \tanh u\,du = \int_0 \frac{\sinh u}{\cosh u}du = \ln\cosh u.$$

Hence,

$$\mathrm{e}^{\int_0 Z(u,1)du} = \mathrm{e}^{\ln\cosh u} = \cosh u.$$

On the other hand, $\mathrm{sn}(u,1) = \tanh u$. The same reasoning is true for functions of the argument v. Hence,

$$\lim_{\frac{L}{D}=\frac{K}{K'}\to\infty} \Lambda(z,k) = \lim_{\frac{L}{D}=\frac{K}{K'}\to\infty} \ln \frac{\mathrm{sn}(u,k)\,\mathrm{e}^{\int_0 Z(u,k)du}}{\mathrm{sn}(v,k)\,\mathrm{e}^{\int_0 Z(v,k)dv}} = \ln \frac{\tanh u \cosh u}{\tanh v \cosh v}\Big|_{k=1}$$

$$= \ln \frac{\sinh u}{\sinh v}\Big|_{k=1} = \ln\sinh\frac{\pi}{2D}(z - z(p,t)) - \ln\sinh\frac{\pi}{2D}(z - \overline{z(p,t)}),$$

and the complex potential becomes (4.21)

$$\Omega(z) = \frac{1}{2\pi i}\int_{-\infty}^{\infty} \gamma(e,t)\frac{\pi}{2D}\left[\ln\sinh(\frac{\pi}{2D}(z - z(s))) - \ln\sinh(\frac{\pi}{2D}(z - \overline{z(s)}))\right] de$$

as desired.

4.1.4 Limiting Case for the Complex Velocity $D \gg 1$, L is Finite

Next we show that as $D \to \infty$ and $L = \pi$ we recover, to the leading order, the periodic extension for the unbounded vortex sheet that has the form

$$(u - iv)(z) = \frac{d\Omega}{dz} = \frac{1}{4\pi i}\int_0^{2\pi} \gamma(p,t)\cot\Big(\frac{1}{2}(z - z(p,t))\Big)dp. \tag{4.32}$$

(For derivation of (4.32), see, for example, [83]). Once again, the velocity at the interface is determined by the principal value of the integral.

Changing to the variable $\zeta = z - \frac{iD}{2}$, we move the strip along the y-axis downward, so now as $D \to \infty$, the strip expands to infinity in both directions. Denote by $\Phi(z,k,K,K')$ the difference of the Jacobi's Z functions in (4.29), i.e.

$$\Phi(z,k,K,K') \equiv Z\Big(\frac{K}{L}(z - z(p,t)) + iK', k\Big) - Z\Big(\frac{K}{L}(z - \overline{z(p,t)}) + iK', k\Big)$$

$$= Z\Big(\frac{K}{L}(\zeta - \zeta(p,t)) + iK', k\Big) - Z\Big(\frac{K}{L}(\zeta - \overline{\zeta(p,t)} + iD) + iK', k\Big).$$

Observe that since $\frac{K}{L}D = K'$, we have

$$\frac{K}{L}(\zeta - \overline{\zeta(p,t)} + iD) + iK' = \frac{K}{L}(\zeta - \overline{\zeta(p,t)}) + 2iK'. \tag{4.33}$$

The following identity is useful ([18], p.152)

$$Z(u+a,k) = Z(u,k) + Z(a,k) - k^2 \operatorname{sn}(u,k)\operatorname{sn}(a,k)\operatorname{sn}(u+a,k). \tag{4.34}$$

Using (4.34) with $a = 2iK'$, we obtain

$$Z(u+2iK',k) = Z(u,k) + Z(2iK',k) - k^2 \operatorname{sn}(u,k)\operatorname{sn}(2iK',k)\operatorname{sn}(u+2iK',k).$$

Note that $\operatorname{sn}(u,k)$ has $2iK'$ as one of its periods, hence $\operatorname{sn}(2iK',k) = \operatorname{sn}(0,k)$, $\operatorname{sn}(u+2iK',k) = \operatorname{sn}(u,k)$. Since $\operatorname{sn}(0,k) = 0$ and $Z(2iK',k) = -\frac{i\pi}{K}$, we conclude that

$$Z(u+2iK',k) = Z(u,k) - \frac{i\pi}{K}. \tag{4.35}$$

Another property of the Jacobi's function $Z(u,k)$ which is useful here, is ([18], p.149)

$$Z(u+iK',k) = Z(u,k) + \frac{\operatorname{cn}(u,k)\operatorname{dn}(u,k)}{\operatorname{sn}(u,k)} - \frac{i\pi}{2K}. \tag{4.36}$$

Using (4.33), (4.35) and (4.36), the function Φ may be written as

$$\Phi(z,k,K,K') = Z\Big(\frac{K}{L}(\zeta - \zeta(p,t)),k\Big) - Z\Big(\frac{K}{L}(\zeta - \overline{\zeta(p,t)}),k\Big)$$
$$+\frac{\operatorname{cn}(\frac{K}{L}(\zeta - \zeta(p,t)),k)\operatorname{dn}(\frac{K}{L}(\zeta - \zeta(p,t)),k)}{\operatorname{sn}(\frac{K}{L}(\zeta - \zeta(p,t)),k)} + \frac{i\pi}{2K}.$$

Extension of the strip to infinity implies the aspect ratio $\frac{D}{L} \to \infty$. For this case, k, k', K and K' become

$$\frac{L}{D} = \frac{K}{K'} = 0, \quad k = 0, \quad k' = 1, \quad K = \frac{\pi}{2}, \quad K' = \infty. \tag{4.37}$$

Note that under the above conditions, the expression $\frac{K}{L}(\zeta - \zeta(p,t))$ is finite. For a finite argument, we can use the relations ([1], p.571 and p.595)

$$\operatorname{cn}(u,0) = \cos u, \quad \operatorname{sn}(u,0) = \sin u, \quad \operatorname{dn}(u,0) = 1, \quad Z(u,0) = 0. \tag{4.38}$$

Then

$$\begin{aligned}\lim_{\substack{k=0\\K=\frac{\pi}{2}\\K'=\infty}} \Phi(z,k,K,K') &= 0+\frac{\cos(\frac{\pi}{2L}(\zeta-\zeta(p,t)))}{\sin(\frac{\pi}{2L}(\zeta-\zeta(p,t)))}-0+i\\ &= \cot(\frac{\pi}{2L}(\zeta-\zeta(p,t)))+i.\end{aligned}$$

As the period $2L=2\pi$, $\frac{\pi}{2L}=\frac{1}{2}$, so we obtain

$$(u-iv)(\zeta)=\frac{d\Omega}{d\zeta}=\frac{1}{2\pi i}\int_0^{2\pi}\gamma(p,t)\frac{1}{2}\left[\cot\left(\frac{1}{2}(\zeta-\zeta(p,t))\right)+i\right]dp.$$

As point ζ approaches the interface, i.e. $\zeta-\zeta(p,t)\to 0$, the dominant term in $\cot(\frac{1}{2}(\zeta-\zeta(p,t)))+i$ is $\cot(\frac{1}{2}(\zeta-\zeta(p,t)))$ since cot becomes singular in this case. So, in the limit $\zeta-\zeta(p,t)\to 0$ we recover the formula (4.32).

4.1.5 Limiting Case for the Complex Velocity $L\gg 1$, D is Finite

Another limiting case of (4.29) is when $\frac{L}{D}\to\infty$ with D fixed and $L\to\infty$. We should be able to recover the Birkhoff-Rott equation for the bounded vortex sheet with no periodicity imposed, i.e., equation (4.20).

First we observe that due to the periodicity in e of functions $\gamma(e,t)$, $s(e,t)$, we can shift the interval of integration in (4.29) from $[0,2L]$ to $[-L,L]$. No shift along the y-axis would be necessary.

For this case, k, k', K and K' become (see [18], p.45)

$$k=1,\quad k'=0,\quad K=\infty,\quad K'=\frac{\pi}{2}.$$

Using relation (4.36) and $\frac{K}{L}=\frac{K'}{D}$, we can write

$$\begin{aligned}(u-iv)(z)=\frac{1}{2\pi i}\int_{-L}^{L}\gamma(p)\frac{K'}{D}\Bigg\{&Z(\frac{K'}{D}(z-z(p,t)),k)\\ &+\frac{\mathrm{cn}(\frac{K'}{D}(z-z(p,t)),k)\,\mathrm{dn}(\frac{K'}{D}(z-z(p,t)),k)}{\mathrm{sn}(\frac{K'}{D}(z-z(p,t)),k)}-\frac{i\pi}{2K}-Z(\frac{K'}{D}(z-\overline{z(p,t)}),k)\\ &-\frac{\mathrm{cn}(\frac{K'}{D}(z-\overline{z(p,t)}),k)\,\mathrm{dn}(\frac{K'}{D}(z-\overline{z(p,t)}),k)}{\mathrm{sn}(\frac{K'}{D}(z-\overline{z(p,t)}),k)}+\frac{i\pi}{2K}\Bigg\}dp.\end{aligned}$$

The argument u in the elliptic functions is finite since we have

$$u = \frac{K'}{D}(z - z(p,t)) = \frac{\pi}{2D}(z - z(p,t))$$

or

$$u = \frac{K'}{D}(z - \overline{z(p,t)}) = \frac{\pi}{2D}(z - \overline{z(p,t)}),$$

so we can use the relations ([1], p.571)

$$\mathrm{sn}(u,1) = \tanh u, \quad \mathrm{cn}(u,1) = \mathrm{sech}\, u, \quad \mathrm{dn}(u,1) = \mathrm{sech}\, u, \quad Z(u,1) = \tanh u.$$

Therefore

$$\frac{\mathrm{cn}(u,1)\,\mathrm{dn}(u,1)}{\mathrm{sn}(u,1)} = \coth u.$$

Using the above relations, we obtain the limit of $(u - iv)$ as $\frac{L}{D} \to \infty$, i.e.,

$$\begin{aligned}\lim_{\substack{k\to 1,\, k'\to 0 \\ K'\to \frac{\pi}{2},\, K\to\infty}} (u - iv)(z) = \frac{1}{2\pi i}\int_{-\infty}^{\infty} \gamma(p)\frac{\pi}{2D}\Big\{&\tanh(\frac{\pi}{2D}(z - z(p,t))) \\ &- \tanh(\frac{\pi}{2D}(z - \overline{z(p,t)})) \\ &+ \coth(\frac{\pi}{2D}(z - z(p,t))) - \coth(\frac{\pi}{2D}(z - \overline{z(p,t)}))\Big\}\, dp.\end{aligned}$$

As the point z approaches the interface, i.e., $z - z(p,t)$ and $z - \overline{z(p,t)}$ become small, terms with tanh will approach 0 while terms with coth will become singular and hence dominant. Therefore, we recover the equation for the velocity of the vortex sheet (4.20) when the domain is a bounded channel and no periodicity is imposed.

4.2 Vorticity Evolution Equation

In this section, we derive the evolution equation for the unnormalized vortex sheet strength $\gamma(e,t)$. In our derivation, we follow that given by Baker, Meiron & Orszag [6] and Siegel [83] but set the weight parameter $\beta = 0$. We also incorporate the surface tension term into the vorticity equation.

Consider an interface between inviscid, incompressible, irrotational fluids. The flow of each fluid is governed by an Euler equation

$$\rho_1 \left[\frac{\partial \mathbf{u}_i}{\partial t} + \mathbf{u}_i \cdot \nabla \mathbf{u}_i \right] = -\nabla p_i + \rho_i g, \quad i = 1, 2, \tag{4.39}$$

where the subscripts $i = 1$ and 2 correspond to the upper and lower fluids, respectively. The boundary conditions at the interface are continuity of the normal component of velocity, i.e., $\mathbf{u}_1 \cdot \mathbf{n} = \mathbf{u}_2 \cdot \mathbf{n}$ where $\mathbf{n}$ is the outward normal to the interface, a kinematic condition, and the pressure difference across the interface that can be expressed by Laplace's equation $p_1 - p_2 = \sigma_0 \kappa$, where σ_0 is the surface tension coefficient, and κ is the curvature of the interface.

Let the interface be a curve $c(e)$ parametrized by $\mathbf{x} = (x(e), y(e))$, where e is a Lagrangian variable, and $\hat{s}$ a unit tangential vector at $\mathbf{x}$. Then the pressure difference can be written as

$$p_1 - p_2 = \sigma_0 \cdot \frac{x_e y_e - x_e y_e}{(x_e^2 + y_e^2)^{3/2}}. \tag{4.40}$$

Define the vorticity density σ by

$$\sigma = (\mathbf{u}_2 - \mathbf{u}_1) \cdot \hat{s}. \tag{4.41}$$

The quantity defined in (4.41) is equivalent to that in (4.4) from the previous section as $\varepsilon \to 0$. This can be shown by using Stokes' theorem.

Recall that the *unnormalized vortex sheet strength* $\gamma(e,t)$ was defined in (4.15) as

$$\gamma(e,t) = \sigma(e,t) \frac{\partial s}{\partial e},$$

where s is the arc length. The velocity of a Lagrangian point at the interface labelled by e is defined as the average of the velocities across the interface. In terms of the complex velocity $u - iv$, this definition is

$$(u - iv)(x(e), y(e)) = \frac{(u_1 - iv_1) + (u_2 - iv_2)}{2}, \tag{4.42}$$

where $u_i - iv_i \equiv q_i$, $i = 1, 2$, are the complex velocities evaluated at each side of the interface near point $(x(e), y(e))$ and defined in (4.17), (4.18). Then the unnormalized vortex sheet strength can be written as

$$\gamma = \sigma(e,t)s_e = (\mathbf{u}_2 - \mathbf{u}_1)\hat{s}s_e = (\bar{q}_2 - \bar{q}_1)z_e = ((u_2 - iv_2) - (u_1 - iv_1))z_e, \tag{4.43}$$

where $z_e = x_e + iy_e$ is the complex analog of the vector (x_e, y_e).

Let $\phi(x, y, t)$ be the complex potential of the flow at point (x, y) and time t. Define

$$\phi_1(x(e,t), y(e,t), t) = \lim_{\substack{(x,y)\to(x(e)^+, y(e)^+) \\ z\in \text{ upper fluid}}} \phi(x, y, t), \tag{4.44}$$

$$\phi_2(x(e,t), y(e,t), t) = \lim_{\substack{(x,y)\to(x(e)^-, y(e)^-) \\ z\in \text{ lower fluid}}} \phi(x, y, t). \tag{4.45}$$

Since the flow in each fluid is irrotational, we can evaluate Bernoulli's equation on either side of the interface to get

$$\frac{\partial \phi_1}{\partial t}\Big|_{x,y} + \frac{1}{2}\bar{q}_1 q_1 + \frac{p_1}{\rho_1} + gy = 0, \tag{4.46}$$

$$\frac{\partial \phi_2}{\partial t}\Big|_{x,y} + \frac{1}{2}\bar{q}_2 q_2 + \frac{p_2}{\rho_2} + gy = 0, \tag{4.47}$$

where $\frac{\partial}{\partial t}\Big|_{x,y}$ is used to denote the Eulerian time derivative; $q_i = u_i - iv_i$ are the complex velocities of the upper and lower fluids near point $(x(e), y(e))$ from above and below, respectively. The Eulerian time derivative and the Lagrangian time derivative of ϕ_i, $i = 1, 2$, are related as follows [83]:

$$\frac{\partial \phi_i}{\partial t}\Big|_e = \frac{\partial \phi_i}{\partial x}\frac{\partial x}{\partial t}\Big|_e + \frac{\partial \phi_i}{\partial y}\frac{\partial y}{\partial t}\Big|_e + \frac{\partial \phi_i}{\partial t}\Big|_{x,y} = u_i u_{sheet} + v_i v_{sheet} + \frac{\partial \phi_i}{\partial t}\Big|_{x,y}$$

where $u_{sheet} = \frac{\partial x}{\partial t}\Big|_e$, $v_{sheet} = \frac{\partial y}{\partial t}\Big|_e$. Since

$$q_{sheet} = u_{sheet} + iv_{sheet} = \left(\frac{\partial x}{\partial t} + i\frac{\partial y}{\partial t}\right)\Big|_e = \frac{\partial z}{\partial t}\Big|_e,$$

we obtain

$$\frac{\partial \phi_i}{\partial t}\Big|_e = \mathrm{Re}\{\bar{q}_{sheet} q_i\} + \frac{\partial \phi_i}{\partial t}\Big|_{x,y}. \tag{4.48}$$

Solving equation (4.48) for $\frac{\partial \phi_i}{\partial t}\Big|_{x,y}$ and substituting the resulting expression into (4.46), (4.47) yields

$$\frac{\partial \phi_1}{\partial t}\Big|_e - \mathrm{Re}\{\bar{q}_{sheet} q_1\} + \frac{1}{2}\bar{q}_1 q_1 + \frac{p_1}{\rho_1} + gy = 0, \tag{4.49}$$

$$\frac{\partial \phi_2}{\partial t}\Big|_e - \mathrm{Re}\{\bar{q}_{sheet} q_2\} + \frac{1}{2}\bar{q}_2 q_2 + \frac{p_2}{\rho_2} + gy = 0. \tag{4.50}$$

Denote by

$$a = \frac{\partial \phi_1}{\partial t}\Big|_e - \mathrm{Re}\{\bar{q}_{sheet} q_1\} + \frac{1}{2}\bar{q}_1 q_1,$$

$$b = \frac{\partial \phi_2}{\partial t}\Big|_e - \mathrm{Re}\{\bar{q}_{sheet} q_2\} + \frac{1}{2}\bar{q}_2 q_2.$$

Multiply equation (4.49) by ρ_1 and equation (4.50) by ρ_2. In terms of a and b, the resulting equations are

$$\rho_1 a + p_1 + \rho_1 gy = 0, \tag{4.51}$$

$$\rho_2 b + p_2 + \rho_2 gy = 0. \tag{4.52}$$

Subtract equation (4.51) from equation (4.52) and notice

$$\rho_2 b - \rho_1 a = \frac{1}{2}(2\rho_2 b - 2\rho_1 a) = \frac{1}{2}(\rho_2 b + \rho_2 b + \rho_2 a - \rho_2 a + \rho_1 b - \rho_1 b - \rho_1 a$$

$$- \rho_1 a) = \frac{1}{2}(\rho_2(a+b) + \rho_2(b-a) + \rho_1(b-a) - \rho_1(a+b))$$

$$= \frac{1}{2}((\rho_2 - \rho_1)(a+b) + (\rho_1 + \rho_2)(b-a)).$$

Hence,

$$\frac{1}{2}\Bigg[(\rho_2-\rho_1)\left(\frac{\partial(\phi_1+\phi_2)}{\partial t}\Big|_e - \mathrm{Re}\{\bar{q}_{sheet}(q_1+q_2)\}\right) + \frac{1}{2}(q_1\bar{q}_1+q_2\bar{q}_2) + (\rho_1+\rho_2)\left(\tfrac{\partial(\phi_2-\phi_1)}{\partial t}\Big|_e - \mathrm{Re}\{\bar{q}_{sheet}(q_2-q_1)\} + \tfrac{1}{2}(q_2\bar{q}_2-q_1\bar{q}_1)\right)\Bigg] + p_2 - p_1 + (\rho_2-\rho_1)gy = 0. \tag{4.53}$$

Denote

$$\Phi = \frac{\phi_1(e,t)+\phi_2(e,t)}{2}, \quad \mu(e,t) = \phi_2(e,t) - \phi_1(e,t)$$

where Φ is the average value and μ is the jump of the potential across the interface. We can also interpret μ as the strength of the dipole layer distributed along the interface (see Baker, Meiron & Orszag [6]).

In "q"-notation, the expressions for the vortex sheet velocity (4.43) and the unnormalized vortex sheet strength (4.42) become

$$\bar{q}_{sheet} = \frac{\bar{q}_1+\bar{q}_2}{2}, \quad \text{and} \quad \gamma = (\bar{q}_2-\bar{q}_1)z_e.$$

Then $\bar{q}_1$ and $\bar{q}_2$ may be expressed in terms of q_{sheet} as

$$\bar{q}_1 = \bar{q}_{sheet} - \frac{\gamma}{2z_e}, \tag{4.54}$$

$$\bar{q}_2 = \bar{q}_{sheet} + \frac{\gamma}{2z_e}. \tag{4.55}$$

Dividing equation (4.53) by $\rho_1+\rho_2$ and using there relations (4.54), (4.55) together with the definitions for μ, Φ, and the Atwood ratio $\alpha = \frac{\rho_2-\rho_1}{\rho_1+\rho_2}$, we get

$$\frac{1}{2}\left[\alpha\left(2\frac{\partial\Phi}{\partial t}\Big|_e - q\bar{q} + \frac{\gamma^2}{4z_e\bar{z}_e}\right) + \frac{\partial\mu}{\partial t}\Big|_e\right] + p_2 - p_1 + \alpha gy = 0. \tag{4.56}$$

Differentiate equation (4.56) with respect to e and use the relation between the unnormalized vortex sheet strength γ and the dipole strength μ (see Baker, Meiron & Orszag [6])

$$\gamma = \frac{\partial\mu}{\partial e},$$

to obtain

$$2\alpha\left[\mathrm{Re}\left\{\frac{\partial\bar{q}}{\partial t}z_e\right\}+\frac{1}{8}\frac{\partial}{\partial e}\left\{\frac{\gamma^2}{z_e\bar{z}_e}\right\}+gy_e\right]+\frac{\partial\gamma}{\partial t}\Big|_e-2\frac{\sigma_0\kappa_e}{\rho_1+\rho_2}=0,$$

where we used the Young-Laplace equation for the pressure difference across the interface, i.e. $p_2-p_1=-\sigma_0\kappa$, σ_0 being surface tension coefficient, $\kappa=\frac{x_e y_e-x_e y_e}{\left(x_e^2+y_e^2\right)^{3/2}}$. Therefore,

$$\frac{\partial\gamma}{\partial t}\Big|_e=-2\alpha\left[\mathrm{Re}\left\{\frac{\partial\bar{q}}{\partial t}z_e\right\}+\frac{1}{8}\frac{\partial}{\partial e}\left\{\frac{\gamma^2}{z_e\bar{z}_e}\right\}+gy_e\right]+2\frac{\sigma_0\kappa_e}{\rho_1+\rho_2}. \tag{4.57}$$

This is a desired evolution equation for γ in dimensional variables.

In view of the fact that the velocity of the vortex sheet may be expressed as a Birkhoff-Rott type integro-differential equation, it follows that equation (4.57) is a Fredholm integral equation of the second kind.

Equation (4.57) and various other slightly different forms have been derived and rederived by many investigators. See, for example, Zaroodny & Greenberg [93], Tryggvason [90]; Zalosh [92] (and the correction by Rottman & Olfe [78], Glimm et al [33]).

CHAPTER 5

CONCLUSIONS

The nonlinear flow is studied which results when two immiscible inviscid incompressible fluids of different densities and separated by an interface which is free to move and which supports surface tension, are caused to flow in a straight infinite channel. Gravity is taken into consideration and the velocities of each phase can be different, thus giving rise to the Kelvin-Helmholtz instability. The competing effects of the Kelvin-Helmholtz instability coupled with a stably or unstably stratified fluid system (Rayleigh-Taylor instability) when surface tension is present to regularize the dynamics, are investigated. The approach involves the derivation of two- and three-dimensional model evolution equations using long-wave asymptotics and the ensuing analysis and computation of these models. The appropriate Birkhoff-Rott integro-differential equation for two-phase inviscid flows in channels of arbitrary aspect ratios is also derived.

A long wave asymptotic analysis is undertaken to develop a theory for fully nonlinear interfacial waves allowing amplitudes as large as the channel thickness. The result is a set of evolution equations for the interfacial shape and the velocity jump across the interface. Linear stability analysis reveals that capillary forces stabilize short-wave disturbances in a dispersive manner and the effect of surface tension on the fully nonlinear dynamics described by our models is studied. In the case of two-dimensional interfacial deflections, traveling waves of permanent form are constructed and it is shown that solitary waves are possible for a range of physical parameters. All solitary waves are expressed implicitly in terms of incomplete elliptic integrals of the third kind. When the upper layer has zero density, two explicit solitary-wave solutions have been found whose amplitudes are equal to $h/4$ or $h/9$ where $2h$ is the channel thickness. In the absence of gravity, solitary waves are not

possible but periodic ones are. Numerically constructed traveling and solitary waves are given for representative physical parameters. The initial value problem for the partial differential equations is also addressed numerically in periodic domains, and the regularizing effect of surface tension is investigated. An explicit pseudo-spectral scheme is used in numerical analysis. The system of evolution equations has three conserved quantities, corresponding to mass, total circulation and energy. These constants of motion are used as a check on the accuracy of computational solutions.

It is shown that the system of governing equations terminates in infinite slope singularities. This is achieved by studying a 2×2 system of nonlinear conservation laws in the complex plane and by numerical solution of the evolution equations. This analysis shows that a sinusoidal perturbation of the flat interface and a cosinusoidal perturbation to the unit velocity jump across causes the interface to develop a singularity at time $t_c = \ln \frac{1}{\varepsilon} + O\left(\ln(\ln \frac{1}{\varepsilon})\right)$ where ε is the initial amplitude of the disturbances. This result is asymptotic for small ε and is derived by studying the asymptotic form of the flow characteristics in the complex plane.

The problem under consideration is generalized to the three-dimensional case, where two fluids with different density and velocities bounded between two infinite horizontal plates are considered. Three-dimensional long-wave model equations are derived by assuming that the wavelengths in the principal horizontal directions are large compared to the channel thickness. Surface tension is again incorporated to regularize short-wave Kelvin-Helmholtz instabilities and the equations are solved numerically subject to periodic boundary conditions. Evidence of singularity formation is found. In particular, it is observed that singularities occur at isolated points starting from general initial conditions. This finding is consistent with numerical studies of unbounded three-dimensional vortex sheets, in particular, with the results by Hou & Hu [40]. Integral invariants of motion that correspond to mass,

total circulation in the principal horizontal directions, and energy provided a useful accuracy check for the numerics.

The vortex-sheet formulation of the exact nonlinear two-dimensional motion of the interface is developed for the case when the vortex sheet is bounded by the channel walls. The model includes a Birkhoff-Rott type integro-differential evolution equation for the velocity of the interface in terms of the vorticity as well as the evolution equation for the unnormalized vortex sheet strength. For the case of a periodic vortex sheet, this Birkhoff-Rott type equation is written in terms of Jacobi's functions. The equation is shown to recover the limits of unbounded and non-periodic flows which are known in the literature.

APPENDIX A

GENERAL PROBLEM FORMULATION

We consider a system of two incompressible, inviscid and immiscible fluids which are bounded between two parallel infinite plates. Denote the upper and lower fluids by subscripts 1 and 2, respectively. In dimensional variables, the height of the upper and lower walls of the channel are h_1 and h_2, respectively. The densities are assumed to be ρ_1 and ρ_2. Cartesian coordinates (x, y, z) will be used with the undisturbed interface at $z = 0$. At later times, the deformed interface is given by the function $z = S(x, y, t)$. The geometry of the problem is given in Figure 3.1.

The velocity components in Cartesian coordinates are denoted by (u_i, v_i, w_i) and the pressure by p_i; the governing equations are the continuity equation and the Euler equations in each layer Ω_i,

$$\nabla \vec{u}_i + w_{i_z} = 0, \tag{A.1}$$

$$u_{i_t} + \vec{u}_i \cdot \nabla u_i + w_i u_{i_z} = -\frac{1}{\rho_i} p_{i_x}, \tag{A.2}$$

$$v_{i_t} + \vec{u}_i \cdot \nabla v_i + w_i v_{i_z} = -\frac{1}{\rho_i} p_{i_y}, \tag{A.3}$$

$$u_{i_t} + \vec{u}_i \cdot \nabla u_i + w_i u_{i_z} = -\frac{1}{\rho_i} p_{i_z} - g \tag{A.4}$$

where $\vec{u}_i = (u_i, v_i)$, $\nabla = (\partial_x, \partial_y)$, the subscripts x, y, z, and t mean partial differentiations with respect to x, y, z, and t, respectively, and g is the gravitational acceleration.

One of the boundary conditions at the interface $z = S(x, y, t)$ is the continuity of the normal component of velocity. This condition is called a *kinematic condition* and it reflects the fact that the boundary between the two fluids is a material surface. In other words, a particle of the interface stays on it during the course of its evolution (see, for example, [2] p. 65). i.e., two fluids cannot occupy the same point at the

same time and a cavity cannot be formed between two fluids [30]. The equation of the interface may be written as $F(x,y,z,t) = z - S(x,y,t) = 0$. Then the kinematic condition implies $\frac{DF}{Dt} = 0$ on the interface, where the operator $\frac{D}{Dt}$, called the material derivative, is given by

$$\frac{D}{Dt} = \partial_t + u\partial_x + v\partial_y + w\partial_z.$$

Therefore, we have

$$-S_t + u_i(-S_x) + v_i(-S_y) + w_i \cdot 1 = 0 \quad \text{on} \quad z = S^{\pm}(x,y,t)$$

or

$$S_t + u_i S_x + v_i S_y = w_i \quad \text{on} \quad z = S^{\pm}(x,y,t), \tag{A.5}$$

with $S^{\pm}$ being values of the function $z = S(x,y,t)$ immediately above and below the interface.

Another condition at the interface is the continuity of the normal component of the stress with allowance for the effect of surface tension (this condition is called the *dynamic condition* [7]). The difference between the values of the stress on two surface elements parallel to the boundary and immediately on either side of it, is a normal force due wholly to surface tension. The total stress $T_i = (\sigma_i^{kj})_{k,j=1}^3$, $i = 1,2$, can be written as

$$\sigma_i^{kj} = -p_i\delta^{kj} + 2\mu_i(e_i^{kj} - \frac{1}{3}\Delta_i\delta^{kj})$$

where

$$e_i^{kj} = \frac{1}{2}\left(\frac{\partial u_i^k}{\partial x_j} + \frac{\partial u_i^j}{\partial x_k}\right) \quad \text{and} \quad \Delta_i = e_i^{kk},$$

with μ_i, $i = 1,2$, being the viscosity of the lower/upper fluid, respectively; δ^{kj} the Kronecker delta symbol

$$\delta^{kj} = \begin{cases} 1, & k = j, \\ 0, & k \neq j. \end{cases}$$

Here we derive the dynamic condition in the general case when the fluids are viscous and then set $\mu_i = 0$, since we restrict our attention to inviscid fluids.

Denote by $\vec{n}$, the outward normal to the interface, and $\vec{t}^{(1)}$, $\vec{t}^{(2)}$ mutually orthogonal vectors in the plane tangent to the surface. For the component of the surface tension normal to the interface (in the direction $\vec{n}$) we have

$$[\vec{n} \cdot T_i \cdot \vec{n}]_2^1 = -\sigma_0 \kappa, \tag{A.6}$$

whereas tangential components (in directions $\vec{t}^{(1)}$ and $\vec{t}^{(2)}$, respectively) are

$$[\vec{t}^{(1)} \cdot T_i \cdot \vec{n}]_2^1 = 0, \tag{A.7}$$

$$[\vec{t}^{(2)} \cdot T_i \cdot \vec{n}]_2^1 = 0, \tag{A.8}$$

where $\kappa = -\operatorname{div} \vec{n}$ is the curvature of the interface; $[\ ]_2^1$ denotes the jump between side 1 and side 2, that is, the value on side 1 minus the value on side 2.

Rewrite equations (A.6)-(A.8) in terms of components of the stress tensor σ_i^{kj}.

$$\vec{n} \cdot T_i \cdot \vec{n} = \begin{pmatrix} n^1 & n^2 & n^3 \end{pmatrix} \begin{pmatrix} \sigma_i^{11} & \sigma_i^{12} & \sigma_i^{13} \\ \sigma_i^{21} & \sigma_i^{22} & \sigma_i^{23} \\ \sigma_i^{31} & \sigma_i^{32} & \sigma_i^{33} \end{pmatrix} \begin{pmatrix} n^1 \\ n^2 \\ n^3 \end{pmatrix} = n^k \sigma_i^{kj} n^j.$$

Then

$$\begin{aligned} [\vec{n} \cdot T_i \cdot \vec{n}]_2^1 &= n^k \sigma_1^{kj} n^j - n^k \sigma_2^{kj} n^j = \left(-p_1 \delta^{kj} + 2\mu_1 (e_1^{kj} - \frac{1}{3} \Delta_1 \delta^{kj}) \right) n^k n^j \\ &- \left(-p_2 \delta^{kj} + 2\mu_2 (e_2^{kj} - \frac{1}{3} \Delta_\perp \delta^{kj}) \right) n^k n^j = -p_1 + 2\mu_1 (e_1^{kj} n^k n^j \\ &- \frac{1}{3} \Delta_1) - \left(-p_2 + 2\mu_2 (e_2^{kj} n^k n^j - \frac{1}{3} \Delta_\perp) \right) = p_2 - p_1. \end{aligned}$$

In the last equality, we used the fact that in our problem both fluids are inviscid and we can set $\mu_i = 0$, $i = 1, 2$. Therefore, equation (A.6) simplifies to

$$p_2 - p_1 = -\sigma_0 \kappa \tag{A.9}$$

giving the dynamic condition at the free surface $z = S(x, y, t)$. Similarly, for the tangential components of the stress in the directions $\vec{t}^{(l)}$, $l = 1, 2$, we have

$$\begin{aligned} 0 = [\vec{t}^{(l)} \cdot T_i \cdot \vec{n}]_2^1 &= t^{(l)k}\sigma_1^{kj}n^j - t^{(l)k}\sigma_2^{kj}n^j = \left(-p_1\delta^{kj} + 2\mu_1(e_1^{kj} - \frac{1}{3}\Delta_1\delta^{kj})\right) \\ &* \quad t^{(l)k}n^j - \left(-p_2\delta^{kj} + 2\mu_2(e_2^{kj} - \frac{1}{3}\Delta_\perp\delta^{kj})\right)t^{(l)k}n^j \\ &= -p_1 t^{(l)k}n^k + 2\mu_1(e_1^{kj}t^{(l)k}n^j - \frac{1}{3}\Delta_1 t^{(l)k}n^k) \\ &- \left(-p_2 t^{(l)k}n^k + 2\mu_2(e_2^{kj}t^{(l)k}n^j - \frac{1}{3}\Delta_\perp t^{(l)k}n^k)\right). \end{aligned}$$

Since $\vec{n} \perp \vec{t}^{(l)}$, it follows that $t^{(l)k}n^k = 0$ and hence,

$$0 = [\vec{t}^{(l)} \cdot T_i \cdot \vec{n}]_2^1 = 2\mu_1 e_1^{kj}t^{(l)k}n^j - 2\mu_2 e_2^{kj}t^{(l)k}n^j.$$

For inviscid fluids, the above equation is satisfied automatically since $\mu_1 = \mu_2 = 0$, therefore, the same is true for equations (A.7) and (A.8).

The upper and lower rigid surfaces are assumed to be impermeable, therefore, the normal component of the velocity is zero there, i.e.

$$w_1(x, y, z, t) = 0 \quad \text{at} \quad z = h_1 \tag{A.10}$$

and

$$w_2(x, y, z, t) = 0 \quad \text{at} \quad z = -h_2. \tag{A.11}$$

We assume that the flow is irrotational away from the interface and we can introduce the potential functions ϕ_i, $i = 1, 2$, for the lower and upper fluids, respectively, such that

$$u_i = \phi_{i_x}, \quad v_i = \phi_{i_y}, \quad w_i = \phi_{i_z}. \tag{A.12}$$

In terms of the potential functions ϕ_i, $i = 1, 2$, the continuity equation (A.1) becomes

$$(\Delta + \partial_{zz})\,\phi_i = 0 \tag{A.13}$$

where $\Delta = \partial_{xx} + \partial_{yy}$.

The momentum equation in the x-direction (A.2) can be written as

$$\left\{\phi_{i_t} + \frac{1}{2}\left(\phi_{i_x}\right)^2 + \frac{1}{2}\left(\phi_{i_y}\right)^2 + \frac{1}{2}\left(\phi_{i_z}\right)^2 + \frac{1}{\rho_i}\, p_i\right\}_x = 0. \tag{A.14}$$

Similarly, equations (A.3) and (A.4) may be written as

$$\left\{\phi_{i_t} + \frac{1}{2}\left(\phi_{i_x}\right)^2 + \frac{1}{2}\left(\phi_{i_y}\right)^2 + \frac{1}{2}\left(\phi_{i_z}\right)^2 + \frac{1}{\rho_i}\, p_i\right\}_y = 0, \tag{A.15}$$

$$\left\{\phi_{i_t} + \frac{1}{2}\left(\phi_{i_x}\right)^2 + \frac{1}{2}\left(\phi_{i_y}\right)^2 + \frac{1}{2}\left(\phi_{i_z}\right)^2 + \frac{1}{\rho_i}\, p_i + gz\right\}_z = 0. \tag{A.16}$$

After integration, equations (A.14)-(A.16) give

$$\phi_{i_t} + \frac{1}{2}\left(\phi_{i_x}\right)^2 + \frac{1}{2}\left(\phi_{i_y}\right)^2 + \frac{1}{2}\left(\phi_{i_z}\right)^2 + \frac{1}{\rho_i}\, p_i = -gz + C_i(t) \tag{A.17}$$

where $C_i(t)$, $i = 1, 2$, are arbitrary functions of time t. Function $C_i(t)$ can be absorbed into ϕ_i without changing the velocities if we introduce new potential functions

$$\tilde{\phi}_i = \phi_i - \int^t C_i(\tau) d\tau,$$

and then drop tildes in the modified equations. Therefore the momentum equation (A.17) becomes

$$\phi_{i_t} + \frac{1}{2}\left(\phi_{i_x}\right)^2 + \frac{1}{2}\left(\phi_{i_y}\right)^2 + \frac{1}{2}\left(\phi_{i_z}\right)^2 + \frac{1}{\rho_i}\, p_i = -gz. \tag{A.18}$$

The boundary conditions on the rigid plates are

$$\phi_{1_z} = 0 \quad \text{at} \quad z = h_1, \tag{A.19}$$

and

$$\phi_{2_z} = 0 \quad \text{at} \quad z = -h_2. \tag{A.20}$$

The kinematic condition evaluated from the upper side of the interface becomes

$$\phi_{1_z} = S_t + (\nabla\phi_1 \cdot \nabla S) \quad \text{on} \quad z = S^+(\vec{x}, t), \tag{A.21}$$

and similarly, that from the lower side gives

$$\phi_{2_z} = S_t + (\nabla\phi_2 \cdot \nabla S) \quad \text{on} \quad z = S^-(\vec{x}, t). \tag{A.22}$$

The curvature κ of the interface $F(x, y, z, t) = z - S(x, y, t) = 0$ is

$$\kappa = -\operatorname{div}\vec{n}, \quad \text{where} \quad \vec{n} = \frac{\operatorname{grad} F}{|\operatorname{grad} F|} = \frac{(-S_x, -S_y, 1)}{(S_x^2 + S_y^2 + 1)^{1/2}},$$

and written out in full becomes

$$\kappa = \frac{1}{[1 + S_x^2 + S_y^2]^{3/2}} \left(S_{xx} + S_y^2 S_{xx} + S_{yy} + S_x^2 S_{yy} - 2S_x S_y S_{xy}\right).$$

Hence, the dynamic condition (A.9) at the free surface becomes is

$$\begin{aligned} p_2 - p_1 &= -\frac{\sigma_0}{[1 + S_x^2 + S_y^2]^{3/2}} \left(S_{xx} + S_y^2 S_{xx} + S_{yy}\right. \\ &+ \left. S_x^2 S_{yy} - 2S_x S_y S_{xy}\right) \quad \text{at} \quad z = S(x, y, t). \end{aligned} \tag{A.23}$$

Multiply equation (A.17) with $i = 1$ by ρ_1, equation (A.17) with $i = 2$ by ρ_2 and subtract the resulting equations to obtain

$$\begin{aligned} \rho_1 [\phi_{1t} &+ \frac{1}{2}\left(\phi_{1_x}\right)^2 + \frac{1}{2}\left(\phi_{1_y}\right)^2 + \frac{1}{2}\left(\phi_{1_z}\right)^2 + gz\Big] - \rho_2 [\phi_{2t} \\ &+ \frac{1}{2}\left(\phi_{2_x}\right)^2 + \frac{1}{2}\left(\phi_{2_y}\right)^2 + \frac{1}{2}\left(\phi_{2_z}\right)^2 + gz\Big] = p_2 - p_1. \end{aligned}$$

Now use relation (A.23) for the pressure difference across the interface to get the following Bernoulli equation

$$\begin{aligned} &\rho_1 \left[\phi_{1t} + \frac{1}{2}\left(\Delta + \partial_{zz}\right)\phi_1 + gz\right] - \rho_2 \left[\phi_{2t} + \frac{1}{2}\left(\Delta + \partial_{zz}\right)\phi_2 + gz\right] \\ &= -\frac{\sigma_0}{[1 + S_x^2 + S_y^2]^{3/2}} \left(S_{xx} + S_y^2 S_{xx} + S_{yy} + S_x^2 S_{yy} - 2S_x S_y S_{xy}\right). \end{aligned} \tag{A.24}$$

The resulting problem consists of equation (A.13) subject to boundary conditions (A.19), (A.20), (A.21), (A.22) and (A.24).

APPENDIX B

DETAILS OF THE DERIVATION OF (2.58)

Here we provide a derivation of (2.58), which is central in the construction of nonlinear travelling waves. Multiplication of (2.58) by S' and integration gives the following equation:

$$\begin{aligned} -c\int W(1-\alpha S)dS &- \alpha\int(1+S^2)W^2dS + 2\int SW^2dS \\ &= \frac{\alpha}{2F}S^2 - \frac{1}{2}\gamma S_x^2 + BS + D \end{aligned} \tag{B.1}$$

where B and D are the same constants appearing in (2.58). Making use of the expression (2.56) for W, we have the following results:

$$\begin{aligned} -c\int W(1-\alpha S)dS &= \frac{c}{2}\left\{c\alpha S - \frac{(c+A)(1-\alpha)}{2}\ln|1-S|\right. \\ &- \left.\frac{(c-A)(1+\alpha)}{2}\ln|1+S|\right\}, \end{aligned} \tag{B.2}$$

$$\begin{aligned} \int W^2(-\alpha S^2+2S-\alpha)dS &= -\frac{\alpha}{4}c^2S + \frac{L_1}{4}\int\frac{dS}{1-S} + \frac{L_2}{4}\int\frac{dS}{(1-S)^2} \\ &+ \frac{L_3}{4}\int\frac{dS}{1+S} + \frac{L_4}{4}\int\frac{dS}{(1+S)^2}, \end{aligned} \tag{B.3}$$

where

$$L_1 = c(A+c)(\alpha-1), \quad L_2 = \frac{1}{2}(1-\alpha)(A+c)^2,$$

$$L_3 = c(1+\alpha)(c-A), \quad L_4 = -\frac{1}{2}(1+\alpha)(A-c)^2.$$

The integrals in (B.2) can be obtained analytically by elementary methods. Combining the results described above, it is found that the logarithmic terms cancel leaving equation (2.58) as the final expression.

APPENDIX C

ELLIPTIC FUNCTIONS

In this chapter, we give some necessary definitions, relations and properties of Legendre's Elliptic Integrals, Jacobi's Elliptic Functions and Jacobi's Z, Π, Θ and H Functions. Material presented here is based on works by Cayley [18] and Milne-Thomson in [1], Chapters 16 and 17.

Let $R(x)$ be a rational function of x and X a rational and integral quartic function of x with real coefficients. The integral

$$\int \frac{R dx}{\sqrt{X}} \tag{C.1}$$

is called an *elliptic integral*. The values of x are real, and such that X is positive, or $\sqrt{X}$ real. The rational function R is the sum of an even function and an odd function of x. The odd part of the differential expression in (C.1) may be integrated by circular and logarithmic functions. There still remains to consider the part when R is even. Thus we may take R to be an even rational function of x.

By a real substitution [18], we can transform the differential expression in (C.1) into the form

$$\frac{R dx}{\sqrt{(1-x^2)(1-k^2x^2)}}, \tag{C.2}$$

where $0 < x < 1$ and $0 < k < 1$. By decomposing R into an integral and fractional part, and the fractional part into simple fractions, and by integrating by parts, the integration is made to depend upon that of the three terms

$$\frac{dx}{\sqrt{(1-x^2)(1-k^2x^2)}}, \quad \frac{x^2 dx}{\sqrt{(1-x^2)(1-k^2x^2)}}, \quad \frac{dx}{\sqrt{(1+nx^2)(1-x^2)(1-k^2x^2)}},$$

where n is real or imaginary.

Writing the substitution $x = \sin\phi$, we can introduce the three kinds of *Elliptic Integrals*: viz. these are

$$F(k,\phi) = \int_0^\phi \frac{d\theta}{\sqrt{1-k^2\sin^2\theta}} \quad \textbf{First Kind}, \tag{C.3}$$

$$E(k,\phi) = \int_0^\phi \sqrt{1-k^2\sin^2\theta} \quad \textbf{Second Kind}, \tag{C.4}$$

$$\Pi(k,\phi) = \int_0^\phi \frac{d\theta}{(1+n\sin^2\theta)\sqrt{1-k^2\sin^2\theta}} \quad \textbf{Third Kind}. \tag{C.5}$$

In the above integrals, ϕ is called the *amplitude*, k the *modulus*, n the parameter. The amplitude is a real angle, the modulus k, as already mentioned, is positive and less than 1; whence also $k' = \sqrt{1-k^2}$, called the *complimentary modulus*, is real, positive and less then 1.

Instead of the complete notation $F(k,\phi)$, we frequently express only the amplitude ϕ, and write simply $F\phi$ and similar $E\phi$, etc. if it is understood what the unexpressed letters k, or k and n, are.

We have spoken of ϕ as the amplitude of $F\phi$. Denote $\Delta\phi = 1-k^2\sin^2\theta$. Writing $F\phi = u$, then ϕ is the amplitude of u, say $\phi = \operatorname{am} u$, and then $\sin\phi$, $\cos\phi$, $\Delta\phi$ are the sine, cosine and delta of $\operatorname{am} u$, which may be written as $\sin\operatorname{am} u$, $\cos\operatorname{am} u$, $\Delta\operatorname{am} u$ or in abbreviated form as

$$\operatorname{sn} u, \quad \operatorname{cn} u \quad \operatorname{dn} u.$$

Functions $\operatorname{sn} u$, $\operatorname{cn} u$ and $\operatorname{dn} u$ are sorts of cosine-functions of u. They are called *Elliptic Functions*. Some of their properties are

$$\operatorname{cn}^2 u = 1 - \operatorname{sn}^2 u, \quad \operatorname{dn}^2 u = 1 - k^2\operatorname{sn}^2 u,$$

$$\frac{d}{du}\operatorname{cn} u = -\operatorname{sn} u \operatorname{dn} u, \quad \frac{d}{du}\operatorname{dn} u = -k^2\operatorname{sn} u \operatorname{cn} u, \quad \frac{d}{du}\operatorname{sn} u = \operatorname{cn} u \operatorname{dn} u.$$

These five equations constitute a foundation of the theory. We also observe that

$$\operatorname{sn} 0 = 0, \quad \operatorname{cn} 0 = 1, \quad \operatorname{dn} 0 = 1$$

and

$$\operatorname{sn}(-u) = -\operatorname{sn} u, \quad \operatorname{cn}(-u) = -\operatorname{cn} u, \quad \operatorname{dn}(-u) = -\operatorname{dn} u,$$

the last three equations imply that functions $\operatorname{sn} u$, $\operatorname{cn} u$ and $\operatorname{dn} u$ are odd functions of u. Moreover, as $k = 0$ or $k = 1$, the elliptic functions reduce to trigonometric functions, viz.

$$\begin{aligned}
&\operatorname{sn}(u, 0) = \sin u, \quad \operatorname{sn}(u, 1) = \tanh u,\\
&\operatorname{cn}(u, 0) = \cos u, \quad \operatorname{cn}(u, 1) = \operatorname{sech} u,\\
&\operatorname{dn}(u, 0) = 1, \qquad \operatorname{dn}(u, 1) = \operatorname{sech} u.
\end{aligned}$$

Elliptic functions $\operatorname{sn} u$, $\operatorname{cn} u$ and $\operatorname{dn} u$ satisfy the following addition equations.

$$\operatorname{sn}(u \pm v) = \frac{\operatorname{sn} u \operatorname{cn} v \operatorname{dn} v \pm \operatorname{sn} v \operatorname{cn} u \operatorname{dn} u}{1 - k^2 \operatorname{sn}^2 u \operatorname{sn}^2 v},$$

$$\operatorname{cn}(u \pm v) = \frac{\operatorname{cn} u \operatorname{cn} v \mp \operatorname{sn} u \operatorname{dn} u \operatorname{sn} v \operatorname{dn} v}{1 - k^2 \operatorname{sn}^2 u \operatorname{sn}^2 v},$$

$$\operatorname{dn}(u \pm v) = \frac{\operatorname{dn} u \operatorname{dn} v \mp k^2 \operatorname{sn} u \operatorname{cn} u \operatorname{sn} v \operatorname{cn} v}{1 - k^2 \operatorname{sn}^2 u \operatorname{sn}^2 v}.$$

The integrals, taken up to the value $\phi = \pi/2$ of the amplitude are said to have their *complete* value. We will denote these by $F(k, \pi/2) = F_1 k$ or simply F_1, and so on $E_1 k$, E_1 etc. The complete function F_1 is also denoted by

$$K = \int_0^{\pi/2} \frac{d\phi}{\sqrt{1 - k^2 \sin^2 \phi}} = \int_0^1 \frac{dx}{\sqrt{(1 - x^2)(1 - k^2 x^2)}},$$

where K is a function of k, moreover $\operatorname{sn} K = 1$, $\operatorname{cn} K = 0$, $\operatorname{dn} K = k'$. It should be noted that functions $\operatorname{sn} u$, $\operatorname{cn} u$ and $\operatorname{dn} u$ have a real period $4K$.

The form of the integral suggests the consideration of another complex quantity

$$\begin{aligned}
&\int_0^{1/k} \frac{dx}{\sqrt{(1 - x^2)(1 - k^2 x^2)}}\\
&= \int_0^1 \frac{dx}{\sqrt{(1 - x^2)(1 - k^2 x^2)}} + i \int_0^1 \frac{dx}{\sqrt{(1 - x^2)(1 - k'^2 x^2)}} = K + iK',
\end{aligned}$$

where K' being the same function of the complimentary modulus k' as K is of k. The elliptic functions $\operatorname{sn} u$, $\operatorname{cn} u$ and $\operatorname{dn} u$ satisfy equations

$$\operatorname{sn}(K+iK') = \frac{1}{k'}, \quad \operatorname{cn}(K+iK') = \frac{ik'}{k}, \quad \operatorname{dn}(K+iK') = 0,$$

from which we deduce that another period is $4iK'$. Therefore, the elliptic functions are doubly periodic. More specifically, the function $\operatorname{sn} u$ has periods $2iK'$, $4K+4iK'$, $4K$; function $\operatorname{cn} u$ has periods $4iK'$, $2K+2iK'$, $4K$; finally, the function $\operatorname{dn} u$ has periods $4iK'$, $4K+4iK'$ and $2K$.

By introducing u as the argument if the integrals of the second (C.4) and third (C.5) kinds, we obtain

$$E(k,\phi) \equiv E(k,u) = \int_0 (1-k^2 \operatorname{sn}^2 u)du,$$

$$\Pi(n,k,\phi) \equiv \Pi(n,k,u) = \int_0 \frac{du}{1+n\operatorname{sn}^2 u}.$$

In place of the integral of the second kind Jacobi considers a function

$$Zu = u\left(1-\frac{E}{K}\right) - k^2 \int_0 \operatorname{sn}^2 u\, du,$$

where E, K denote the complete functions $E_1 k$, $F_1 k$ respectively. The complete expression is $Z(k,u)$, thus, Zu is a functions of k.

From the function $\operatorname{sn} u$ we derive a new function Θu by the equation

$$\Theta u = \sqrt{\frac{2Kk'}{\pi}}\, \mathrm{e}^{\frac{1}{2}u^2\left(1-\frac{E}{K}\right)-k^2\int_0 du \int_0 \operatorname{sn}^2 u du}$$

or using the function Zu, we may write

$$\Theta u = \sqrt{\frac{2k'K}{\pi}}\, \mathrm{e}^{\int_0 Z(u,k)du}.$$

This may be regarded as one of four functions Θu, $\Theta(u+K)$, $\Theta(u+iK')$, $\Theta(u+K+iK')$. Writing

$$Hu = -i\, \mathrm{e}^{\frac{i\pi}{2K}(u+\frac{1}{2}iK')}\, \Theta(u+iK'),$$

the functions may be taken to be Θu, $\Theta(u+K)$, Hu, $H(u+K)$.

The function Zu may be expressed in terms of Θu and its derivative $\frac{d}{du}\Theta u \equiv \Theta' u$ as

$$Zu = \frac{\Theta' u}{\Theta u}.$$

The elliptic functions $\operatorname{sn} u$, $\operatorname{cn} u$, $\operatorname{dn} u$ may be written in terms of Jacobi's functions Θu, $\Theta(u+K)$, Hu, $H(u+K)$ as

$$\operatorname{sn} u = \frac{1}{\sqrt{k}}\frac{Hu}{\Theta u}, \quad \operatorname{cn} u = \sqrt{\frac{k'}{k}}\frac{H(u+K)}{\Theta u}, \quad \operatorname{dn} u = \sqrt{k'}\frac{\Theta(u+K)}{\Theta u}.$$

It may be remarked here that the functions H, Θ are not doubly periodic.

The functions H, Θ may be expressed in terms of doubly infinite products, viz. writing for shortness

$$\begin{aligned}
(m, m') &= 2mK + 2m'iK', \\
(\bar{m}, m') &= (2m+1)K + 2m'iK', \\
(m, \bar{m}') &= 2mK + (2m'+1)iK', \\
(\bar{m}, \bar{m}') &= (2m+1)K + (2m'+1)iK'.
\end{aligned}$$

Then, we have

$$\begin{aligned}
Hu &= \sqrt{k}\sqrt{\frac{2k'K}{\pi}}u \prod_{m,m'}\left\{1 + \frac{u}{(m,m')}\right\}, \\
H(u+K) &= \sqrt{\frac{2k'K}{\pi}} \prod_{m,m'}\left\{1 + \frac{u}{(\bar{m},m')}\right\}, \\
\Theta u &= \sqrt{\frac{2k'K}{\pi}} \prod_{m,m'}\left\{1 + \frac{u}{(m,\bar{m}')}\right\}, \\
\Theta(u+K) &= \sqrt{\frac{2k'K}{\pi}} \prod_{m,m'}\left\{1 + \frac{u}{(\bar{m},\bar{m}')}\right\},
\end{aligned} \tag{C.6}$$

where (except that in the first product the simultaneous values $m = 0$, $m' = 0$ are to be omitted) m, m' have all positive or negative integer values, including zero, but under the following condition, viz. taking μ, μ' to denote each of them an indefinitely

large positive integer, μ being also indefinitely large in comparison with μ', so that $\mu'/\mu = 0$, then for m the limits are $m = -\mu$ to $+\mu$; for m' the limits are $m = -\mu'$ to $+\mu'$; for $\bar{m}$ the limits are $m = -\mu - 1$ to $+\mu$; for m the limits are $\bar{m}' = -\mu' + 1$ to $+\mu'$.

Consider the expression $\frac{K'}{K}$. It is convenient to notice (see also Figure C.1) the following limiting values for k, k', K and K'

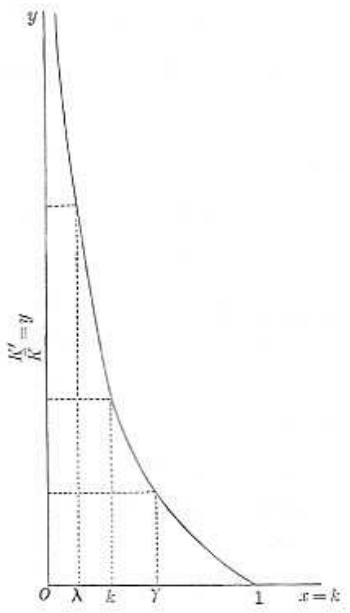

Figure C.1 Dependence of $\frac{K'}{K}$ on k. Taken from Cayley [18], p.44.

$$k = 0, \quad k' = 1, \quad K = \frac{\pi}{2}, \quad K' = \infty, \quad \frac{K'}{K} = \infty,$$

$$k = 1, \quad k' = 0, \quad K = \infty, \quad K' = \frac{\pi}{2}, \quad \frac{K'}{K} = 0,$$

i.e., as k increases from 0 to 1, $\frac{K'}{K}$ diminishes from ∞ to 0.

There is no proper addition-equation for the functions H, Θ. The nearest analogue is the system of equations

$$\Theta(u+v)\Theta(u-v) = \frac{\Theta^2 u \Theta^2 v - H^2 u H^2 v}{\Theta^2 0},$$

$$H(u+v)H(u-v) = \frac{H^2\Theta^2 v - \Theta^2 u H^2 v}{\Theta^2 0},$$

where $\Theta 0 = \sqrt{\frac{2k'K}{\pi}}$.

However, there is the addition-equation for the function Zu, viz.

$$Zu + Zv - Z(u+v) = k^2 \operatorname{sn} u \operatorname{sn} v \operatorname{sn}(u+v).$$

Finally, we give some values of the Zu function for certain values of the arguments.

$$Z(0,k) = 0, \qquad Z(K,k) = 0, \quad Z(2iK',k) = -\tfrac{i\pi}{K}, \qquad Z(iK',k) = \infty,$$
$$Z(u,1) = \tanh u, \quad Z(u,0) = 0, \quad Z(-u,k) = -Z(u,k).$$

APPENDIX D

SOKHOTSKI-PLEMELJ FORMULAE

In this chapter, we present Sohotskij-Plemelj Formulae used in the derivation of a Birkhoff-Rott type integro-differential equation in Section 4.1.

Consider the integral

$$F(z) = \frac{1}{2\pi i} \int_C \frac{f(\zeta)}{\zeta - z} d\zeta \tag{D.1}$$

where C is a smooth curve (C may be an arc or a closed contour), function $f(z)$ defined on C and continuous everywhere except possibly at a finite number of points where it has an integrable discontinuity. The integral (D.1) is called the *Cauchy type integral*. Let the function $f(\zeta)$ satisfy the *Hölder condition* on C, that is for any two points ζ and ζ_1 of C

$$|f(\zeta) - f(\zeta_1)| \leq \Lambda |\zeta - \zeta_1|^\lambda, \quad \Lambda > 0, \quad 0 < \lambda \leq 1.$$

The integral (D.1) is well defined and $F(z)$ is analytic provided that z is not on C. However, if z is on C, this integral becomes ambiguous. To give it a unique meaning we have to define how z approaches C. We denote by $+$ the region that is on the left of the positive direction of C and by $-$ the region on the right (see Figure D.1). Then, as the next theorem shows, $F(z)$ has a limit $F^+(\zeta_0)$, ζ_0 on C, when z approaches C along a curve entirely in the $+$ region. Similarly, $F(z)$ has a limit $F^-(\zeta_0)$, when z approaches C along a curve entirely in the $-$ region. These limits are given by so called *Sokhotski-Plemelj Formulae*.

Theorem (Sokhotski-Plemelj Formulae) *Let C be a smooth contour (closed or open) and let $f(z)$ satisfy a Hölder condition on C. The Cauchy type integral $F(z)$, defined in (D.1), has the limiting values $F^+(\zeta_0)$ and $F^-(\zeta_0)$ as z approaches C from*

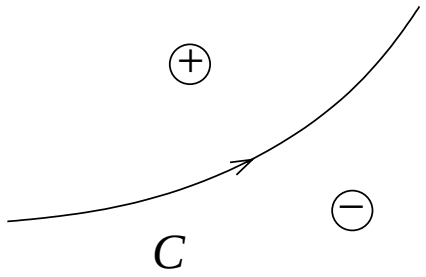

Figure D.1 Regions on either side of C.

the left and the right, respectively, and ζ_0 is not an endpoint of C. These limiting values are given by

$$F^+(\zeta_0) = F(\zeta_0) + \frac{1}{2}f(\zeta_0), \tag{D.2}$$

$$F^-(\zeta_0) = F(\zeta_0) - \frac{1}{2}f(\zeta_0) \tag{D.3}$$

where

$$F(\zeta_0) = \frac{1}{2\pi i}\fint_C \frac{f(\zeta)}{\zeta - \zeta_0}d\zeta. \tag{D.4}$$

In equation (D.4), $\fint$ denotes the principal value integral defined by

$$\fint_C \frac{f(\zeta)}{\zeta - \zeta_0}d\zeta = \lim_{\varepsilon\to 0}\int_{C\setminus C_\varepsilon} \frac{f(\zeta)}{\zeta - \zeta_0}d\zeta \tag{D.5}$$

where C_ε is the portion of the curve C contained within a small circle of radius ε, centered on ζ_0, as depicted in Figure D.2.

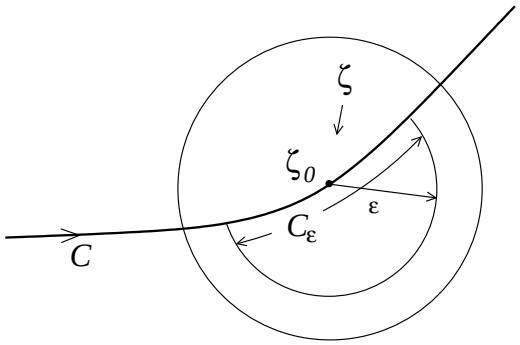

Figure D.2 Neighborhood of point ζ_0 on C.

Formulae (D.2), (D.3) were first proved by Sokhotski in 1873, then by Plemelj in 1908, and finally under more general assumptions by Privalov in 1918 [55].

BIBLIOGRAPHY

[1] Abramowitz, M., and Stegun, I. A. *Handbook of mathematical functions with formulas, graphs, and mathematical tables*, vol. 55 of *National Bureau of Standards Applied Mathematics Series*. Superintendent of Documents, U.S. Government Printing Office, Washington, D.C., 1964.

[2] Acheson, D. J. *Elementary fluid dynamics*. Oxford Applied Mathematics and Computing Science Series. The Clarendon Press Oxford University Press, New York, 1990.

[3] Baker, G., Caflisch, R. E., and Siegel, M. Singularity formation during Rayleigh-Taylor instability. *J. Fluid Mech. 252* (1993), 51–78.

[4] Baker, G., Meiron, D., and Orszag, S. Vortex simulations of the Rayleigh-Taylor instability. *Phys. Fluids 23* (1980), 1485–1490.

[5] Baker, G., and Nachbin, A. Stable methods for vortex sheet motion in the presence of surface tension. *SIAM J. Sci. Comput. 19*, 5 (1998), 1737–1766 (electronic).

[6] Baker, G. R., Meiron, D. I., and Orszag, S. A. Generalized vortex methods for free-surface flow problems. *J. Fluid Mech. 123* (1982), 477–501.

[7] Batchelor, G. *An introduction to Fluid Dynamics*, paperback ed. Cambridge Mathematical Library. Cambridge University Press, Cambridge, 1999.

[8] Beale, J. T., Hou, T. Y., and Lowengrub, J. Convergence of a boundary integral method for water waves. *SIAM J. Numer. Anal. 33*, 5 (1996), 1797–1843.

[9] Beale, J. T., Hou, T. Y., and Lowengrub, J. S. On the well-posedness of two fluid interfacial flows with surface tension. In *Singularities in fluids, plasmas and optics (Heraklion, 1992)*, vol. 404 of *NATO Adv. Sci. Inst. Ser. C Math. Phys. Sci.* Kluwer Acad. Publ., Dordrecht, 1993, pp. 11–38.

[10] Benjamin, T. Internal waves of finite amplitude and permanent form. *J. Fluid Mech. 25* (1966), 241–270.

[11] Benjamin, T. Internal waves of permanent form in fluids of great depth. *J. Fluid Mech. 29* (1967), 559–592.

[12] Birkhoff, G. Helmholtz and Taylor instability. In *Proc. Sympos. Appl. Math., Vol. XIII*. American Mathematical Society, Providence, R.I., 1962, pp. 55–76.

[13] Brady, M., and Pullin, D. I. On singularity formation in three-dimensional vortex sheet evolution. *Phys. Fluids 11*, 11 (1999), 3198–3200.

[14] Byrd, P. F., and Friedman, M. D. *Handbook of elliptic integrals for engineers and scientists*. Second edition, revised. Die Grundlehren der mathematischen Wissenschaften, Band 67. Springer-Verlag, New York, 1971.

[15] Caflisch, R. E., and Orellana, O. F. Long time existence for a slightly perturbed vortex sheet. *Comm. Pure Appl. Math. 39*, 6 (1986), 807–838.

[16] Caflisch, R. E., and Orellana, O. F. Singular solutions and ill-posedness for the evolution of vortex sheets. *SIAM J. Math. Anal. 20*, 2 (1989), 293–307.

[17] Carrier, G. F., Krook, M., and Pearson, C. E. *Functions of a complex variable: Theory and technique*. McGraw-Hill Book Co., New York, 1966.

[18] Cayley, A. *An elementary treatise on elliptic functions*, 2nd ed. Dover Publications, Inc., New York, 1961.

[19] Chandrasekhar, S. *Hydrodynamic and hydromagnetic stability*. The International Series of Monographs on Physics. Clarendon Press, Oxford, 1961.

[20] Chen, B., and Saffman, P. Steady gravity-capillary waves on deep water. I. Weakly nonlinear waves. *Stud. Appl. Math. 60*, 3 (1979), 183–210.

[21] Chen, B., and Saffman, P. Steady gravity-capillary waves on deep water. II. Numerical results for finite amplitude. *Stud. Appl. Math. 62*, 2 (1980), 95–111.

[22] Choi, W., and Camassa, R. Weakly nonlinear internal waves in a two-fluid system. *J. Fluid Mech. 313* (1996), 83–103.

[23] Choi, W., and Camassa, R. Fully nonlinear internal waves in a two-fluid system. *J. Fluid Mech. 396* (1999), 1–36.

[24] Choi, Y., and Humphrey, J. A. Analytical prediction of tow-dimensional potential flow due to fixed vortices in a rectangular domain. *J. Comp. Phys. 56* (1984), 15–27.

[25] Cowley, S. J., Baker, G. R., and Tanveer, S. On the formation of Moore curvature singularities in vortex sheets. *J. Fluid Mech. 378* (1999), 233–267.

[26] Crapper, G. An exact solution for progressive capillary waves of arbitrary amplitude. *J. Fluid Mech. 2* (1957), 532–540.

[27] Daly, B. Numerical study of two fluid rayleigh-taylor instability. *Phys. Fluids 10* (1967), 297–307.

[28] Daly, B. Numerical study of the effect of surface tension on interface instability. *Phys. Fluids 12* (1969), 1340–1354.

[29] Davis, R. E., and Acrivos, A. Solitary internal waves in deep water. *J. Fluid Mech. 29* (1967), 593–607.

[30] Drazin, P. G., and Reid, W. H. *Hydrodynamic stability*. Cambridge University Press, Cambridge, 1981. Cambridge Monographs on Mechanics and Applied Mathematics.

[31] Fink, P., and Soh, W. A new approach to roll-up calculations of vortex sheets. *Proc. Roy. Soc. London A362* (1978), 195–209.

[32] Fornberg, B., and Whitham, G. A numerical and theoretical study of certain nonlinear wave phenomena. *Philos. Trans. Roy. Soc. London Ser. A 289*, 1361 (1978), 373–404.

[33] Glimm, J., McBryan, O., Menikoff, R., and Sharp, D. H. Front tracking applied to Rayleigh-Taylor instability. *SIAM J. Sci. Statist. Comput. 7*, 1 (1986), 230–251.

[34] Gradshteyn, I. S., and Ryzhik, I. M. *Table of integrals, series, and products*. Academic Press [Harcourt Brace Jovanovich Publishers], New York, 1980. Corrected and enlarged edition edited by Alan Jeffrey, Incorporating the fourth edition edited by Yu. V. Geronimus [Yu. V. Geronimus] and M. Yu. Tseytlin [M. Yu. Tseĭtlin], Translated from the Russian.

[35] Greengard, L. Potential flow in channels. *SIAM J. Sci. Statist. Comput. 11*, 4 (1990), 603–620.

[36] Harlow, F., and Welch, J. Numerical study of large-amplitude free-surface motions. *Phys.Fluids 9* (1966), 842–851.

[37] Helfrich, K. R., Melville, W. K., and Miles, J. W. On interfacial solitary waves over slowly varying topography. *J. Fluid Mech. 149* (1984), 305–317.

[38] Hirt, C., Cook, J., and Butler, T. A lagrangian method for calculating the dynamics of an incompressible fluid with free surface. *J. Comp. Phys. 5* (1970), 103–124.

[39] Hogan, S. Some effects of surface tension on steep water waves. *J. Fluid Mech. 91*, 1 (1979), 167–180.

[40] Hou, T., and Hu, G. Singularity formation in three-dimensional vortex sheets. *Phys. Fluids 15*, 1 (2003), 147–172.

[41] Hou, T. Y., Lowengrub, J. S., and Shelley, M. J. Removing the stiffness from interfacial flows with surface tension. *J. Comput. Phys. 114*, 2 (1994), 312–338.

[42] Hou, T. Y., Lowengrub, J. S., and Shelley, M. J. Boundary integral methods for multicomponent fluids and multiphase materials. *J. Comput. Phys. 169*, 2 (2001), 302–362.

[43] Hunter, J. K., and Vanden-Broeck, J.-M. Solitary and periodic gravity—capillary waves of finite amplitude. *J. Fluid Mech. 134* (1983), 205–219.

[44] Ishihara, T., and Kaneda, Y. Spontaneous singularity formation in the shape of vortex sheet in three-dimensional flow. *J. Phys. Soc. Japan 63* (1994), 388–392.

[45] Ishihara, T., and Kaneda, Y. Singularity formation in three-dimensional motion of a vortex sheet. *J. Fluid Mech. 300* (1995), 339–366.

[46] Joseph, R. I. Solitary waves in a finite depth fluid. *J. Phys. A 10*, 12 (1977), 225–227.

[47] Kakutani, T., and Yamasaki, N. Solitary waves on a two-layer fluid. *J. Phys. Soc. Japan 45* (1978), 674–679.

[48] Kang, Y., and Vanden-Broeck, J.-M. Gravity-capillary waves in the presence of constant vorticity. *Eur. J. Mech. B Fluids 19*, 2 (2000), 253–268.

[49] Kelvin, L. *Mathematical and Physical Papers*, vol. 4. Cambridge University Press, Cambridge, 1910.

[50] Kinnersley, W. Exact large amplitude capillary waves on sheets of fluid. *J. Fluid Mech. 77*, 2 (1976), 229–241.

[51] Koop, C. G., and Butler, G. An investigation of internal solitary waves in a two-fluid system. *J. Fluid Mech. 112* (1981), 225–251.

[52] Korn, G. A., and Korn, T. M. *Mathematical handbook for scientists and engineers*. Second, enlarged and revised edition. McGraw-Hill Book Co., New York, 1968.

[53] Krasny, R. A study of singularity formation in a vortex sheet by the point-vortex approximation. *J. Fluid Mech. 167* (1986), 65–93.

[54] Kubota, T., Ko, D., and Dobbs, L. Weakly-nonlinear, long internal gravity waves in stratified fluids of finite depth. *J. Hydronautics 12* (1978), 157–165.

[55] Lavrent'ev, M., and Shabat, B. *Metody teorii funktsiy kompleksnogo peremennogo*. Gosudarstvennoe izdatel'stvo fiziko-matematicheskoj literatury, Moscow, 1958. (in Russian). Part I only translated into Spanish; Part II is: B.V. Shabat, *Introduction to complex analysis. Part II. Functions of several variables*, Translations of Mathematical Monographs, 110, AMS, Providence, RI, 1992.

[56] Lax, P. D. Development of singularities of solutions of nonlinear hyperbolic partial differential equations. *J. Math. Phys. 5* (1964), 611–613.

[57] Liska, R., Margolin, L., and Wendroff, B. Nonhydrostatic two-layer models of incompressible flow. *Comput. Math. Appl. 29*, 9 (1995), 25–37.

[58] Logan, J. D. *An introduction to nonlinear partial differential equations*. Pure and Applied Mathematics. John Wiley & Sons Inc., New York, 1994. A Wiley-Interscience Publication.

[59] Longuet-Higgins, M. S. Integral properties of periodic gravity waves of finite amplitude. *Proc. Roy. Soc. London Ser. A 342* (1975), 157–174.

[60] Longuet-Higgins, M. S., and Cokelet, E. D. The deformation of steep surface waves on water. I. A numerical method of computation. *Proc. Roy. Soc. London Ser. A 350*, 1660 (1976), 1–26.

[61] Markushevich, A. I. *Theory of functions of a complex variable. Vol. I, II, III*, english ed. Chelsea Publishing Co., New York, 1977. Translated and edited by Richard A. Silverman.

[62] Matsuno, Y. A unified theory of nonlinear wave propagation in two-layer fluid systems. *J. Phys. Soc. Japan 62*, 6 (1993), 1902–1916.

[63] Meiron, D. I., Baker, G. R., and Orszag, S. A. Analytic structure of vortex sheet dynamics. I. Kelvin-Helmholtz instability. *J. Fluid Mech. 114* (1982), 283–298.

[64] Miles, J. Solitary waves. *Ann. Rev. Fluid Mech. 12* (1980), 11–43.

[65] Miles, J. W. On internal solitary waves. II. *Tellus 33*, 4 (1981), 397–401.

[66] Miura, R. M., Gardner, C. S., and Kruskal, M. D. Korteweg-de Vries equation and generalizations. II. Existence of conservation laws and constants of motion. *J. Mathematical Phys. 9*, 8 (1968), 1204–1209.

[67] Moore, D. W. The spontaneous appearance of a singularity in the shape of an evolving vortex sheet. *Proc. Roy. Soc. London Ser. A 365*, 1720 (1979), 105–119.

[68] Moore, D. W. On the point vortex method. *SIAM J. Sci. Statist. Comput. 2*, 1 (1981), 65–84.

[69] Moore, D. W. Numerical and analytical aspects of Helmholtz instability. In *Theoretical and applied mechanics (Lyngby, 1984)*. North-Holland, Amsterdam, 1985, pp. 263–274.

[70] Ono, H. Algebraic solitary waves in stratified fluids. *J. Phys. Soc. Japan 39*, 4 (1975), 1082–1091.

[71] Papageorgiou, D. T., and Orellana, O. Study of cylindrical jet breakup using one-dimensional approximations of the Euler equations. *SIAM J. Appl. Math. 59*, 1 (1999), 286–317 (electronic).

[72] Papageorgiou, D. T., and Smith, F. T. Nonlinear instability of the wake behind a flat plate placed parallel to a uniform stream. *Proc. Roy. Soc. London Ser. A 419*, 1856 (1988), 1–28.

[73] Pullin, D. Numerical studies of surface-tension effects in nonlinear Kelvin-Helmholtz and Rayleigh-Taylor instabilities. *J. Fluid Mech. 119* (1982), 507–532.

[74] Rangel, R., and Sirignano, W. Nonlinear growth of Kelvin-Helmholtz instability: Effect of surface tension and density ratio. *Phys. Fluids A 31* (1988), 1845–1855.

[75] Roberts, A. A stable and accurate numerical method to calculate the motion of a sharp interface between fluids. *IMA J. Appl. Math. 31* (1983), 13–35.

[76] Rosales, R. R., and Papanicolaou, G. C. Gravity waves in a channel with a rough bottom. *Stud. Appl. Math. 68*, 2 (1983), 89–102.

[77] Rosenhead, L. The formation of vortices from a surface of discontinuity. *Proc. R. Soc. London Ser. A 134* (1931), 170–192.

[78] Rottman, J., and Olfe, D. Comment on discretized simulations of vortex sheet evolution with buoyancy and surface tension effects. *AIAA J. 15* (1977), 1214–1215.

[79] Saffman, P. *Vortex dynamics.* Cambridge University Press, Cambridge, 1992.

[80] Schwartz, L. Computer extension and analytic continuation of Stokes' expansion for gravity waves. *J. Fluid Mech. 62* (1974), 553–578.

[81] Schwartz, L. W., and Vanden-Broeck, J.-M. Numerical solution of the exact equations for capillary-gravity waves. *J. Fluid Mech. 95*, 1 (1979), 119–139.

[82] Shelley, M. A study of singularity formation in vortex-sheet motion by a spectrally accurate vortex method. *J. Fluid Mech. 244* (1992), 493–526.

[83] Siegel, M. *An analytical and numerical study of singularity formation in the Rayleigh-Taylor problem.* Ph.D. Thesis, New York University, 1989.

[84] Siegel, M. A study of singularity formation in the Kelvin-Helmholtz instability with surface tension. *SIAM J. Appl. Math. 55*, 4 (1995), 865–891.

[85] Stokes, G. On the theory of oscillatory waves. *Camb. Trans. 8* (1847), 441–473.

[86] Sulem, C., Sulem, P., Bardos, C., and Frisch, U. Finite time analyticity for the two and three dimensional Kelvin-Helmholtz instability. *Commun. Math. Phys. 80* (1981), 485–516.

[87] Tanaka, M. Nonlinear self-modulation of interfacial waves. *J. Phys. Soc. Jpn. 51*, 6 (1982), 2016–2023.

[88] Taylor, G. The instability of liquid surfaces when accelerated in a direction perpendicular to their planes. I. *Proc. Roy. Soc. London. Ser. A. 201* (1950), 192–196.

[89] Thorpe, S. Experiments on the instability of stratified shear flows: missible fluids. Part 2. *J. Fluid Mech. 46* (1971), 299–319.

[90] Tryggvason, G. Numerical simulation of the Rayleigh-Taylor instability. *J. Comp. Phys. 75* (1988), 253–282.

[91] Van Dyke, M. *An Album of Fluid Motion.* Parabolic Press, Stanford, California, 1982.

[92] Zalosh, R. Discretized simulation of vortex sheet evolution with buoyancy and surface tension effects. *AIAA J. 14* (1976), 1517–1523.

[93] Zaroodny, S., and Greenberg, M. On a vortex sheet approach to the numerical calculation of water waves. *J. Comp. Phys. 11* (1973), 440–446.